

# MultHyFuel

## Deliverable 2.2

### Assessment of Dispersion for High-Pressure H<sub>2</sub>

Authors:

James Stewart, HSE  
Elena Vyazmina, Air Liquide  
Guillaume Lecocq, INERIS  
Chris Dixon, Shell

Reviewers:

Matthew Ivings, HSE  
Christophe Proust, INERIS  
Sébastien Quesnel, ENGIE  
Joana Dias Fonseca, Hydrogen Europe

Status: Final

Report Date: 11th November 2022

Confidentiality Level: Public



This project has received funding from the Fuel Cells and Hydrogen 2 Joint Undertaking under Grant Agreement No 101006794. This Joint Undertaking receives support from the European Union's Horizon 2020 Research and Innovation programme, Hydrogen Europe and Hydrogen Europe research.



## Deliverable D2.2

# Assessment of Dispersion for High-Pressure H<sub>2</sub>

Report approved by: Edwina de Lewandowicz, BA (Hons)

Date of Issue: 11/11/2022

Lead Author: James Stewart, BSc (Hons), MSc, CMath, MIMA

Contributing Author(s): Elena Vyazmina (Air Liquide)  
Guillaume Lecocq (INERIS)  
Chris Dixon (Shell)

Customer: MultHyFuel Consortium, coordinated by Hydrogen Europe

Technical & Editorial  
Reviewer: Matthew Ivings, PhD, CPhys, MInstP

Project number: PE20142

HSE Science Division Report  
Number: FD/21/04

### Disclaimer:

This report and the work it describes were undertaken collaboratively by the Health and Safety Executive (HSE), Air Liquide, INERIS and Shell. Its contents, including any opinions and/or conclusions expressed or recommendations made, do not supersede current HSE policy or guidance.



## Executive Summary

The main aim of MultHyFuel Work Package 2 (WP2) is to **produce the data missing to implement usable risk analysis and mitigation activity** for Hydrogen Refuelling Stations (HRS) in a multi-fuel context. This report, deliverable D2.2, is one of four deliverables which will be produced in WP2 and is the main output of *Task 2.1.2 – Dispersion Characteristics*. The principal aim of this task is to study realistic releases of H<sub>2</sub> on representative multi-fuel forecourts using Computational Fluid Dynamics (CFD).

In this report the CFD modelling performed as part of the *Dispersion Characteristics* task is described, the range of realistic release scenarios are discussed and their links to the critical scenarios identified through the risk assessment work conducted in WP3 are presented. The report presents demonstration solutions, including predicted flammable cloud volumes, for a range of critical scenarios.

The task has been conducted in two stages as follows:

- **Model Validation** – to evaluate the CFD models selected by the task partners and to evaluate their performance through comparison to experimental data.
- **Realistic Release Modelling** – to perform demonstration simulations of a range of critical scenarios, identified in WP3.

The model validation exercise shows that the CFD models selected for the Dispersion Characteristics task can reasonably reproduce the measured data across a range of H<sub>2</sub> release scenarios. The experiments used as the basis of the exercise include underexpanded H<sub>2</sub> jet releases in the open atmosphere and issuing into an obstacle array, as well as buoyancy-driven releases inside a naturally ventilated enclosure.

The results of the model validation exercise show that the models produce acceptable solutions when compared to measured data and give confidence in the ability of the models, and the modellers, to capture the behaviour of realistic releases adequately.

For the modelling presented in this report, the choice of CFD model is shown to be of less importance than the definition of the source term used as an input to the CFD simulations. The model validation results suggest that jet release modelling in CFD studies should use source term input values taken from a suitable jet model, with the source specified based on conditions in the jet where the local Mach number is close to 1.

The realistic release simulation results presented span nine base scenarios, taken from the outputs of WP3. Each of these is modelled with two separate wind conditions, giving 18 cases in total. The cases cover three different forecourt configurations, as defined in WP3, and involve H<sub>2</sub> releases ranging from 1.5 to 120 g/s through hole sizes with diameters of 0.2 mm, 10% of the hose diameter (~ 0.95 mm) and full bore rupture of a 3/8 inch hose (~9.5 mm). The wind conditions modelled involve a stable atmospheric boundary layer (ABL) with a wind speed of 1.5 m/s at a reference height of 10 m above the ground (F1.5) and a neutral ABL with a wind speed of 5 m/s at a reference height of 10 m (D5).

The simulation results illustrate a consistent trend, with the F1.5 conditions giving larger flammable cloud volumes than the corresponding scenario with D5 wind conditions for all cases

studied. This illustrates that a stable atmosphere with low wind speed is likely to give a better representation of realistic worst-case conditions for the purposes of risk assessment analyses.

The predicted cloud volumes across the range of scenarios considered ranges from around 0.1 – 230 m<sup>3</sup>, depending on the size of the release, the forecourt geometry and the selected CFD model. The results show that the full bore rupture releases present a significant hazard, with flammable clouds fully engulfing the dispensing area and spreading over a large proportion of the forecourt. Conversely, the medium-sized (10% of the hose diameter) H<sub>2</sub> releases give greatly reduced flammable cloud volumes, although they still present a credible hazard in the vicinity of the release point. For the smallest release considered, the predicted cloud volumes are small and show no interaction with the obstacles present on the forecourt. As such, it would be reasonable to study the smallest releases using simpler, engineering type tools, rather than CFD.

One of the benefits of having studied these scenarios with CFD models is being able to obtain a visual representation of the flammable cloud and to thus be able to see the interaction of the cloud with obstacles on the forecourt. From the results presented in this report, it is clear that there can be extensive interaction of the flammable cloud with the canopy above the dispensing area. As such, it is recommended that additional work is undertaken in a future project to study the influence of canopy design.

The work described in this report has gone as far as it is possible to within the scope and budget of the MultHyFuel *Dispersion Characteristics* task. However, it is clear that this work can only be considered as having taken a first step into the study of H<sub>2</sub> releases on multi-fuel forecourts. There is clearly scope for extension of this modelling study to consider real-world multi-fuel forecourt case studies and to further evaluate the choice of model input parameters and forecourt geometry on predicted flammable cloud volumes. The results of this study highlight the canopy as having a strong influence on the dispersion. It is recommended that future research seeks to continue this work.

# Contents

Executive Summary .....	2
Contents.....	4
Acronyms .....	6
List of Figures.....	7
List of Tables .....	11
1 Introduction.....	13
2 Task Methodology .....	14
2.1 Overview .....	14
2.2 Model Validation.....	14
2.3 Realistic Release Modelling.....	14
3 CFD Model Validation .....	16
3.1 Model Validation Cases .....	16
3.1.1 Unobstructed Free Jet.....	16
3.1.2 Obstructed Free Jet.....	18
3.1.3 Confined Release .....	20
3.2 CFD Models and Approaches.....	21
3.2.1 Selected Models.....	21
3.2.2 Domain and Computational Mesh .....	24
3.2.3 Source Term.....	26
3.2.4 Solver Information and Numerical Sub-Models.....	26
3.3 Model Validation Results .....	29
3.3.1 Unobstructed Free Jet.....	29
3.3.2 Obstructed Free Jet.....	36
3.3.3 Confined Releases .....	42
3.4 Summary.....	43
4 Realistic Release Modelling.....	45
4.1 Selected Scenarios .....	45
4.1.1 Configuration 1 – Ready-to-deploy Multi-fuel Station .....	45
4.1.2 Configuration 2 – On Site H <sub>2</sub> Production Multi-fuel Station.....	45
4.1.3 Configuration 3 – High Capacity & High Filling Multi-fuel Station .....	46
4.1.4 Scenarios.....	46
4.1.5 Atmospheric Conditions.....	52
4.1.6 Release Conditions .....	52
4.2 Modelling Approaches Used.....	53
4.2.1 Forecourt Geometry .....	53

4.2.2	Domain and Computational Mesh .....	56
4.2.3	Wind Profile Boundary Conditions.....	61
4.2.4	H <sub>2</sub> Source Term .....	62
4.3	Simulation Results.....	63
4.3.1	Initial Velocity Field .....	63
4.3.2	Scenarios 1 & 2.....	65
4.3.3	Scenarios 3 & 4.....	67
4.3.4	Scenarios 7 & 8.....	71
4.3.5	Scenarios 9 & 10.....	74
4.3.6	Scenarios 11 & 12.....	75
4.3.7	Scenarios 15 & 16.....	77
4.3.8	Scenarios 17 & 18.....	80
4.3.9	Scenarios 19 & 20.....	81
4.3.10	Scenarios 23 & 24.....	82
4.3.11	Scenarios 25 & 26.....	83
4.3.12	Scenarios 27 & 28.....	84
5	Discussion .....	85
5.1	Summary of Realistic Release Modelling Results.....	85
5.2	Limitations of Modelling Performed .....	88
5.3	Areas for Extending the Research in Future Projects .....	89
6	Conclusions.....	90
7	Appendix .....	92
7.1	Appendix 1 – Forecourt Configurations .....	92
7.1.1	Configuration 1 – Ready-to-Deploy Multi-fuel Station.....	92
7.1.2	Configuration 2 – On Site H <sub>2</sub> Production Multi-fuel Station.....	94
7.1.3	Configuration 3 – High Capacity & High Filling Multi-fuel Station .....	96
7.2	Appendix 2 – Atmospheric Boundary Layer.....	98
8	References .....	101
	What is MultHyFuel? .....	103

## Acronyms

ABL	Atmospheric Boundary Layer
CFD	Computational Fluid Dynamics
HRS	Hydrogen Refuelling Station
JIP	Joint Industry Project
RANS	Reynold's-Averaged Navier-Stokes
SST	Shear Stress Transport
VCE	Vapour Cloud Explosion
WP	Work Package



## List of Figures

Figure 1 – Schematic of the layout for the unobstructed free jet experiments.....	16
Figure 2 – Layout of the instrumentation mast used for the unobstructed free jet experiments.....	17
Figure 3 – Schematic of the experimental setup used for the obstructed free jet releases.....	18
Figure 4 – Instrumentation layout used for the ExJet obstructed free jet experiments.....	19
Figure 5 – Schematic of the confined release test configuration .....	20
Figure 6 – Comparison of measured and predicted centreline $H_2$ molar fraction for the unobstructed free jet .....	29
Figure 7 – Comparison of the measured and predicted radial profiles of $H_2$ for the unobstructed jet scenario.....	30
Figure 8 – Ratio of predicted-to-measured concentration as a function of $H_2$ molar concentration for the unobstructed free jet scenario. Figure includes both centreline and radial data from Figure 6 and Figure 7 .....	31
Figure 9 – Comparison of measured and predicted centreline velocity for the unobstructed free jet.....	32
Figure 10 – Comparison of the measured and predicted radial velocity profiles for the unobstructed jet scenario .....	33
Figure 11 – Comparison of measured and predicted centreline turbulent fluctuating velocity, $u'$ , for the unobstructed jet.....	34
Figure 12 – Comparison of the measured and predicted radial profiles of turbulent fluctuating velocity for the unobstructed jet scenario .....	34
Figure 13 – Comparison of measured and predicted centreline fractional turbulence intensity for the unobstructed jet.....	35
Figure 14 – Comparison of the measured centreline $H_2$ molar fraction for the unobstructed free jet to CFX v19.0 predictions using the Ewan and Moodie (1986) and Shell FRED pseudo source inlet conditions listed in Table 9 .....	36
Figure 15 - Comparison of the measured centreline velocity for the unobstructed free jet to CFX v19.0 predictions using the Ewan and Moodie (1986) and Shell FRED pseudo source inlet conditions (see Table 9).....	36
Figure 16 – Comparison of the measured and predicted centreline $H_2$ molar fraction for the obstructed jet .....	37
Figure 17 – Comparison of the measured and predicted radial $H_2$ molar fraction for the obstructed jet scenario.....	38
Figure 18 – Comparison of the measured and predicted centreline velocity for the obstructed jet .....	39
Figure 19 – Comparison of the measured and predicted radial velocity profiles for the unobstructed jet scenario .....	40
Figure 20 – Comparison of measured and predicted radial profiles of turbulent fluctuating velocity, $u'$ .....	41
Figure 21 - Comparison of the measured centreline $H_2$ molar fraction for the obstructed jet to CFX v19.0 predictions using the Ewan and Moodie (1986) and Shell FRED pseudo source inlet	

conditions listed in Table 9 .....	42
Figure 22 – Comparison of the measured and predicted H <sub>2</sub> concentration profiles with height inside the enclosure for the 10.4 NL min <sup>-1</sup> release .....	43
Figure 23 – Comparison of the measured and predicted H <sub>2</sub> concentration profiles with height inside the enclosure for the 218.3 NL min <sup>-1</sup> release .....	43
Figure 24 – Schematic of the setup for realistic release scenarios 1 – 4 .....	49
Figure 25 – Schematic of the setup for realistic release scenarios 7 – 8 .....	49
Figure 26 – Schematic of the setup for realistic release scenarios 9 – 12 .....	50
Figure 27 – Schematic of the setup for realistic release scenarios 15 – 16 .....	50
Figure 28 – Schematic of the setup for realistic release scenarios 17 – 20 .....	51
Figure 29 – Schematic of the setup for realistic release scenarios 23 - 28 .....	51
Figure 30 – Modelled leak configuration for the external release scenarios .....	52
Figure 31 – Modelled leak configuration for the internal release scenarios .....	53
Figure 32 – Perspective view of the 3D geometry for Configuration 1 .....	54
Figure 33 – Perspective view of the 3D geometry for Configuration 2 .....	55
Figure 34 – Perspective view of the 3D geometry for Configuration 3 .....	56
Figure 35 – Simulation domain used: plan view (left), side view (bottom right) and perspective view (top right) .....	56
Figure 36 – Plan view of the mesh used in CFX on a plane 1.2 m above the ground (the height of the realistic releases) .....	58
Figure 37 – Porosity distribution on the computational mesh used in the FLACS simulations of Scenarios 17-20 .....	59
Figure 38 – Example of the meshing approach used in the OpenFOAM 1812 simulations of realistic releases for forecourt Configuration 2 .....	59
Figure 39 - Example of the meshing approach used in the OpenFOAM 1912+ simulations of realistic releases for forecourt Configuration 3. A focus is made on the area of interest .....	60
Figure 40 – Example of the meshing approach used in KFX for simulation of Scenario 4 .....	60
Figure 41 – Comparison of the wind velocity profiles imposed for the F1.5 and D5 atmospheric conditions considered .....	62
Figure 42 – Initial velocity field for forecourt Configuration 1 with D5 atmospheric wind conditions at a height of 1.2 m above the ground (corresponding to the release height used for the external H <sub>2</sub> leaks) .....	64
Figure 43 – Initial velocity field for forecourt Configuration 1 with F1.5 atmospheric wind conditions at a height of 1.2 m above the ground (corresponding to the release height used for the external H <sub>2</sub> leaks) .....	64
Figure 44 – Plan-view of H <sub>2</sub> /air cloud at the ½ LFL (2% vol.) and LFL (4% vol.) concentrations for Scenarios 1 (F1.5) & 2 (D5) as predicted using CFX .....	65
Figure 45 – Perspective view of the flammable cloud (iso-surface	

showing H <sub>2</sub> at 4% vol.) for Scenario 1 (F1.5) as predicted using CFX.....	66
Figure 46 – Perspective view of the flammable cloud (iso-surface showing H <sub>2</sub> at 4% vol.) for Scenario 2 (D5) as predicted using CFX.....	67
Figure 47 – Plan-view of H <sub>2</sub> /air cloud at the ½ LFL (2% vol.) and LFL (4% vol.) concentrations for Scenarios 3 (F1.5) & 4 (D5) as predicted using CFX.....	68
Figure 48 – Perspective view of the flammable cloud (iso-surface showing H <sub>2</sub> at 4% vol.) for Scenario 3 (F1.5) as predicted using CFX.....	69
Figure 49 – Perspective view of the flammable cloud (iso-surface showing H <sub>2</sub> at 4% vol.) for Scenario 4 (D5) as predicted using CFX.....	70
Figure 50 – Perspective view of the flammable cloud (iso-surface showing H <sub>2</sub> at 4% vol.) for Scenario 4 (D5) as predicted using KFX.....	71
Figure 51 – Plan view of H <sub>2</sub> /air cloud at the ½ LFL (2% vol.) and LFL (4% vol.) concentrations for Scenarios 7 (F1.5) & 8 (D5) as predicted using CFX.....	72
Figure 52 – Perspective view of the flammable cloud (iso-surface showing H <sub>2</sub> at 4% vol.) for Scenario 7 (F1.5) as predicted using CFX.....	73
Figure 53 – Perspective view of the flammable cloud (iso-surface showing H <sub>2</sub> at 4% vol.) for Scenario 8 (D5) as predicted using CFX.....	74
Figure 54 – H <sub>2</sub> /air cloud at the ½ LFL (2% vol.) and the LFL (4% vol.) concentrations for Scenarios 9 (F1.5) & 10 (D5) as predicted using OpenFOAM 1812.....	75
Figure 55 – Plan view of H <sub>2</sub> /air cloud at the ½ LFL (2% vol.) and LFL (4% vol.) concentrations for Scenarios 11 (F1.5) & 12 (D5) as predicted using OpenFOAM 1812.....	76
Figure 56 – H <sub>2</sub> /air cloud at the ½ LFL (2% vol.) and the LFL (4% vol.) concentrations for Scenarios 11 (F1.5) & 12 (D5) as predicted using OpenFOAM 1812.....	77
Figure 57 – H <sub>2</sub> /air cloud at the ½ LFL (2% vol.) and the LFL (4% vol.) concentrations for Scenarios 11 (F1.5) & 12 (D5) as predicted using KFX.....	77
Figure 58 – Plan view of H <sub>2</sub> /air cloud at the ½ LFL (2% vol.) and LFL (4% vol.) concentrations for Scenarios 15 (F1.5) & 16 (D5) as predicted using OpenFOAM 1812.....	78
Figure 59 – H <sub>2</sub> /air cloud at the ½ LFL (2% vol.) and the LFL (4% vol.) concentrations for Scenarios 15 (F1.5) & 16 (D5) as predicted using OpenFOAM 1812.....	79
Figure 60 – H <sub>2</sub> /air cloud at the ½ LFL (2% vol.) and the LFL (4% vol.) concentrations for Scenarios 15 (F1.5) & 16 (D5) as predicted using KFX.....	80
Figure 61 – Perspective view of the H <sub>2</sub> /air cloud at the LFL and ½ LFL concentrations for Scenarios 17 (F1.5) and 18 (D5) as predicted with FLACS.....	81

Figure 62 – Perspective view of the H <sub>2</sub> /air cloud at the LFL and ½ LFL concentrations for Scenarios 19 (F1.5) and 20 (D5) as predicted with FLACS.....	82
Figure 63 – Plan view of H <sub>2</sub> /air cloud at the ½ LFL (2% vol.) and LFL (4% vol.) concentrations for Scenarios 25 (F1.5) & 26 (D5) as predicted using KFX.....	83
Figure 64 – H <sub>2</sub> /air cloud at the ½ LFL (2% vol.) and the LFL (4% vol.) concentrations for Scenarios 25 (F1.5) & 26 (D5) as predicted using KFX .....	84
Figure 65 – Comparison of the predicted flammable cloud volume across the range of realistic release scenarios modelled. Here, the column labels give Configurations 1, 2 and 3 as C1, C2 and C3, respectively, followed by the release pressure as a numerical value and the release size as small-internal (S-I), medium (M) and large (L). Results for the F1.5 and D5 wind conditions are shown as blue and red columns, respectively.....	85
Figure 66 – Comparison of the predicted flammable cloud volumes for the 350 bar, full bore rupture release scenarios across all three forecourt configurations .....	86
Figure 67 – Comparison of the predicted flammable cloud volumes for the 350 bar, 10% hose diameter release scenarios for Configurations 1 and 2.....	87
Figure 68 – Comparison of the predicted flammable cloud volumes for the 700 bar, full bore rupture release scenarios for Configurations 1 and 2.....	88
Figure 69 – Layout of the <i>ready to deploy</i> multi-fuel forecourt from deliverable D3.5. Table 19 presents descriptions of the items included in this forecourt layout .....	92
Figure 70 – Layout of the <i>on site H<sub>2</sub> production</i> multi-fuel forecourt from deliverable D3.5. Table 21 presents descriptions of the items included in this forecourt layout .....	94
Figure 71 – Layout for the <i>high capacity</i> multi-fuel forecourt from deliverable D3.5. Table 23 presents descriptions of the items included in this forecourt layout .....	96

## List of Tables

Table 1 - Measured temperature and pressure just upstream of the nozzle exit for the unobstructed free jet release.....	16
Table 2 – Sensor positions used in the unobstructed free jet experiments.....	17
Table 3 - Measured temperature and pressure just upstream of the nozzle exit for the obstructed free jet release.....	18
Table 4 – Sensor positions used in the obstructed free jet experiments.....	19
Table 5 – Summary of the modelled release conditions for the confined release experiments .....	20
Table 6 – Sensor position for the 1 m <sup>3</sup> enclosure confined release tests .....	21
Table 7 – Summary of the CFD models/codes selected by the task partners.....	21
Table 8 – Summary of the computational domain and mesh choices used with each CFD model for the three model validation scenarios studied.....	25
Table 9 – Summary of the pseudo-source inlet conditions used in the different CFD models evaluated .....	26
Table 10 – Summary of the CFD model numerical details and sub-model selections used for the two jet release validation scenarios .....	27
Table 11 – Summary of the CFD model numerical details and sub-model selections used for the two confined release validation scenarios.....	28
Table 12 – Summary of the H <sub>2</sub> -related critical scenarios associated with the forecourt for both Configurations 1 & 2 .....	46
Table 13 – Summary of the H <sub>2</sub> -related critical scenarios associated with the forecourt for Configuration 3 .....	46
Table 14 – List of realistic release scenarios to be modelled using CFD tools. Cases marked with (*) indicate that the mass flow rate is restricted to the dispenser H <sub>2</sub> delivery flow rate. All other mass flow rates have been estimated using the FCH2 e-Laboratory <i>Jet Parameters</i> tool.....	47
Table 15 – Domain extent used for the realistic release simulations. Refer to Figure 35 for further details. ....	57
Table 16 – Summary of the mesh sizes used for the realistic release simulations described in this report.....	61
Table 17 - Summary of the H <sub>2</sub> jet source term parameters (calculated using Shell's AEROPLOUME model) used by all modellers for the realistic release simulations. Where the mass flow rates include an asterisk (*), this indicates that the flow rate has been capped at the dispenser delivery flow rate .....	63
Table 18 – Assumed distribution of vehicles and members of the public present on the forecourt for Configuration 1.....	92
Table 19 – Summary of the footprint size for equipment and distribution areas for Configuration 1 .....	93
Table 20 – Assumed distribution of vehicles and members of the public present on the forecourt for Configuration 2.....	94
Table 21 – Summary of the footprint size for equipment and distribution areas for Configuration 2 .....	95
Table 22 – Assumed distribution of vehicles and members of the public	

present on the forecourt for Configuration 3.....	96
Table 23 - Summary of the footprint size for equipment and distribution areas for Configuration 3 .....	97

# 1 Introduction

This report is one of four deliverables forming the principal outputs of MultHyFuel Work Package (WP) 2 – *Practical Research to Address Gaps in Current Understanding*. The main aim of WP2 is to **produce the data missing to implement usable risk analysis and mitigation activity** for Hydrogen Refuelling Stations (HRS) in a multi-fuel context. There is extensive interaction across WP2 and WP3 to ensure that knowledge gaps, safety-critical scenarios and safety barriers identified in WP3 are studied in further detail as part of the work conducted under WP2.

The four main objectives of WP2 are as follows:

- Determine leakage frequencies, flow rates, extent of hazardous zones and ignition probabilities for faults on HRS plant
- Reproduce experimentally, and study using Computational Fluid Dynamics (CFD), the key fire and explosion scenarios which cannot be investigated sufficiently using simpler modelling tools
- Test in realistic conditions the performance and reliability of key safety barriers identified in WP3
- Estimate experimentally the consequences of hazards on the hydrogen dispensers affecting the other dispenser types on a multi-fuel forecourt, and vice-versa

This report outlines the work undertaken for WP2 *Task 2.1.2 – Dispersion Characteristics*. The report describes the CFD modelling performed and presents the predicted flammable cloud volumes, and flammable masses, for the critical scenarios considered.

The realistic release scenarios simulated as part of this task are based on the findings from WP3 *Task 3.5 – Identification of Critical Scenarios*. Each scenario was selected due to features deemed to fall outside the scope of application for simpler engineering tools. Further details of the critical scenarios, and the reasons for their inclusion in this CFD modelling task, are given in Section 4 of the present report.

## 2 Task Methodology

### 2.1 Overview

The principal aim of *Task 2.1.2 – Dispersion Characteristics* is to study realistic releases of  $H_2$  on representative multi-fuel forecourts using CFD. The task has been conducted in two stages as follows:

- **Model Validation** – to evaluate the CFD models selected by the task partners and evaluate their performance through comparison to experimental data
- **Realistic Release Modelling** – to perform demonstration simulations of a range of critical scenarios, identified through WP3 HAZID workshops and subsequent risk assessment analyses, which could not be adequately studied using simpler, engineering type modelling tools

Further details of each are given in the following Sections of this report.

### 2.2 Model Validation

Model validation is used to analyse how well a model performs at predicting key quantities through direct comparison to experimental data. A model validation exercise typically aims to evaluate model performance for a range of scenarios which exhibit similar physics to the main scenarios of interest in a given study. The purpose of evaluating a model in this way is to assess a model's strengths and weaknesses through comparison to measured data. Model validation results can then be used to better understand model predictions generated for practical scenarios.

The CFD models selected by each of the task partners have been validated against pre-existing experiments covering the following three release scenarios:

- **Unobstructed free jet** – high-pressure free jet
- **Obstructed free jet** – high-pressure free jet issuing into an obstacle array
- **Confined release** – buoyancy-dominated releases inside a naturally-ventilated enclosure

These three scenarios were selected to collectively span the release physics and geometrical elements relevant for the anticipated realistic release modelling to follow. Further details of each validation scenario studied are given in Section 3.

### 2.3 Realistic Release Modelling

In this task, a series of realistic release scenarios are modelled. The purpose of these simulations is to provide information on the extent of the flammable cloud which would form following an accidental  $H_2$  release on a multi-fuel forecourt. The principal model output used to achieve this task aim is the predicted flammable volume, i.e. the volume of the  $H_2$ /air cloud in which the concentration of  $H_2$  lies between the lower and upper flammability limits, 4% and 75% (v/v), respectively. Additionally, the mass of  $H_2$  in the flammable cloud is also reported for some of the scenarios modelled.



The selected scenarios are based on the outputs of WP3. In particular, the representative forecourt layouts and the high-hazard events associated with releases from H<sub>2</sub> dispensers, as identified in Task 3.5. In this *Dispersion Characteristics* task, the scenarios of interest are those which are not suitable for simulation using simpler modelling tools, e.g. scenarios with jet impingement and significant obstacle interaction.

Whilst Task 3.5 provides the generic definition of the releases to be considered, specific details, such as the release location and orientation, and the modelled wind conditions, have been chosen within the CFD modelling task. The final selection of scenarios was then agreed with the overall MultHyFuel project consortium before the simulations commenced.

Further details of each of the realistic release scenarios modelled are given in Section 4 of this report.

## 3 CFD Model Validation

### 3.1 Model Validation Cases

#### 3.1.1 Unobstructed Free Jet

Daubech et al. (2015) performed a series of horizontally-oriented unobstructed free jet releases of  $H_2$ . Both ignited and unignited tests were performed, with measurements of  $H_2$  concentration, velocity and turbulence intensity obtained during the tests. The experiments involved the release of  $H_2$  through a 12 mm diameter nozzle located 1.5 m above the ground. The release nozzle was connected by a flexible hose to a 5 m<sup>3</sup> storage vessel at 40 bar. Figure 1 shows a schematic of the experimental setup.

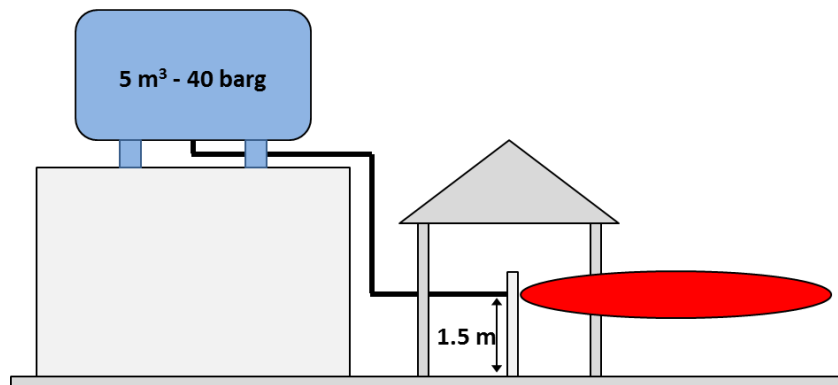


**Figure 1 – Schematic of the layout for the unobstructed free jet experiments**

Measurements of the temperature and pressure were taken just upstream of the nozzle exit, giving conditions which can be used to generate an inlet source term for modelling the releases using CFD. A number of repeat tests were performed, with little variation in the measured release conditions. As such, model predictions for a steady-state release are compared to the experimental data from a number of experimental trials.

Table 1 summarises the measured conditions just upstream of the release plane. The measured ambient temperature was 10 °C for the unobstructed free jet experiments.

Pressure (barg)	Temperature (°C)
34.0±0.1	25.0±1.0

**Table 1 - Measured temperature and pressure just upstream of the nozzle exit for the unobstructed free jet release**

An instrumented mast was used to collect the experimental data. Measurements of  $H_2$  concentration, deduced from  $O_2$  measurements, were taken using SERVOMEX - Type PM1158 paramagnetic oxygen analysers (accuracy to within  $\pm 0.1\%O_2$ ). Velocity measurements were obtained using bi-directional pitot probes coupled with differential pressure sensors, with turbulence intensity information inferred from the measured velocity field. The expected accuracy is typically  $\pm 1.0$  m/s. The instrumentation mast was placed at distances of 1.25, 2.0, 3.0, 4.5, 7.5 and 10.0 m downstream from the release orifice, aligned with the jet centreline. An array of 9 sensors in the vertical direction was used to obtain  $H_2$  concentration measurements, with 7 sensors in the horizontal direction used to measure the velocity field. A schematic of the sensor arrangement is shown in Figure 2. The sensor locations used are given, relative to the release point,

in Table 2, where the jet is aligned along the +X direction and the +Z direction is taken as pointing vertically upwards from the ground.

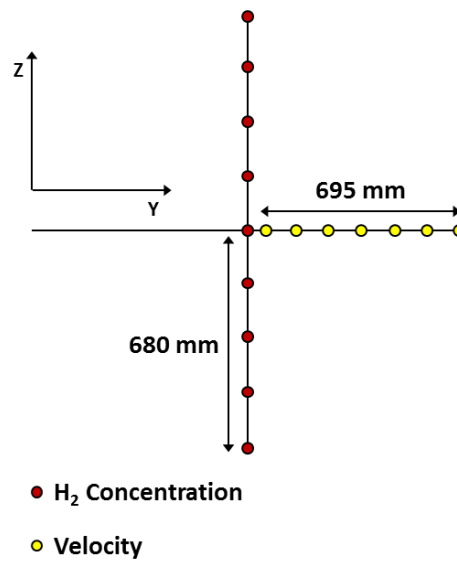


Figure 2 – Layout of the instrumentation mast used for the unobstructed free jet experiments

Measured Variable	Sensor Location		
	X (m)	Y (m)	Z (m)
H <sub>2</sub> Concentration	1.25, 2.0, 3.0, 4.5, 7.5, 10.0	0.0	-0.68
			-0.51
			-0.34
			-0.17
			0.00
			0.17
			0.34
			0.51
			0.68
Velocity	1.25, 2.0, 3.0, 4.5, 7.5, 10.0	0.055	0.0
		0.170	
		0.285	
		0.405	
		0.520	
		0.635	
		0.750	

Table 2 – Sensor positions used in the unobstructed free jet experiments

The unobstructed free jet scenario is included in this model validation exercise primarily as a means of evaluating a range of source term modelling approaches commonly used in CFD. These so-called *pseudo-source*, or *notional nozzle*, approaches are frequently used in preference to simulating high-pressure releases directly from the nozzle. This typically allows for the use of a larger release area in the model, and thus reduces the necessary cell size for the computational

mesh used. Furthermore, it alleviates the need to simulate the expansion zone, which comprises a complex series of shocks, or discontinuities. Resolving this region at the same time as capturing larger scale dispersion effects is extremely difficult with the traditional CFD solvers.

It should be noted that, whilst the release pressure for the two free jet tests modelled here is substantially lower than expected for an HRS dispenser, the resulting mass flow rate of H<sub>2</sub> is similar to the highest dispensing flow rate envisioned. From WP3 release rates are anticipated to be up to 300 g/s, for a 350 bar heavy-duty dispenser. With regards to H<sub>2</sub> concentrations in the jet, the concentration can be shown to be relatively insensitive to release pressure for a given mass flow rate, thus using a lower value of 40 barg is appropriate for the present analysis.

### 3.1.2 Obstructed Free Jet

The unobstructed free jet tests described by Daubech et al. (2015) were performed as a part of the ExJet Joint Industry Project (JIP). Within the same project, a series of obstructed free jet releases was also undertaken. The obstructed releases involved horizontally-oriented H<sub>2</sub> free jets released through a 12 mm diameter nozzle located 0.75 m above the ground. The release nozzle was connected by a flexible hose to a 5 m<sup>3</sup> storage vessel at 40 bar. The jets were directed into an obstacle array comprising numerous 1.5 m long, 0.1 m diameter cylinders oriented perpendicularly to the jet flow. The cylinders were spaced approximately 0.35 m apart in the vertical direction. Figure 3 shows a schematic of the experimental setup.

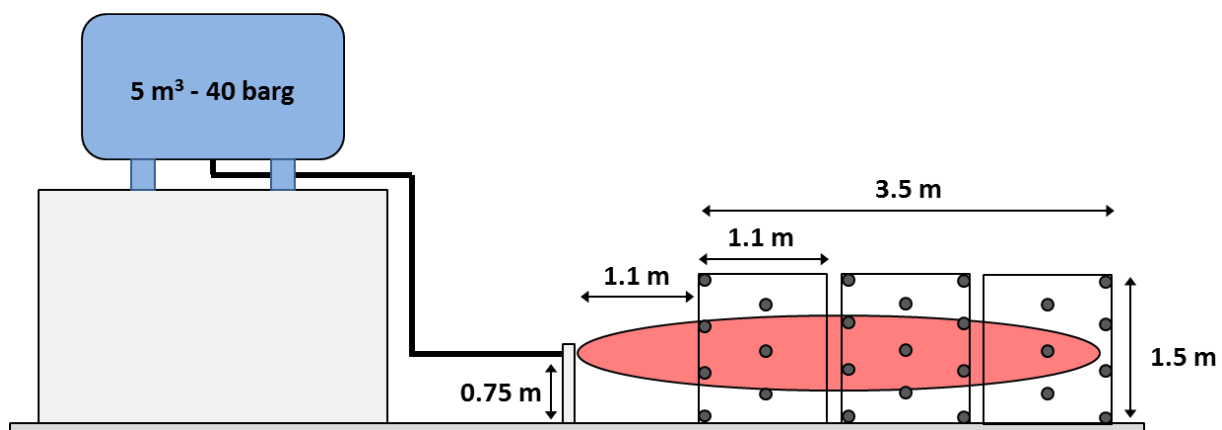


**Figure 3 – Schematic of the experimental setup used for the obstructed free jet releases**

Measurements of the temperature and pressure were taken just upstream of the nozzle exit, giving conditions which can be used to generate an inlet source term for modelling the releases using CFD. Table 3 summarises the measured conditions just upstream of the release plane. The measured ambient temperature was 15 °C for the obstructed free jet experiments.

Pressure (barg)	Temperature (°C)
38.0±0.1	8.0±1.0

**Table 3 - Measured temperature and pressure just upstream of the nozzle exit for the obstructed free jet release**

Measurements of H<sub>2</sub> concentration, deduced from O<sub>2</sub> measurements, were taken during the obstructed jet releases tests using SERVOMEX - Type PM1158 paramagnetic oxygen analysers. Velocity measurements were obtained using bi-directional pitot probes coupled with differential pressure sensors, with turbulence intensity information inferred from the measured velocity field.

A single instrumentation mast was used in each experiment, with three repeat tests performed to collect data 1.4, 2.5 and 4.4 m downstream of the release point. A schematic of the instrumentation mast used is shown in Figure 4, where the lowest sensor positions on the mast were located 0.7 m above the ground, i.e. 0.05 m below the centre of the release point.

The sensor locations used across the obstructed jet tests are summarised in Table 4 with the positions given relative to the release point, again with the jet released along the +X direction and the +Z direction taken as vertically upwards from the ground.

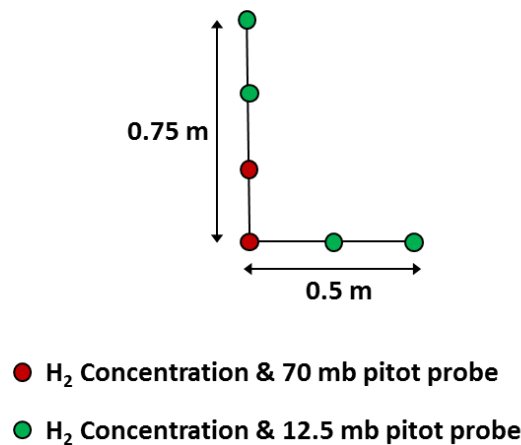


**Figure 4 – Instrumentation layout used for the ExJet obstructed free jet experiments**

Measured Variable	Sensor Location		
	X (m)	Y (m)	Z (m)
H <sub>2</sub> Concentration and velocity	1.4, 2.5, 4.4	0.00	-0.05
		0.00	0.20
		0.00	0.45
		0.00	0.70
		0.25	-0.05
		0.50	-0.05

**Table 4 – Sensor positions used in the obstructed free jet experiments**

Validating the CFD models used in this task against experimental data for an obstructed release enables the performance of the models to be assessed for a scenario with comparable physics to the realistic release scenarios involving obstructions and impinging releases.

On a multi-fuel forecourt, there are a number of obstacles which could be present in the path of an accidental release, for example the dispenser casing, vehicles and any building structures such as the fuel station shop. Thus, it is likely that the majority of realistic releases will interact in some way with obstacles in the flow path. Hence it is critical that model performance is assessed for such releases as part of this model validation exercise, prior to studying the critical scenarios identified through the risk assessment work in WP3.

### 3.1.3 Confined Release

Bernard-Michel and Houssin-Agbomson (2017) performed a series of confined  $H_2$  releases inside naturally ventilated  $1\text{ m}^3$  and  $2\text{ m}^3$  enclosures. In the present study, the  $1\text{ m}^3$  enclosure results are used as the smaller enclosure volume more closely represents the anticipated volume of a representative  $H_2$  dispenser.

The  $1\text{ m}^3$  enclosure experiments involved vertically upward releases of  $H_2$  at a height of 80 mm above the enclosure base. Two circular release nozzles were used in the tests with 4 mm and 27.2 mm internal diameter, with  $H_2$  flow rates of approximately 5 to 218  $\text{NL min}^{-1}$ . Two of the tests using the 27.2 mm nozzle are used in this model validation exercise. The release conditions for each are summarised in Table 5

Nozzle Diameter (mm)	Flow Rate ( $\text{NL min}^{-1}$ )	Velocity ( $\text{m/s}$ )	Temperature ( $^{\circ}\text{C}$ )
27.2	10.4	0.31	12.4
	218.3	6.56	12.3

**Table 5 – Summary of the modelled release conditions for the confined release experiments**

The experiments used a 1 m high enclosure with a 0.995 m square base. The enclosure included two ventilation openings, one at the top and the other at the bottom of two opposing walls, each 960 mm wide and 180 mm high. Figure 5 shows a schematic of the test configuration.

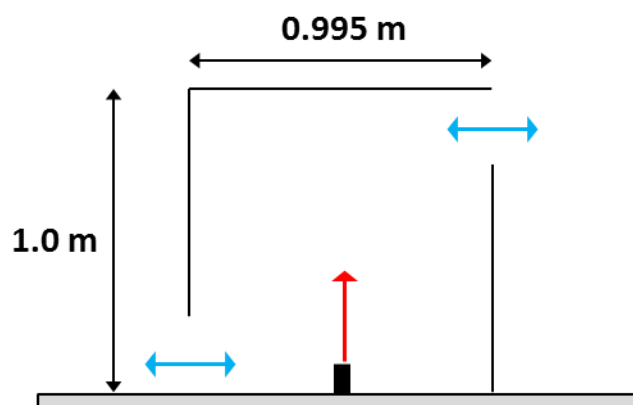


**Figure 5 – Schematic of the confined release test configuration**

Measurements of  $H_2$  concentration were taken using 15 Xen-TCG3880 minicatharometers mounted to a single, vertical sensor tree positioned close to one of the walls perpendicular to the two containing ventilation openings. Table 6 gives the position of each sensor relative to the centre of the enclosure base with the Y direction perpendicular to the two ventilation openings and the +Z direction pointing vertically upwards.

Measured Variable	Sensor Location		
	X (m)	Y (m)	Z (m)
H <sub>2</sub> Concentration	0.0	-0.45	0.040
			0.105
			0.170
			0.235
			0.300
			0.365
			0.430
			0.495
			0.560
			0.625
			0.690
			0.755
			0.820
			0.885
			0.950

**Table 6 – Sensor position for the 1 m<sup>3</sup> enclosure confined release tests**

Validation of the CFD models used in this task with data for confined releases is necessary to capture the physics associated with realistic releases inside the dispenser casing. There is a substantial number of fixtures and fittings inside the dispenser which could lead to releases of H<sub>2</sub>. Testing of relevant components has been performed as part of Task 2.1.1 – Leakage Characterisation, as a means of quantifying the leakage flow rates and component failures which may occur. Such releases will be similarly confined as for the scenarios tested by Bernard-Michel and Houssin-Agbomson (2017).

## 3.2 CFD Models and Approaches

### 3.2.1 Selected Models

Each task partner has selected different CFD model(s), or model version(s), for the simulation work involved in the *Dispersion Characteristics* task, as summarised in Table 7.

Task Partner	Selected CFD Models
Air Liquide	FLACS v10.4 & v10.6
HSE	CFX v19.0
INERIS	OpenFOAM v1912+
Shell	OpenFOAM v1812, KFX 3.6.8,

**Table 7 – Summary of the CFD models/codes selected by the task partners**

In addition to CFD model predictions, the consequence modelling package FRED (Betteridge, 2022) has also been used to model the jet release scenarios. Specifically, the jet dispersion model, AEROPUME (McFarlane, 1991) within the FRED package has been used in order to enable comparison between the CFD predictions and results using a simpler modelling approach. Details

of the AEROPLUME approach are briefly described in Section 3.2.1.5.

References to model versions are not included in the remainder of this report, other than to distinguish between the two versions of OpenFOAM used.

#### 3.2.1.1 CFX

CFX (ANSYS, 2019) is a general-purpose CFD code. As used here, the model is based around an unstructured tetrahedral mesh. The solver is based on the SIMPLE algorithm and uses 2nd order numerical schemes. Both steady-state and transient versions of the solver have been used in this work. Where the model was used for transient calculations, a 2nd order backward Euler scheme was used for time-stepping.

With regards to turbulence, a range of two-equation Reynold's-Averaged Navier Stokes (RANS) approaches have been used. For the model validation simulations, the  $k-\varepsilon$  RNG model was used. However, results of a turbulence model sensitivity analysis showed little variation between this model and the standard  $k-\varepsilon$  model. For the purposes of consistency with the other models, the standard  $k-\varepsilon$  model was used for all of the realistic release simulations described in Section 4. Full buoyancy modelling was also used, with corrections to both the turbulence production and dissipation terms in the turbulence model.

Species transport was modelled using a scalar transport equation for  $H_2$ , with air modelled as a constraint species, i.e. not tracked, but inferred from the  $H_2$  concentration field.

With the use of an unstructured mesh it is possible to resolve all of the obstacles in the flow field directly, although the level of resolution is dependent on how fine the computational mesh is in the vicinity of the obstructions. This is beneficial for the realistic release simulations, in particular, which are described in Section 4.

#### 3.2.1.2 OpenFOAM

OpenFOAM<sup>1</sup> is an open source CFD toolkit in which users can construct solvers for their individual problem. The distribution of OpenFOAM is supplied with a large number of solvers already available which, in many cases, can be used directly without modification.

In this work, the simulations performed by Shell have been carried out using modified versions of the standard solvers intended for buoyancy problems. The two solvers used as the basis were the steady-state *buoyantSimpleFoam* solver and the transient *buoyantPimpleFoam* solver. Aside from the time dependence, these two solvers are essentially the same and are intended for flows either driven by buoyancy or where density differences due to temperature variation are important. The Boussinesq approximation is not used and the solver is described in the relevant OpenFOAM documentation as being appropriate for compressible flow simulations.

However, the solvers selected by Shell do not allow for species transport by default, thus some modification was required to incorporate thermodynamics from another OpenFOAM solver. The chosen thermodynamics is a thermo-physical model for reacting mixtures. The reactions are

---

<sup>1</sup> <https://openfoam.org/>



turned off in the calculations presented here and only the ability to deal with multiple species is used. As a consequence, the modelling includes an equation for species transport.

For the modelling performed by INERIS, a different version of OpenFOAM was used as compared to that used by Shell. INERIS made use of the *rhoReactingFoam* solver without modification for modelling the two high-speed H<sub>2</sub> jet release validation cases. For computing the buoyancy-driven flows in the naturally ventilated 1 m<sup>3</sup> box, the solver *rhoReactingBuoyantFoam* was used. The same solver was used as the basis for the realistic release modelling exercise discussed in Section 4.

Turbulence is handled using the standard two-equation k- $\epsilon$  model in both the Shell and INERIS modelling. Whilst there are known deficiencies of this model for the simulation of jet flows, alternative approaches do not readily include buoyancy effects in OpenFOAM. Since the influence of buoyancy is considered important in the simulations described in this report, using the standard k- $\epsilon$  model is deemed to be a better approach than employing a more comprehensive, and computationally expensive, turbulence model given the other approximations made in the modelling.

### 3.2.1.3 FLACS

FLACS (Gexcon, 2014) is a CFD toolbox specifically designed for the simulation of process safety related applications, such as dispersion of flammable gases.

FLACS is based on the use of structured Cartesian grids and the so-called *distributed porosity* concept, whereby complex geometries are represented on a relatively coarse numerical grid using volume and area porosities in each cell to represent sub-grid scale obstacles. Where possible, it is advisable to align larger obstructions with grid lines to ensure that they are adequately captured in the model.

The CFD code within FLACS solves 3D Favre-averaged transport equations for mass, momentum, enthalpy, turbulence properties and species concentrations. Turbulence closure is achieved via the two-equation RANS k- $\epsilon$  turbulence model. The solver utilises the SIMPLE algorithm (Patankar, 1980).

### 3.2.1.4 KFX

KFX<sup>2</sup> (DNV, 2001) is a CFD code distributed by Det Norsk Veritas (DNV) originally intended as a fire simulator but also capable of gas dispersion calculations and with a user interface specialised to these two applications. KFX was developed at the Norwegian University of Science and Technology and SINTEF and now developed and marketed by DNV. It is a proprietary solver so only a brief overview will be given.

KFX uses a finite volume technique with a single block Cartesian grid to solve the transport equations. The gas density is calculated from an ideal gas law. Turbulent transport effects are modelled as gradient diffusion with turbulent viscosity calculated from the k- $\epsilon$  turbulence model including buoyancy effects.

---

<sup>2</sup> Kameleon FireEx (KFX): <https://www.dnv.com/services/cfd-simulation-kfx-110662>

KFX is a transient code and cannot carry out steady-state calculations. Steady state results are obtained by allowing the solution to reach a steady state over time, transiently. Hence, initially, calculated jets will grow and take some time to reach a steady state. However, the code is implicit and very stable so that large time steps can be used (i.e. a large Courant number) so that a steady state can be reached quickly.

### 3.2.1.5 AEROPLUME

AEROPLUME (McFarlane, 1991) is a steady-state integral model which is used to simulate the gas jet/plume development in a release from a pressurised vessel or from a stack/vent. The release can consist of a mixture of several non-reacting components, which can form one or more single or multi-component aerosols. It can handle gaseous and two-phase jet releases in the open atmosphere. AEROPLUME is based on conservation of mass, momentum and energy, together with an entrainment assumption, and assumptions describing the mixture thermodynamics. The model is included as a component of the Shell FRED consequence modelling software (Betteridge, 2022).

## 3.2.2 Domain and Computational Mesh

Table 8 summarises the domain size used and computational mesh settings selected by each task partner for the three model validation scenarios considered. The details given in the Table illustrate that there are some significant differences between the modelling approaches used, particularly with regards to the type of mesh and the mesh resolution used to capture the inlet. Both of these choices are, to a certain extent, a consequence of the choice of CFD model. For example, the FLACS grid guidelines stipulate the mesh resolution for simulating a jet release, whereas the model user has more choice on how best to resolve the inlet in the other CFD models used in the present study.

It is good practice to undertake a mesh sensitivity analysis when performing a CFD modelling study to ensure that the model predictions are not affected by the choice of computational grid. The task partners have undertaken such an analysis prior to submitting their results for the model validation simulations. The grid sensitivity analysis results are not presented here.

With regards to simulating the influence of the ground for the jet release scenarios, all of the models used a smooth-wall with a zero-slip approximation for velocity.

	FLACS v10.4/10.6	CFX v19.0	OpenFOAM v1912+	OpenFOAM v1812
<b>Unobstructed Free Jet</b>				
Mesh Type	Structured Cartesian	Unstructured tetrahedral	Structured Cartesian	Hexahedral with mesh adaptation
Grid at Inlet	1 cell	108 nodes	10 cells	44 faces
Mesh Node Count	4,179,175	1,956,404	9,100,000	1,401,218
Domain Dimensions	65 m x 30 m x 17 m	22 m x 6 m x 5 m	20 m x 8 m x 5 m	17 m x 10 m x 8 m
<b>Obstructed Free Jet</b>				
Mesh Type	Structured Cartesian	Unstructured tetrahedral	Structured Cartesian	Hex dominant with mesh adaptation
Grid at Inlet	1 cell	115 nodes	6 cells	52 faces
Mesh Node Count	2,664,750	2,589,006	2,100,000	2,337,376
Domain Dimensions	17 m x 14 m x 8.1 m	22 m x 8 m x 5 m	8.5 m x 4 m x 4 m	17 m x 10 m x 5 m
<b>Confined Releases</b>				
Mesh Type	Structured Cartesian	Unstructured tetrahedral	Structured Cartesian	Hexahedral with mesh adaptation
Grid at Inlet	1 cell	120 nodes	6 cells	24 faces
Mesh Node Count	891,075	1,014,353	1,000,000	2,765,550
Domain Dimensions	1.96 m x 1.38 m x 1.75 m	4 m x 4 m x 2.5 m	4 m x 4 m x 2 m	8 m x 9 m x 6 m

**Table 8 – Summary of the computational domain and mesh choices used with each CFD model for the three model validation scenarios studied**

### 3.2.3 Source Term

Modelling high-pressure, underexpanded jet releases directly from the orifice presents a significant challenge numerically. The associated pressure, temperature and velocity gradients, and the presence of discontinuities, or shocks, require a highly refined computational mesh to capture the structure of the jet core. Additionally, all of this takes place in a region very close to the jet exit plane, whereas the region of interest could be much further downstream. This leads to a disparity in mesh requirements in different areas of the simulation domain, which often leads to substantial model run times as a result.

To mitigate this, it is common practice for modellers to make use of so-called *pseudo-source* or *notional nozzle* approaches, which are used to approximate the jet conditions downstream of the shock structure. This substantially reduces the computational mesh size requirement, and consequently the simulation run time. Papanikolaou et al. (2012) presents, and evaluates the use of, a range of notional nozzle approaches for CFD modelling of underexpanded H<sub>2</sub> releases.

There are a range of approaches for specifying the inlet conditions used with a pseudo-source, with each modeller involved in the present study adopting a different source term model. The source conditions used for the two jet release scenarios used for the model validation exercise described here are summarised in Table 9. Full details of the pseudo source modelling approaches can be found in the original research papers or model user guides, as appropriate.

	Unobstructed	Obstructed	Unobstructed	Obstructed
CFD Model	FLACS v10.4		OpenFOAM 1812	
Source Model	FLACS Jet Program		FRED	
Diameter (mm)	74.0	74.0	68.0	72.0
Velocity (m/s)	704.6	704.6	775.0	768.0
Temperature (K)	280.7	280.7	255.6	245.9
H <sub>2</sub> Mass Fraction	1.0	1.0	0.894	0.895
CFD Model	CFX 19.0		OpenFOAM 1912+	
Source Model	Ewan & Moodie (1986)		EXORIS Model	
Diameter (mm)	51.2	54.0	46.4	48.9
Velocity (m/s)	1199.5	1164.8	1170.0	1170
Temperature (K)	247.4	233.3	248.0	225.0
H <sub>2</sub> Mass Fraction	1.0	1.0	1.0	1.0

**Table 9 – Summary of the pseudo-source inlet conditions used in the different CFD models evaluated**

### 3.2.4 Solver Information and Numerical Sub-Models

Table 10 summarises the settings used for each for the two jet release validation scenarios. Table 11 provides equivalent details for the two confined release cases studied.

Task Partner	CFX v19.0	FLACS v10.4/6	OpenFOAM 1812	OpenFOAM 1912+
<b>Numerical Details</b>				
<b>Solver type</b>	Compressible, pressure-based solver, method based on the SIMPLE algorithm	Compressible, pressure-based solver, method based on the SIMPLE algorithm	Compressible, pressure-based solver, method based on the SIMPLE algorithm	Compressible, density-based solver using PIMPLE algorithm
<b>Steady-state or transient</b>	Transient	Transient	Steady-state	Transient
<b>Temporal scheme</b>	2 <sup>nd</sup> order backward Euler	1 <sup>st</sup> order backward Euler	n/a	Implicit-Euler
<b>Advection scheme</b>	CFX high-resolution scheme, 2 <sup>nd</sup> order min.	Hybrid scheme between 2 <sup>nd</sup> order upwind and 2 <sup>nd</sup> order central difference	2 <sup>nd</sup> order upwind	2 <sup>nd</sup> order upwind
<b>Turbulence</b>				
<b>Formulation</b>	Reynolds-Averaged Navier Stokes (RANS)	RANS	RANS	RANS
<b>Turbulence Model</b>	k-ε RNG model	k-ε model	k-ε model	k-ε model
<b>Heat Transfer</b>				
<b>Formulation</b>	Full energy equation	Full energy equation	Enthalpy equation	Sensible energy equation
<b>Model</b>	Total Energy model (full enthalpy)	Total Energy model (full enthalpy)		
<b>Buoyancy</b>	Full buoyancy	Boussinesq approximation	Full buoyancy	No buoyancy model
<b>Species Transport</b>				
<b>Equation of State</b>	Ideal Gas	Ideal Gas	Ideal Gas	Ideal Gas
<b>Modelled Species</b>	Scalar transport of H <sub>2</sub> , air as a constraint	Scalar transport of H <sub>2</sub> , air as a constraint	Scalar transport of H <sub>2</sub> & O <sub>2</sub> , with N <sub>2</sub> as the constraint	Scalar transport of H <sub>2</sub> & O <sub>2</sub> , with N <sub>2</sub> as the constraint

Table 10 – Summary of the CFD model numerical details and sub-model selections used for the two jet release validation scenarios

Task Partner	CFX v19.0	FLACS v10.4/6	OpenFOAM 1812	OpenFOAM 1912+
<b>Numerical Details</b>				
<b>Solver type</b>	Compressible, pressure-based solver, method based on the SIMPLE algorithm	Compressible, pressure-based solver, method based on the SIMPLEC algorithm	Compressible, pressure-based solver, method based on the SIMPLE algorithm	Compressible, density-based solver using PIMPLE algorithm
<b>Steady-state or transient</b>	Transient	Transient	Transient	Transient
<b>Temporal scheme</b>	2 <sup>nd</sup> order backward Euler	1 <sup>st</sup> order backward Euler	Implicit Euler	Implicit Euler
<b>Advection scheme</b>	CFX high-resolution scheme, 2 <sup>nd</sup> order min.	Hybrid scheme between 2 <sup>nd</sup> order upwind and 2 <sup>nd</sup> order central difference	2 <sup>nd</sup> order upwind	2 <sup>nd</sup> order upwind
<b>Turbulence</b>				
<b>Formulation</b>	RANS	RANS	RANS	RANS
<b>Turbulence Model</b>	k-ε RNG model	k-ε model	k-ε model	k-ε model
<b>Heat Transfer</b>				
<b>Formulation</b>	Full energy equation	Full energy equation	Enthalpy equation	Sensible energy equation
<b>Model</b>	Total Energy model (full enthalpy)	Total Energy model (full enthalpy)		
<b>Buoyancy</b>	Full buoyancy	Boussinesq approximation	Full buoyancy	Full buoyancy
<b>Species Transport</b>				
<b>Equation of State</b>	Ideal Gas	Ideal Gas	Ideal Gas	Ideal Gas
<b>Modelled Species</b>	Scalar transport of H <sub>2</sub> , air as a constraint	Scalar transport of H <sub>2</sub> , air as a constraint	Scalar transport of H <sub>2</sub> & O <sub>2</sub> , with N <sub>2</sub> as the constraint	Scalar transport of H <sub>2</sub> & O <sub>2</sub> , with N <sub>2</sub> as the constraint

**Table 11 – Summary of the CFD model numerical details and sub-model selections used for the two confined release validation scenarios**

## 3.3 Model Validation Results

### 3.3.1 Unobstructed Free Jet

#### 3.3.1.1 Hydrogen Concentration

Figure 6 shows a comparison of the measured and predicted centreline  $H_2$  molar fraction for the unobstructed free jet scenario (Daubech et al., 2015). The Figure includes predictions made using each of the model configurations described in Section 3.2. Predictions made using the AEROPULME jet dispersion model within the consequence modelling package FRED are also included to give results from an *engineering tool* for the purposes of further comparison. The results presented in Figure 6 illustrate that, overall, all of the models used give predictions in broadly reasonable agreement with the measurements. To summarise:

- The CFX calculations over-predict the centreline  $H_2$  molar fraction at distances of 1.25 m and 2 m downstream from the release, before giving close agreement with the measured data at the measurement locations further downstream
- The FLACS predictions give very good agreement with the measured data at all measurement locations along the jet centreline.
- The OpenFOAM 1812 simulations also gives predictions in excellent agreement with the measured data along the jet centreline, similar to predictions made using FLACS.
- The OpenFOAM 1912+ calculations over-predict the measured  $H_2$  molar fraction at most measurement locations.
- The Shell FRED (AEROPULME) results fall broadly in line with the CFD model predictions. The Figure shows that the FRED calculations over-predict the measured data and thus gives a conservative estimate of the  $H_2$  concentration along the jet centreline.

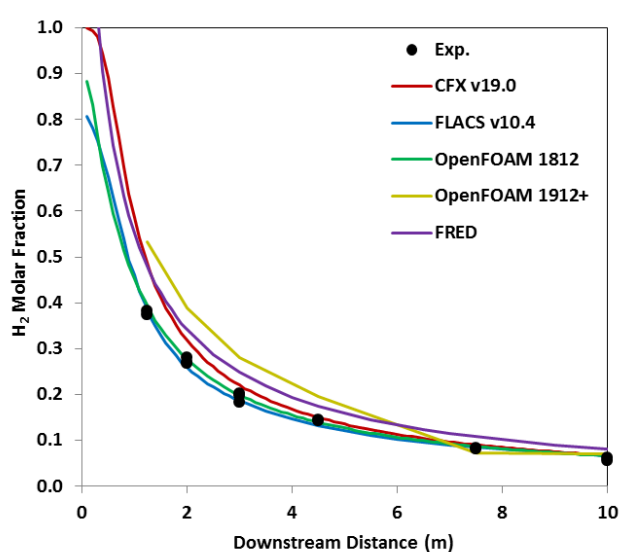


Figure 6 – Comparison of measured and predicted centreline  $H_2$  molar fraction for the unobstructed free jet

Clearly the two versions of OpenFOAM are giving very different predictions of centreline concentration. This is likely as a result of the choice of computational grid, source term

representation and small differences in the model set up (see Table 8 and Table 10), rather than any substantial differences between the two versions of the CFD code.

Figure 7 compares the predicted and measured radial profiles of  $H_2$  molar fraction for each of the models evaluated. The Figure demonstrates that:

- The CFX simulations over-predict the centreline concentration and under-predict the jet width at the first measurement location, but then give better agreement with both the jet width and concentrations moving further away from the release.
- The FLACS calculations give good agreement with the experimental data, capturing the concentration and jet widths well.
- The OpenFOAM 1812 modelling gives good agreement with the measured results at most of the measurement locations, but slightly under-predicts the jet width at the first measurement location.
- The OpenFOAM 1912+ predictions give good agreement with the measured jet widths at most measurement locations but over-predict the centreline concentrations significantly.

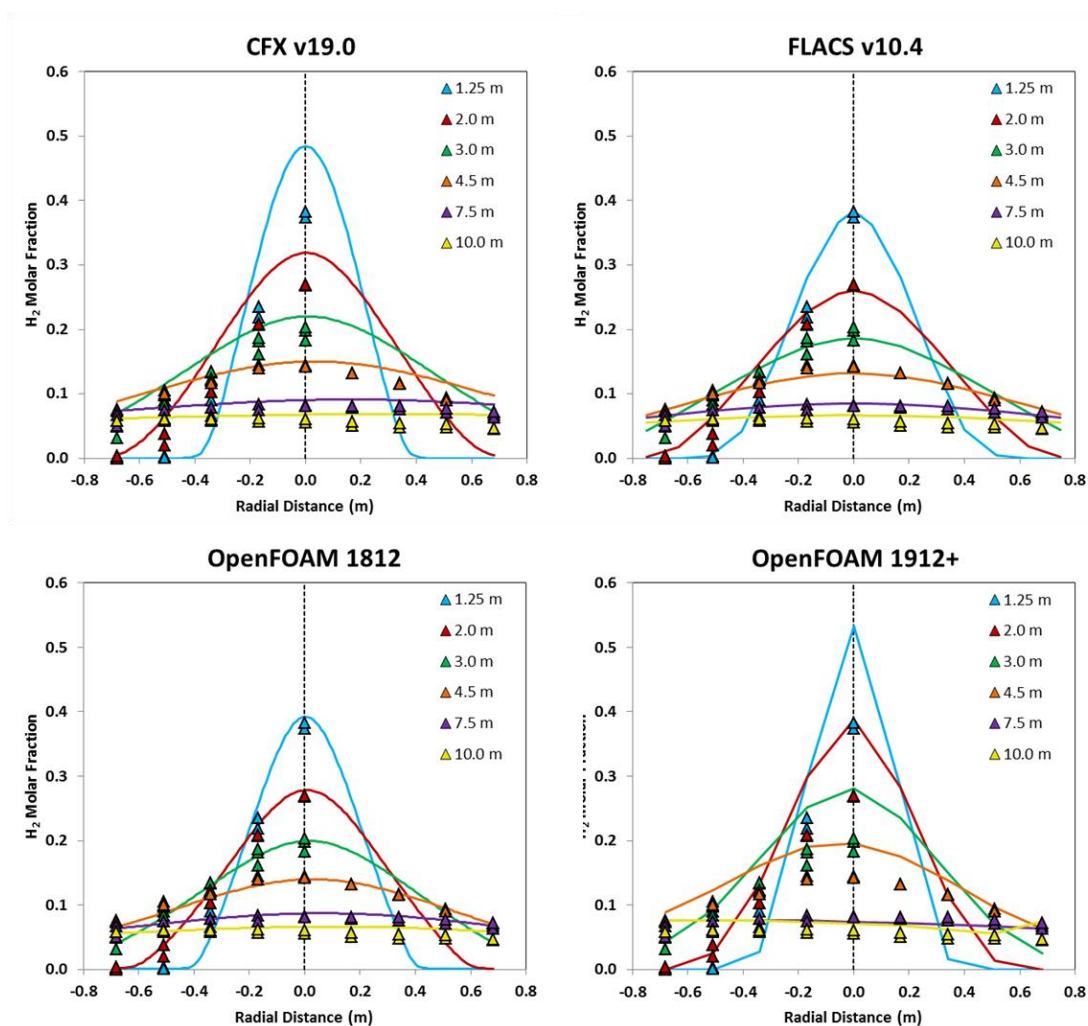


**Figure 7 – Comparison of the measured and predicted radial profiles of  $H_2$  for the unobstructed jet scenario**



Figure 8 presents ratios of the predicted-to-measured  $H_2$  concentration as a function of the measured  $H_2$  molar fraction for all measurement locations used in the unobstructed jet scenario. The Figure illustrates how the various models compare across the range of measured  $H_2$  concentrations to give an idea of where the models perform best. The horizontal black dashed line shows a ratio of 1, i.e. that the predicted concentration equals the measured value. The two horizontal red dashed lines indicate predictions at  $\pm 50\%$  of the measured data.

From Figure 8 it is clear that for the majority of the concentration measurements, all of the models assessed here give predictions within 50% of the measured data. Deviations to this general trend are found where the measured  $H_2$  concentrations are small, for example at the extremes of the jet width (see Figure 7).

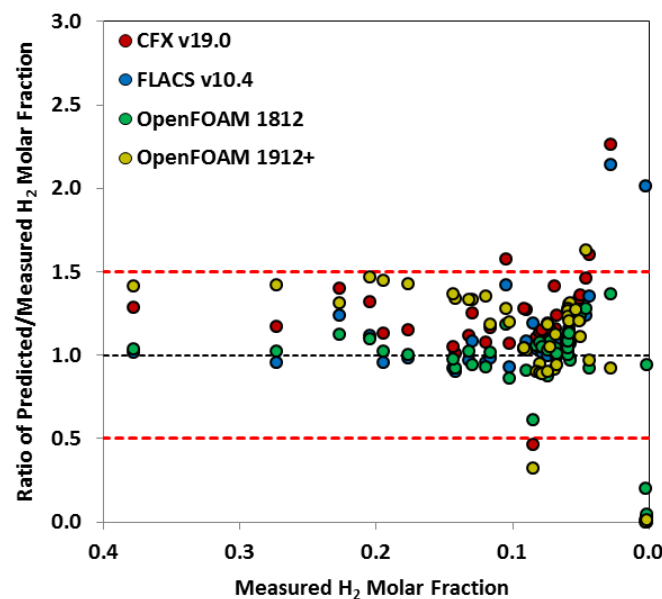


**Figure 8 – Ratio of predicted-to-measured concentration as a function of  $H_2$  molar concentration for the unobstructed free jet scenario. Figure includes both centreline and radial data from Figure 6 and Figure 7**

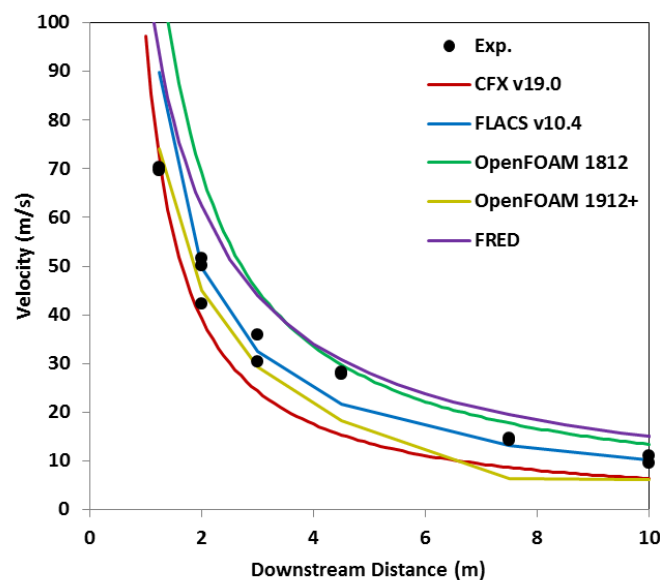
### 3.3.1.2 Velocity

Figure 9 compares the measured and predicted velocity along the centreline of the unobstructed jet. The Figure includes predictions made using the FRED consequence modelling package for comparison of different model types. Overall, the Figure illustrates that the model predictions bound the experimental data on both sides, giving both over-prediction and under-prediction of the measured data.

It is worth noting that the velocity sensors used experimentally were saturated at distances less than 3 m from the release, and thus there is some uncertainty in the measured data at those sensors. The results show that there is greater variation in the model predictions of velocity than for predictions of  $H_2$  molar fraction. Specifically, Figure 9 shows that:

- The CFX modelling gives good agreement with the measured velocity 1.25 m downstream of the release, but then under-predicts the remaining measurements reasonably significantly.

- The FLACS simulations give generally good agreement with the measured data but over-predict the measured velocity at the first measurement location 1.25 m downstream and under-predict the measured velocity 4.5 m downstream of the release.
- The OpenFOAM 1812 calculations over-predict the centreline velocity at all measurement locations. The model outputs most closely matches the data point located 3 m downstream of the release.
- The OpenFOAM 1912+ modelling gives good agreement with the measured data for the first three measurement locations, but under-predicts at distances of 4.5, 7.5 and 10 m downstream of the release.
- The predictions made using the AEROPLUME jet dispersion model in FRED are very similar to those obtained with OpenFOAM 1812. This model bounds the experimental data on the upper side.



**Figure 9 – Comparison of measured and predicted centreline velocity for the unobstructed free jet**

Figure 10 shows a comparison of the measured and predicted radial profiles of velocity for each of the models evaluated. The results in this Figure show that:

- The CFX results give reasonable approximation of the jet widths (based on velocity) for measurements to 3 m downstream of the release point. Beyond this, the jet width is over-predicted, most notably at a distance of 4.5 m downstream of the release.
- The FLACS modelling gives generally good agreement with the measured data but over-predicts the centreline velocity and the jet width at 4.5 m downstream of the release. The latter is common across all four models used.
- The OpenFOAM 1812 simulations over-predict the centreline velocity at all measurement locations, but give good approximations of the jet widths, except at 4.5 m downstream of the release, as for the other models.
- The OpenFOAM 1912+ predictions give good agreement with the jet widths and the

centreline velocity measurements. Although, as for the other model results, the jet width at 4.5 m downstream of the release is over-predicted.

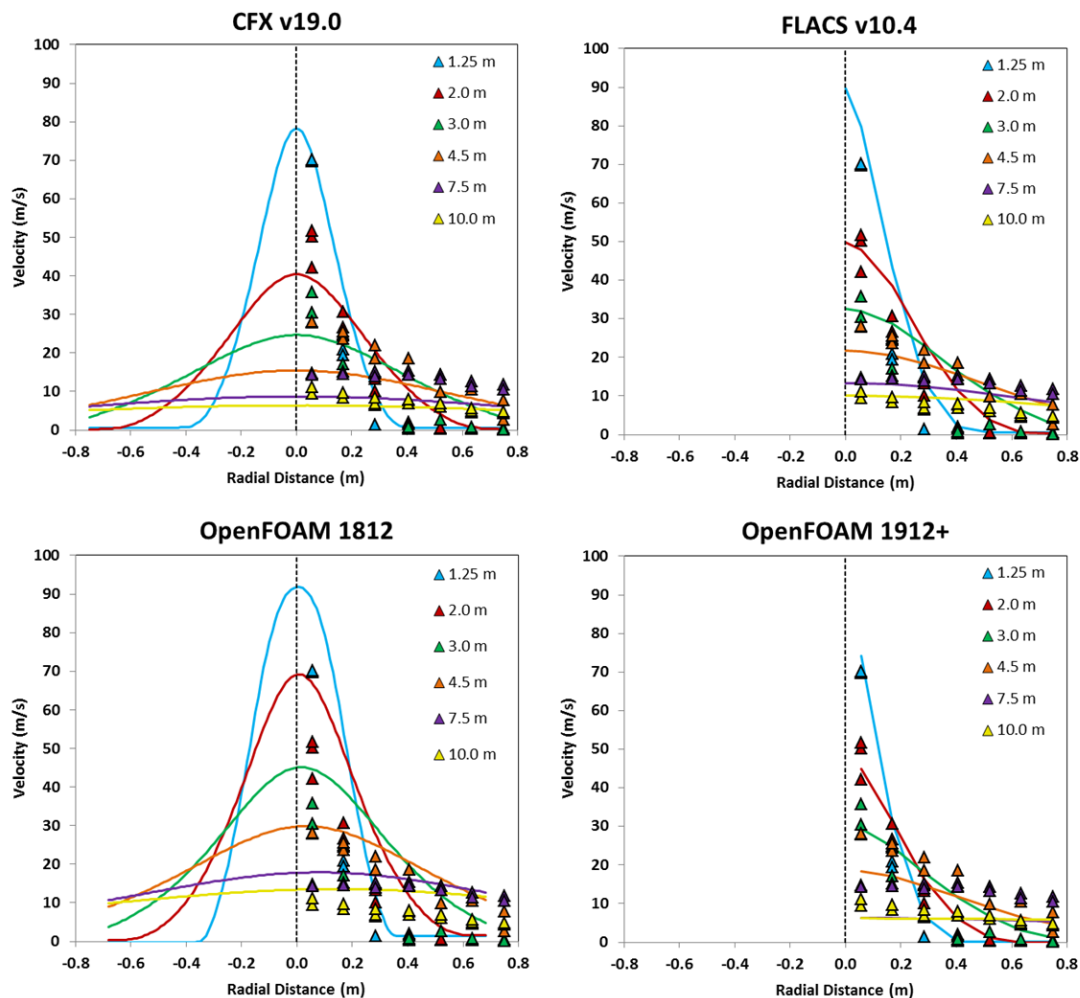


**Figure 10 – Comparison of the measured and predicted radial velocity profiles for the unobstructed jet scenario**

### 3.3.1.3 Turbulence

Figure 11 and Figure 12 present comparisons between the measured and predicted fluctuating velocity component,  $u'$  (m/s) along the jet centreline and radially within the jet, respectively. These Figures show that:

- The predictions made using CFX, FLACS and OpenFOAM 1812 are comparable and give good agreement with the measured data at distances of 4.5 m and more downstream of the release. In the nearfield, these models significantly over-predict  $u'$ . This could be due to saturation of the velocity sensors used in the experiment, thus giving uncertain results in the near-field. Furthermore, it is worth bearing in mind that the fluctuating velocity is inferred from velocity measurements in the experiments and that the level of accuracy of the data is not clear.
- The results obtained with OpenFOAM 1912+ are initially in line with the other model predictions before dropping away to give zero turbulent fluctuating velocity at downstream distances of 7.5 m and greater.

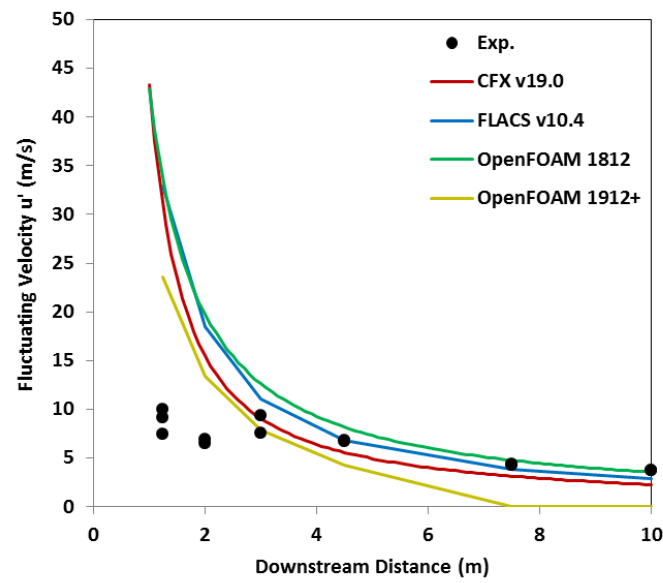


Figure 11 – Comparison of measured and predicted centreline turbulent fluctuating velocity,  $u'$ , for the unobstructed jet

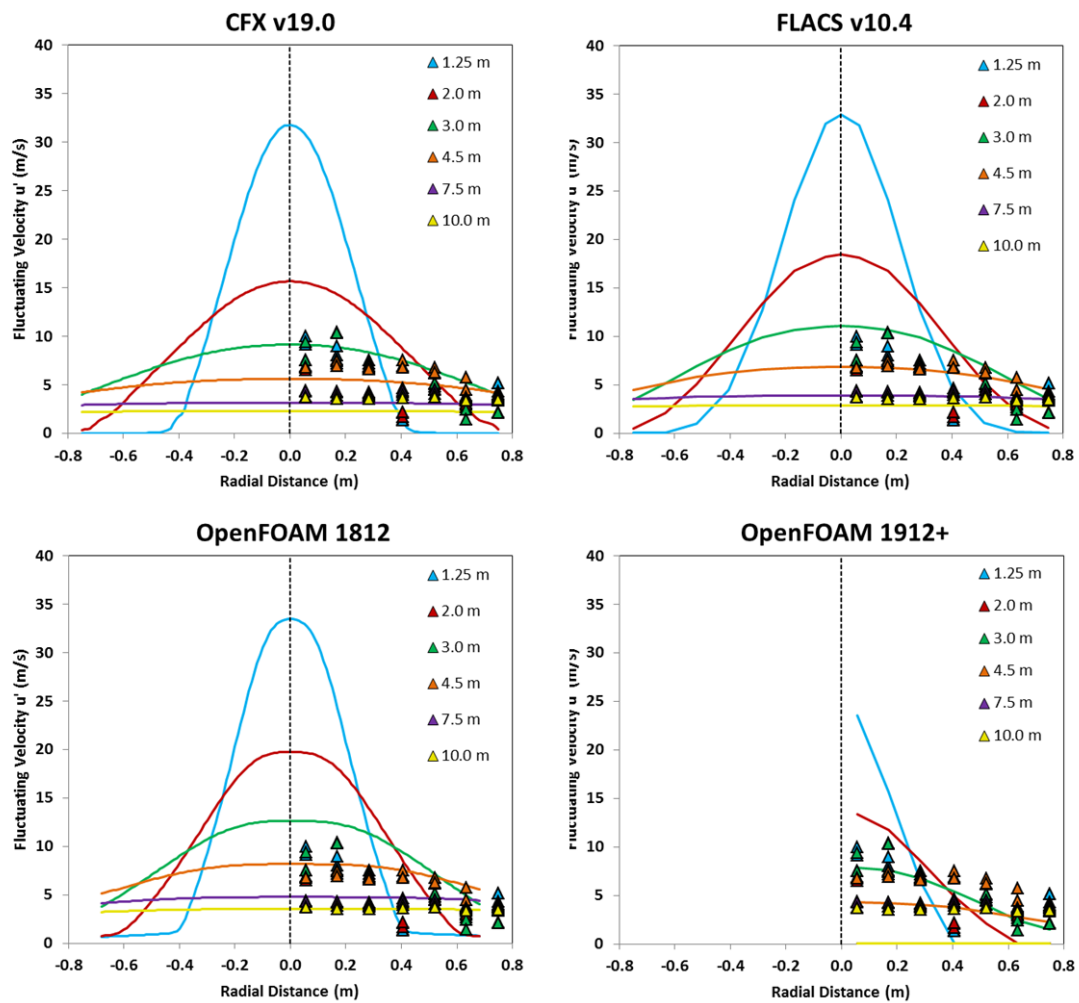
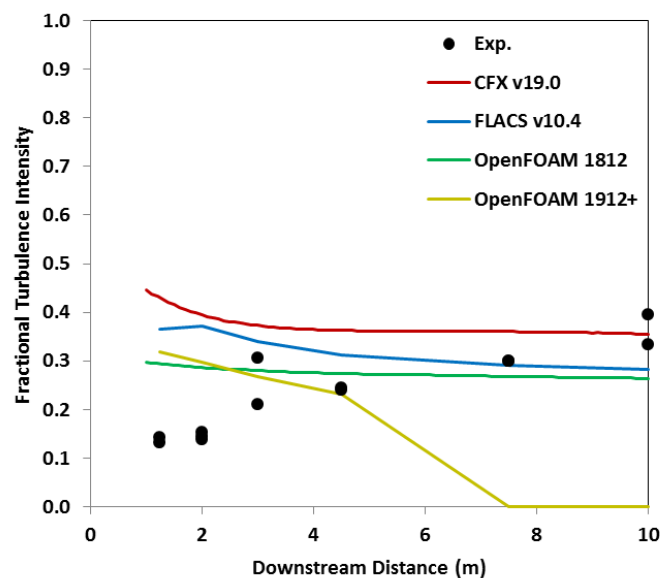


Figure 12 – Comparison of the measured and predicted radial profiles of turbulent fluctuating velocity for the unobstructed jet scenario

Figure 13 compares the inferred fractional turbulence intensity from the measured data and model predictions. The Figure shows that:

- The CFX predictions give a fractional turbulence intensity of 0.43 at the first measurement location, before this value drops to a near-constant value of 0.36.
- The FLACS predictions give a fractional turbulence intensity of around 0.37 at the first two measurement locations downstream of the release, before the turbulence intensity decays to a near-constant value of 0.30.
- The OpenFOAM 1812 results show a near-constant fractional turbulent intensity of around 0.27 at all measurement locations.
- The OpenFOAM 1912+ calculations give a fractional turbulence intensity which starts at around 0.32 at a distance of 1.25 m from the release point, before the turbulence intensity decays to zero 7.5 m downstream of the release.



**Figure 13 – Comparison of measured and predicted centreline fractional turbulence intensity for the unobstructed jet**

#### 3.3.1.4 Influence of Source Term

To further illustrate the effect the choice of source term can have on model predictions, CFX was used with source conditions estimated using both the Ewan and Moodie (1986) approach (as presented above) and using outputs from the Shell FRED model; see Table 9 for a comparison between the two sets of inlet conditions. As shown in Figure 14, the choice of source term has a reasonable influence on the results, with CFX giving predictions closer to the measured data when using the source term generated with FRED than with the Ewan and Moodie (1986) approach. Similar findings were found for predictions of the centreline jet velocity, as discussed in Section 3.3.1.2 and presented in Figure 15.

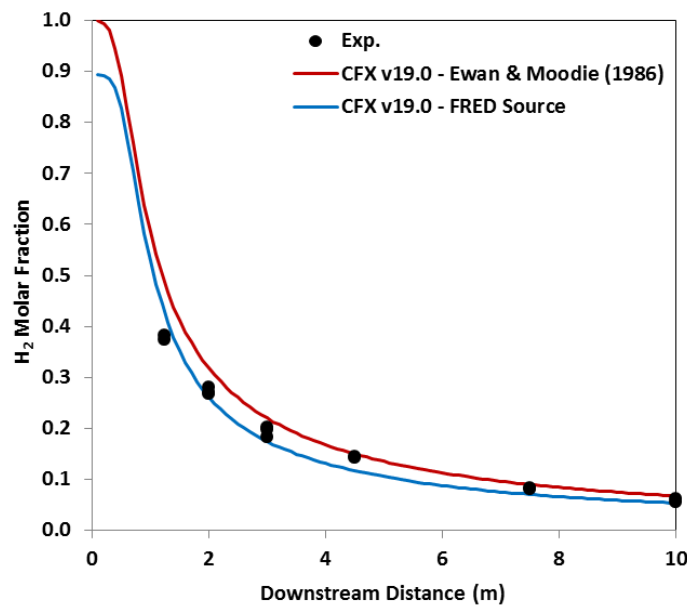


**Figure 14 – Comparison of the measured centreline H<sub>2</sub> molar fraction for the unobstructed free jet to CFX v19.0 predictions using the Ewan and Moodie (1986) and Shell FRED pseudo source inlet conditions listed in Table 9**

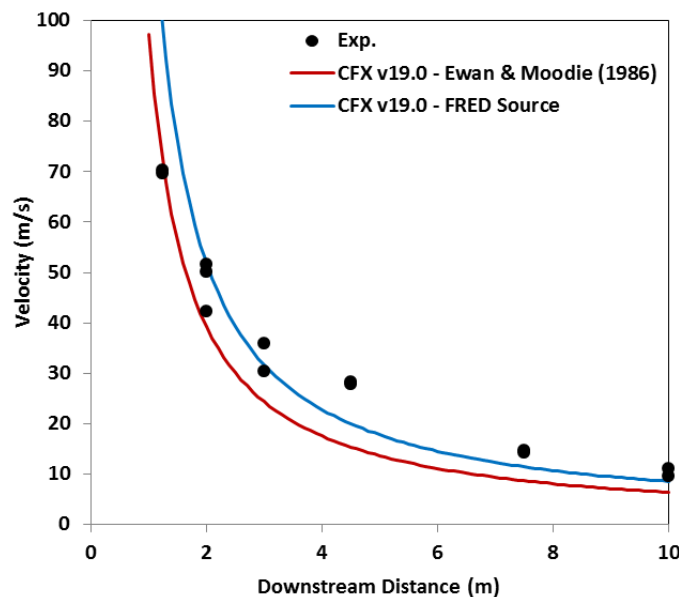


**Figure 15 - Comparison of the measured centreline velocity for the unobstructed free jet to CFX v19.0 predictions using the Ewan and Moodie (1986) and Shell FRED pseudo source inlet conditions (see Table 9)**

### 3.3.2 Obstructed Free Jet

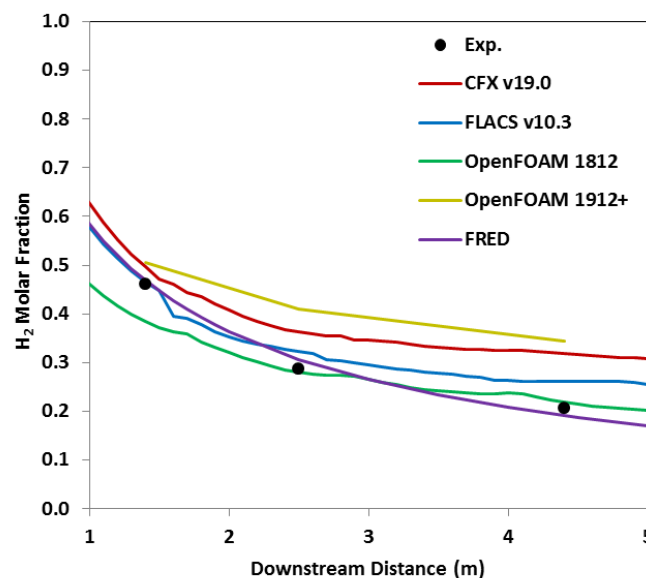
#### 3.3.2.1 Hydrogen Concentration

Figure 16 compares the predicted and measured centreline H<sub>2</sub> molar fraction for the obstructed jet release scenario. Again, the Figure includes AEROPLUME predictions from FRED (which do not account for the obstructions) for reference. The Figure shows that:

- The CFX modelling over-predicts the centreline H<sub>2</sub> concentration at all measurement

locations. The level of over-prediction at the first measurement location is small but increases with increased distance from the release point.

- The FLACS simulations give excellent agreement with the first measurement point, but also over-predict the measured centreline concentration. As is the case for the CFX results, the magnitude of the over-prediction increases with increased distance from the release point.
- The OpenFOAM 1812 results under-predict the concentration at the first measurement location before giving excellent agreement with the measured data further downstream.
- The OpenFOAM 1912+ predictions give similar results to CFX, over-predicting the measured  $H_2$  molar fraction at all of the measurement locations.
- The FRED results give the closest agreement with the measured data.



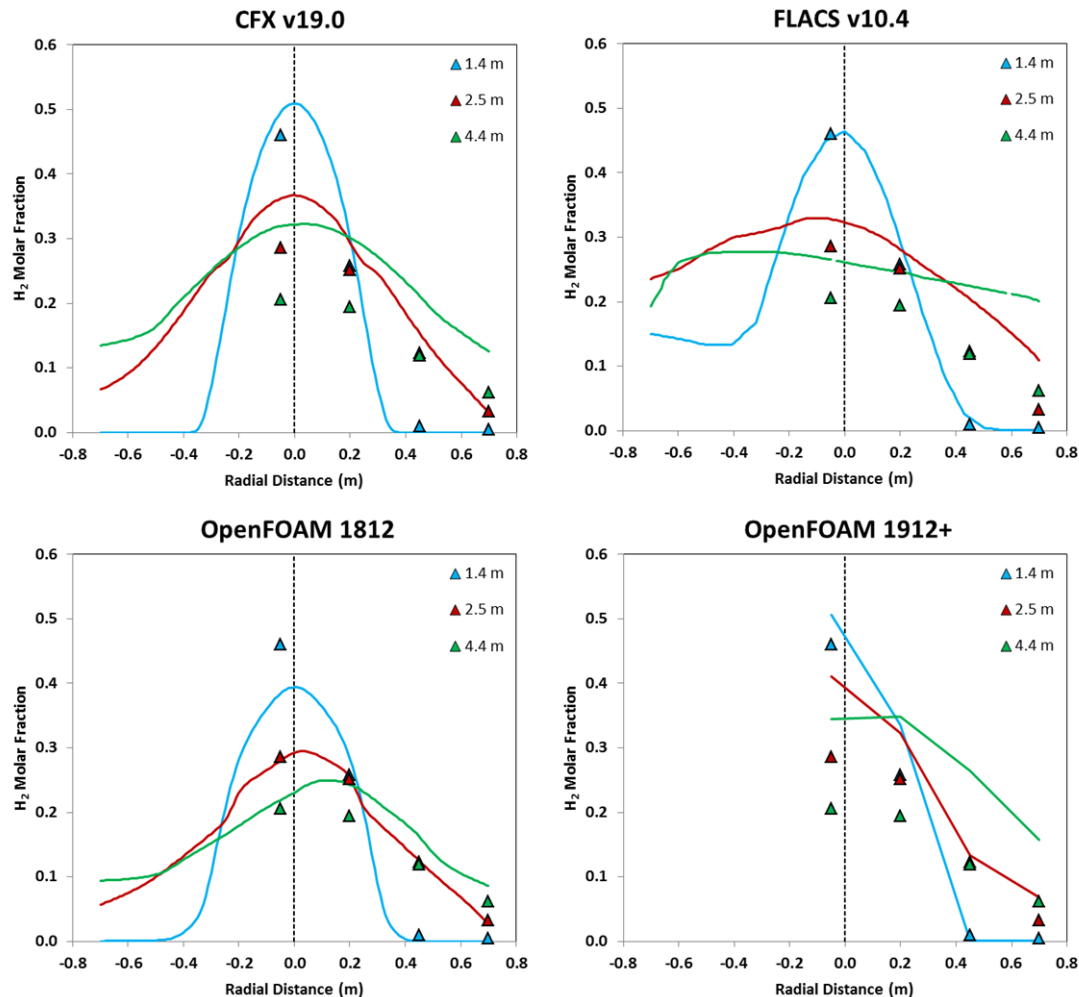
**Figure 16 – Comparison of the measured and predicted centreline  $H_2$  molar fraction for the obstructed jet**

Figure 17 compares the predicted and measured  $H_2$  molar fraction for the unobstructed jet scenario radially within the jet. The results demonstrate that:

- The CFX calculations capture the jet width relatively well but over-predict the measured concentrations.
- The FLACS simulations reproduce the measured concentrations well at the first downstream distance of 1.4 m, but over-predict concentrations and jet widths further downstream.
- The OpenFOAM 1812 modelling gives excellent agreement at a distance of 2.5 m downstream of the release point, but slightly over-predicts the measured concentration data at 4.4 m downstream. Again, the jet width is reproduced well in the model.
- The OpenFOAM 1912+ simulations give good agreement with the measured jet widths but over-predict specific concentration measurements quite substantially at the 4.4 m

measurement location.

- The CFX, FLACS and OpenFOAM 1812 calculations all predict some asymmetry in the radial profiles. This is most pronounced in the FLACS modelling and is due to jet interaction with the obstacle array and the influence of gravity, since the measurement sensor array is on the vertical plane (see Section 3.1.2)



**Figure 17 – Comparison of the measured and predicted radial H2 molar fraction for the obstructed jet scenario**

### 3.3.2.2 Velocity

Figure 18 and Figure 19 show comparisons of the measured and predicted centreline and radial profiles of velocity in the obstructed jet, respectively. The Figures illustrate that:

- The OpenFOAM 1812 calculations give centreline velocity decay in closest agreement with the measured data, whilst the other three models generally under-predict the velocity measurements.
- The CFX, FLACS and OpenFOAM 1812 all exhibit the same behaviour in the predicted velocity, with the centreline decay showing drops in velocity slightly further downstream of each measurement location, which result from interactions between the jet and the



obstacle array. Similarly, in the radial velocity profiles at 2.5 m and 4.4 m downstream of the release point, all three of these models show drops in velocity either side of the centreline, again as a consequence of the obstacles. In the FLACS models, the obstacles are represented using porosities, whereas in CFX and OpenFOAM 1812 the obstacles are resolved (to some extent) by the mesh.

- All of the models capture the jet width relatively well, as shown by predictions of radial velocity profiles.
- The OpenFOAM 1912+ modelling gives under-prediction of the centreline velocity at measurement locations 1.4 m and 4.4 m downstream, but reproduces well the measured data at 2.5 m downstream of the release point.
- The FRED predictions bisect the measured data points, initially under-predicting at a distance of 1.4 m downstream of the release before giving over-predictions of the centreline velocity for the other two measurement locations.

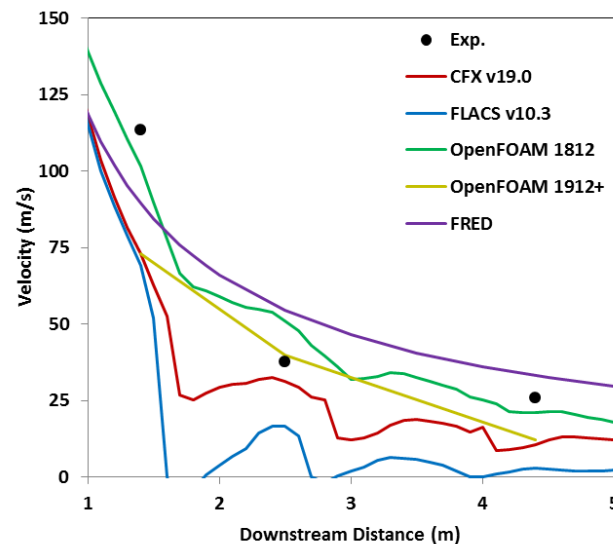


**Figure 18 – Comparison of the measured and predicted centreline velocity for the obstructed jet**

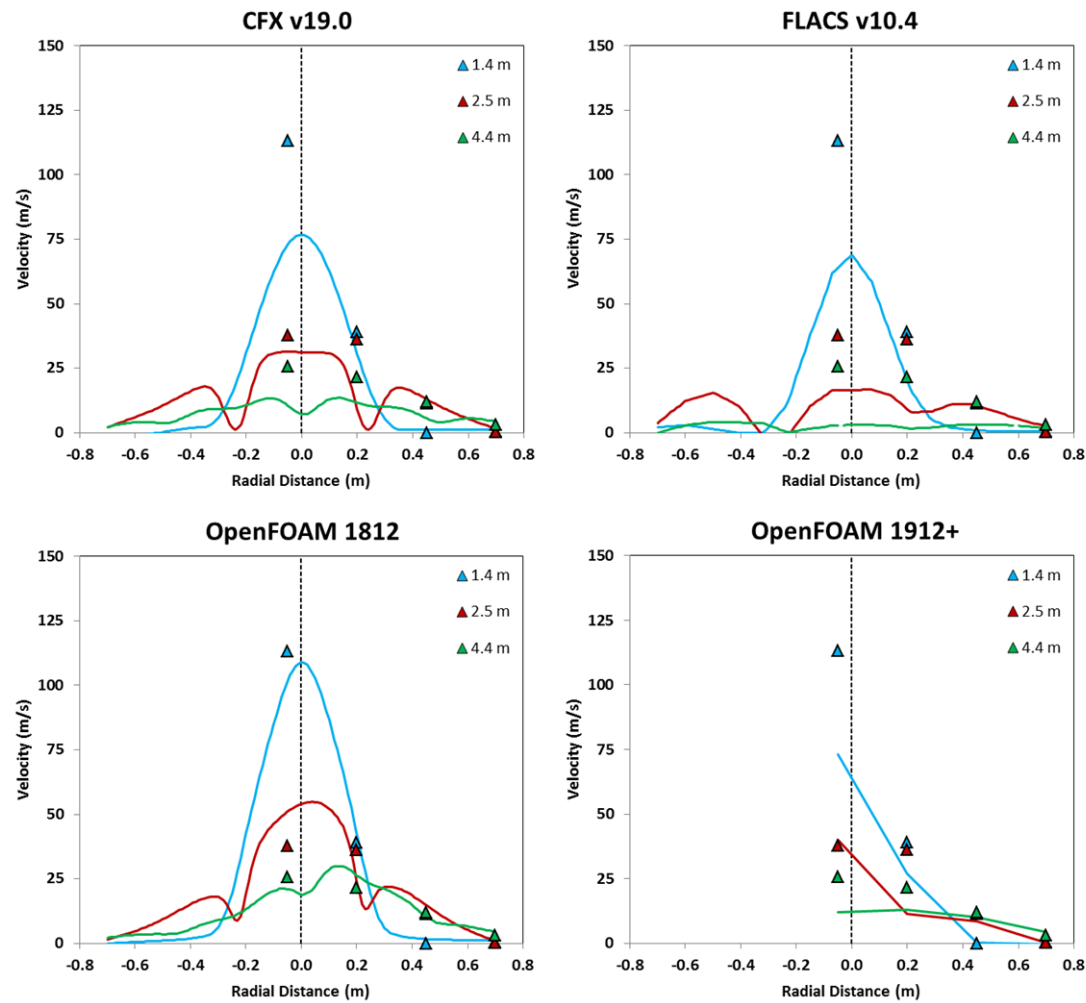


**Figure 19 – Comparison of the measured and predicted radial velocity profiles for the unobstructed jet scenario**

### 3.3.2.3 Turbulence

With regards to the turbulence field, experimental data for radial profiles of the turbulent fluctuating velocity,  $u'$  (m/s), is compared to predictions made using three of the four models tested, as shown in Figure 20. The results show that:

- The three models give generally similar results, with some asymmetry across the radial profiles.
- The experimental fluctuating velocity close to the jet centreline at a distance of 1.4 m is substantially lower than the predictions made using all three models. It is worth bearing in mind that the fluctuating velocity is inferred from velocity measurements in the experiments and that the level of accuracy of the data is not clear.
- The predicted values of  $u'$  at the extremities of the radial profile at 1.4 m are significantly under-predicted, but are in closer agreement with the data at 2.5 m and 4.4 m downstream of the release point.

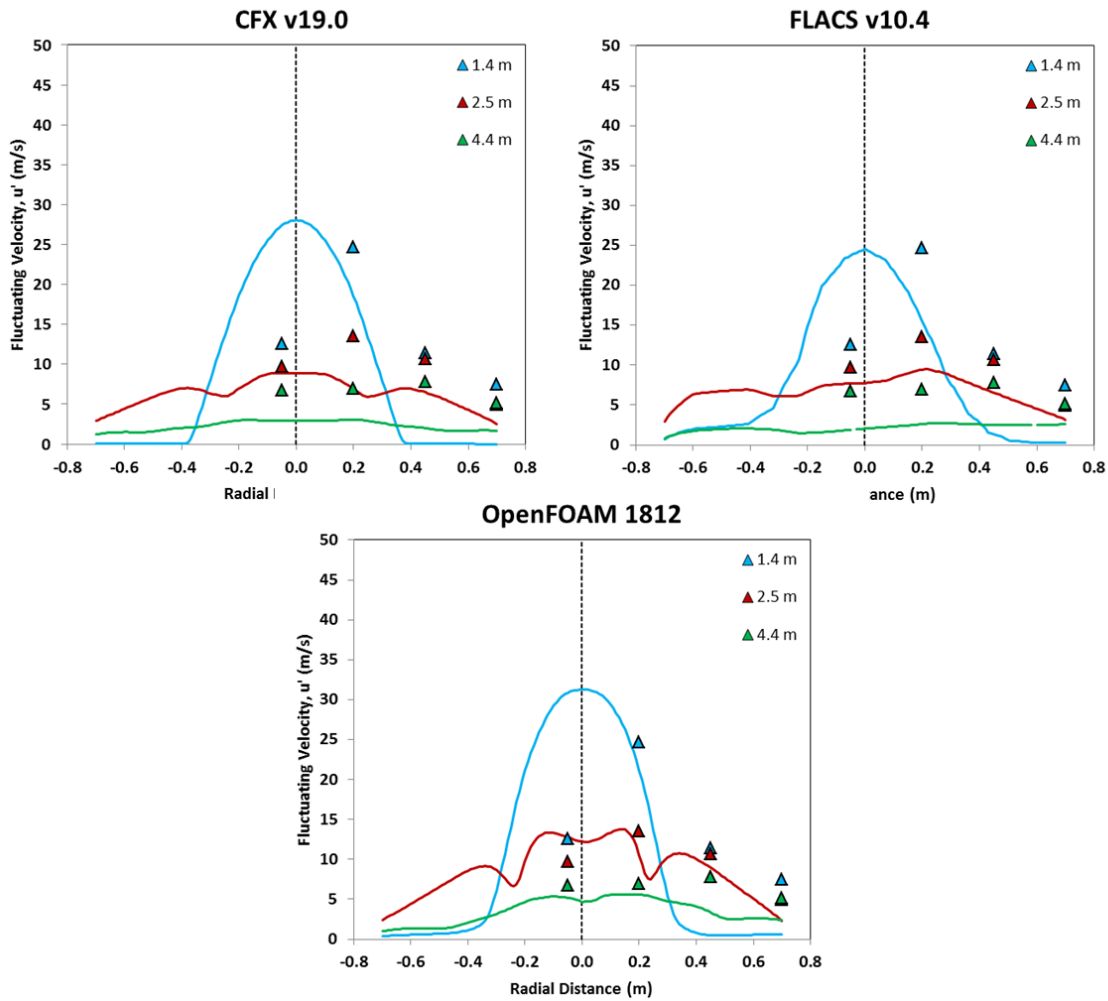


**Figure 20 – Comparison of measured and predicted radial profiles of turbulent fluctuating velocity,  $u'$**

#### 3.3.2.4 Influence of Source Term

As was the case for the unobstructed jet, CFX has also been used with source conditions estimated using both the Ewan and Moodie (1986) approach and the Shell FRED model to simulate the obstructed jet scenario. Table 9 summarises the two sets of inlet conditions used. CFX predictions of the centreline  $H_2$  molar fraction are shown in Figure 21 using the two source terms. The results indicate that using the model with the source conditions taken from FRED gives closer agreement with the measured data, similarly to the findings for the unobstructed jet case. Furthermore, the results from CFX with this source condition are comparable with those produced using OpenFOAM 1812. This indicates a good level of agreement across the two models, modelling approaches and different modellers, provided that the same source term is used. This will be an important consideration for the realistic release modelling to follow.

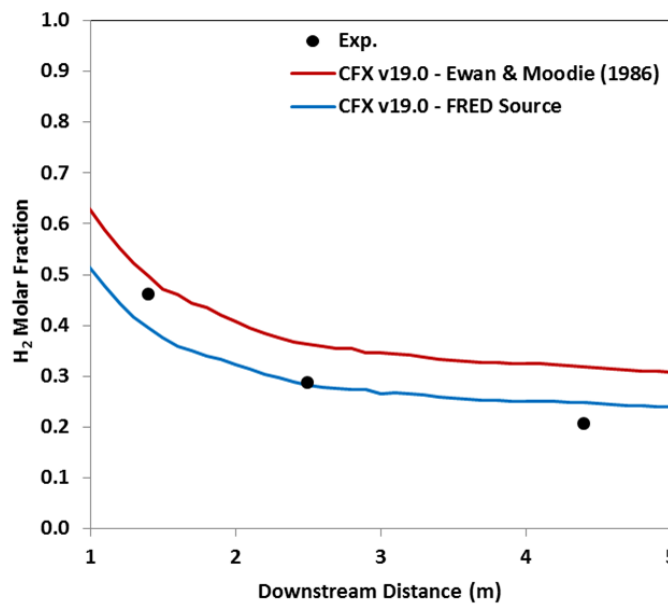


**Figure 21 - Comparison of the measured centreline H<sub>2</sub> molar fraction for the obstructed jet to CFX v19.0 predictions using the Ewan and Moodie (1986) and Shell FRED pseudo source inlet conditions listed in Table 9**

### 3.3.3 Confined Releases

Figure 22 and Figure 23 compare the measured and prediction vertical H<sub>2</sub> concentration profiles for the 10.4 NL min<sup>-1</sup> and 218.3 NL min<sup>-1</sup> confined release scenarios, respectively. The two Figures illustrate that closer agreement between the model predictions and the measured concentrations is obtained, in general, for the higher release rate scenario. For both releases, the predicted concentrations in the transition layer, i.e. 0.6 to 0.8 m above the enclosure base, show less good agreement with the measured data for most of the models tested.

Overall, predictions of the upper layer concentration, where the H<sub>2</sub> concentrations are greatest, are in good agreement with the data for the 218.3 NL min<sup>-1</sup> release for all of the models used. However, the simulations for both versions of OpenFOAM show some over-prediction of the upper layer concentrations for the 10.4 NL min<sup>-1</sup> release. For the lower release rate scenario, the depth of the upper layer is under-predicted in the modelling using OpenFOAM 1912+ and CFX, as indicated by under-prediction of the concentration at around 0.8 m above the enclosure base.

For the purposes of further comparison Figure 22 and Figure 23 include predictions of the concentration based on the approach of Linden (1999), as implemented by Air Liquide (Jallais et al., 2013). The Linden (1999) modelling gives predictions in good agreement with the measured concentration. This approach will later form the basis of estimating source conditions for realistic releases inside the dispenser casing, so it is reassuring that the model gives good agreement with the measured data here.

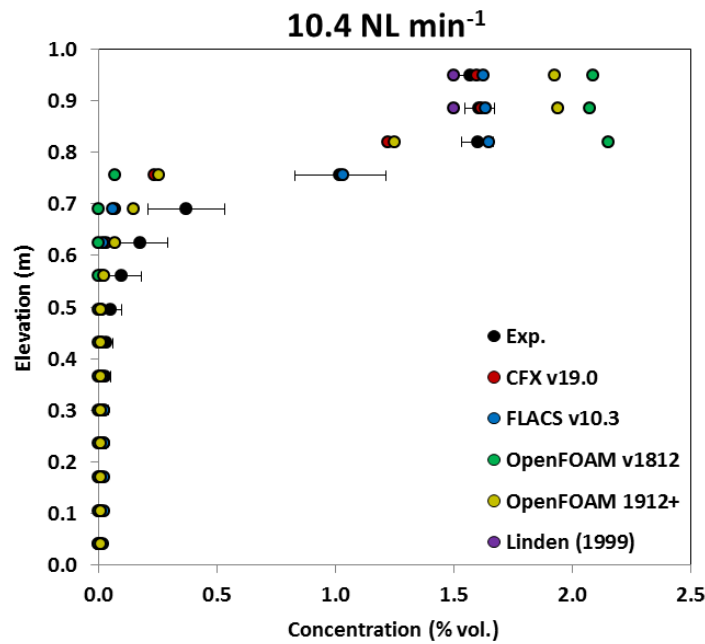


Figure 22 – Comparison of the measured and predicted H<sub>2</sub> concentration profiles with height inside the enclosure for the 10.4 NL min<sup>-1</sup> release

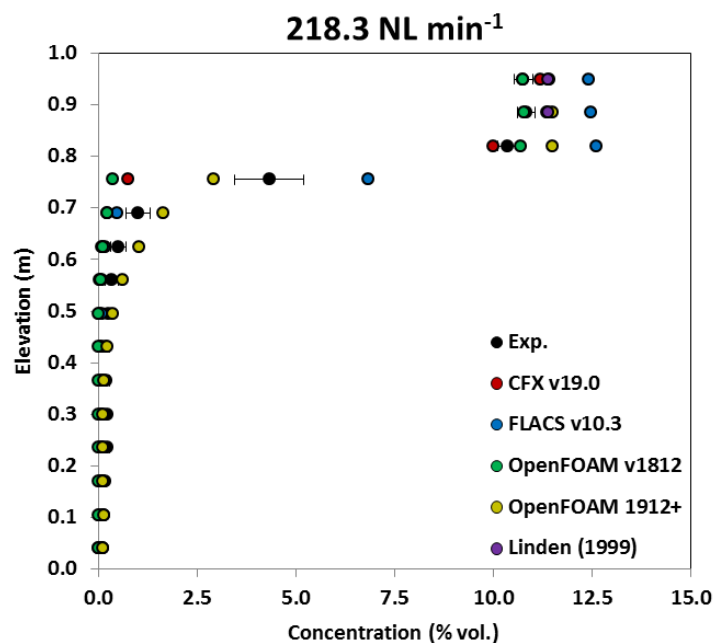


Figure 23 – Comparison of the measured and predicted H<sub>2</sub> concentration profiles with height inside the enclosure for the 218.3 NL min<sup>-1</sup> release

### 3.4 Summary

To summarise, the model validation exercise has shown that the CFD models selected by the task partners can reasonably reproduce the measured data across the selected range of scenarios considered. This gives confidence that the models will produce acceptable solutions for the realistic release modelling to follow.

Whilst the model validation results show some scatter in predictions, with both over-prediction and under-prediction of the measured data, for the purposes of the present study, the level of agreement is considered acceptable. This is because the realistic release modelling to be performed will include a range of approximations and simplifications, so the CFD modelling results will be heavily influenced by the choices made to set up and define the cases to be studied. Furthermore, model predictions for those critical scenarios will not be compared with measured data at specific locations, instead the aim is to generate representative solutions of expected flammable cloud shapes, size and spread across the forecourt configurations defined in WP3. What the model validation work has shown is that the models are likely to be capable of achieving this successfully.

One specific outcome to note from the model validation cases involving jet releases is that the specification of the source term has been shown to be important. Results presented in this report indicate that model predictions made with OpenFOAM 1812 and CFX are comparable when the same source conditions are used. Furthermore, using the source term from FRED (refer back to Table 9) gave better agreement with the measurements when used in CFX than the Ewan and Moodie (1986) approach also tested. As such, for jet simulations it is recommended that a suitable jet model is used to estimate the conditions within the expanded jet where the local Mach number of 1, or just below. These conditions can then be used to specify inlet conditions for CFD calculations. The approach used in the realistic release modelling, described in Section 4, is based on the use of FRED (AEROPULME) to generate jet inlet conditions for the CFD models.

## 4 Realistic Release Modelling

### 4.1 Selected Scenarios

Deliverable D3.5 – *Identification of Critical Scenarios* presents matrices of severity and likelihood for a range of H<sub>2</sub> release scenarios identified through a series of HAZID workshops for each of three representative forecourt configurations. Three separate forecourt layouts were defined in WP3 to ensure that the different design options normally considered by HRS operators were captured in the risk analysis. Although these forecourt configurations are not intended to represent real forecourts, configuration 1 is designed to resemble a *ready-to-deploy* multi-fuel station, configuration 2 includes *on-site H<sub>2</sub> production* and configuration 3 represents a *high-capacity* station. Appendix 1 contains further details of the layouts for each forecourt configuration and Section 4.2.1 presents the 3D representations of these layouts as used in the CFD analysis described in the present report.

As part of Task 3.5, each release scenario was modelled using engineering tools to assess the possible severity of the post-ignition consequences, either as a jet fire, flash fire or vapour cloud explosion (VCE). Full details of the scenarios considered and the modelling and risk ranking analysis performed can be found in the WP3 deliverables. Here, the focus is on the subset of releases which are considered critical, due to the combination of the anticipated likelihood and severity of the modelled events.

Appendix 3 of deliverable D3.5 outlines the critical scenarios for each configuration. For the CFD modelling task, and WP2 more generally, the focus is on scenarios involving H<sub>2</sub> releases on the forecourt. Thus, we can discount all scenarios associated with the storage and process area of each configuration and all scenarios involving fuels other than H<sub>2</sub>. The CFD modelling task takes into account the scenarios identified as high risk for their effect on people both on and off site. Deliverable D3.5 presents findings for two sets of vehicle occupancy levels as follows:

- **Option 1:** Each bus contains 50 people, each truck contains only 1 person
- **Option 2:** Each bus and each truck contains 2 people

Here the focus is on the results for Option 2. Since buses are unlikely to be permitted to refuel whilst full of passengers, the option in which each bus contains a driver and reserve driver only is considered to be more realistic.

The following Sections of this report present the critical scenarios associated with H<sub>2</sub> releases on the forecourt as defined in deliverable D3.5. Further information on the forecourt designs is also included in Appendix 1.

#### 4.1.1 Configuration 1 – Ready-to-deploy Multi-fuel Station

Table 12 summarises the critical scenarios identified in Task 3.5 which relate to H<sub>2</sub> releases on the forecourt for Configurations 1 & 2. The findings of Task 3.5 define the same set of critical scenarios for both configurations.

#### 4.1.2 Configuration 2 – On Site H<sub>2</sub> Production Multi-fuel Station

As discussed in Section 4.1.1, the same set of critical scenarios was identified for both Configurations 1 & 2.

Scenario Description	Hole Sizes	Pressures (barg)
H <sub>2</sub> dispenser – loss of H <sub>2</sub> containment on hose (external release)	10% hose diameter Full bore rupture	350, 700 & 1000
H <sub>2</sub> dispenser – loss of H <sub>2</sub> containment at vent line exit (external release)	Vent line outlet	350 & 700

**Table 12 – Summary of the H<sub>2</sub>-related critical scenarios associated with the forecourt for both Configurations 1 & 2**

As shown in Table 12, the key scenarios for configurations 1 & 2 relate to loss of H<sub>2</sub> containment principally on the hose, but also at the vent line exits. Both 10% hose diameter and full bore rupture releases were identified as critical events associated with the dispensing hose.

#### 4.1.3 Configuration 3 – High Capacity & High Filling Multi-fuel Station

Table 13 summarises the critical scenarios identified in Task 3.5 which relate to H<sub>2</sub> releases on the forecourt for Configuration 3. Through comparison of Table 12 with Table 13 it is clear that there are a larger number of critical scenarios for Configuration 3 than for the other two forecourt designs. This is principally due to the assumptions inherent in the risk assessment analysis, particularly relating to the assumed location of Configuration 3 being adjacent to a motorway, which leads to higher severity than for Configurations 1 and 2 for some of the scenarios considered.

Scenario Description	Hole Sizes	Pressures (barg)
H <sub>2</sub> dispenser – loss of containment on pipe/valve (internal release)	0.2 mm	350, 700 & 1000
H <sub>2</sub> dispenser & cooling system – loss of containment on hose (external release)	0.2 mm	350 & 700
H <sub>2</sub> dispenser & cooling system – loss of containment on pipework (internal release)	10% pipe diameter	350 & 700
H <sub>2</sub> dispenser – loss of H <sub>2</sub> containment on hose (external release)	10% hose diameter Full bore rupture	350, 700 & 1000

**Table 13 – Summary of the H<sub>2</sub>-related critical scenarios associated with the forecourt for Configuration 3**

Table 13 shows that critical scenarios involving releases at the hose include 0.2 mm diameter, 10% hose diameter and full bore rupture scenarios. For Configuration 3, releases on pipework inside the dispenser cabinet through 0.2 mm or 10% pipe diameter holes are also identified as critical cases.

#### 4.1.4 Scenarios

The intention of the realistic release modelling is to use CFD to provide information on the extent of the steady-state flammable cloud formed following an H<sub>2</sub> release on a representative multi-fuel



forecourt. The simulations are intended to provide demonstration solutions for a range of key scenarios, rather than to form an exhaustive analysis across the full range of critical events identified through WP3.

Simulating the full range of permutations of critical scenario and forecourt configuration is beyond the remit of the present task. Thus, a subset of the scenarios has been selected for consideration as part of the realistic release modelling exercise, as summarised in Table 14.

Scenario No.	Release Type	Release Location	Leak Size	Pressure (barg)	Mass Flow Rate (g/s)	Wind Condition	Configuration
1	External	Hose	Medium	350	14.8	F1.5	1
2						D5	
3			Large		120.0 *	F1.5	
4						D5	
5			Medium	700	25.9	F1.5	
6						D5	
7			Large		60.0 *	F1.5	
8						D5	
9	External	Hose	Medium	350	14.8	F1.5	2
10						D5	
11			Large		120.0 *	F1.5	
12						D5	
13			Medium	700	25.9	F1.5	
14						D5	
15			Large		60.0 *	F1.5	
16						D5	
17	Internal	Pipe/Valve	Small	1000	1.5	F1.5	3
18						D5	
19			Medium	350	14.8	F1.5	
20						D5	
21	External	Hose	Small	350	0.7	F1.5	
22						D5	
23			Medium		14.8	F1.5	
24						D5	
25			Large		120.0 *	F1.5	
26						D5	
27			Large	700	300.0 *	F1.5	
28						D5	

**Table 14 – List of realistic release scenarios to be modelled using CFD tools. Cases marked with (\*) indicate that the mass flow rate is restricted to the dispenser H2 delivery flow rate. All other mass flow rates have been estimated using the FCH2 e-Laboratory Jet Parameters tool**

Comparing the scenarios listed in Table 14 to those summarised in Table 12 and Table 13 shows that the following assumptions and limitations have been applied to the scenario selection:

- **Configurations 1 & 2:**

- The 1000 bar hose release has been discounted, since it is out of scope of the present work. The project focusses on dispensing pressures of 700 and 350 bar only.
- The full bore vent line exit releases have also been discounted as they do not offer a substantially different release condition to a full bore rupture of the hose.

- **Configuration 3:**

- The focus is on a dispensing pressure of 350 bar, since this is consistent with the delivery pressure currently used for heavy duty vehicle refuelling.
- However, a 700 bar release scenario has been included for the purposes of comparison.
- For the 0.2 mm diameter internal release within the dispenser housing, a release pressure of 1000 bar was selected to represent a possible worst case.

As shown in Table 14, there are 14 base scenarios to be modelled with two wind conditions each, giving a total of 28 realistic release scenarios. Leak sizes are listed as *Small*, *Medium* or *Large* in the table, which correspond to a 0.2 mm diameter hole, 10% of the pipe/hose diameter and full bore rupture, respectively.

Following discussion with the MultHyFuel project consortium and the Task 2.1.2 partners, it was decided that Scenarios 5/6 and 13/14 would be omitted, since the mass release rate of H<sub>2</sub> for these cases is not sufficiently different to the release rate for other scenarios considered. Furthermore, scenarios 21 & 22 are also excluded from the analysis since the mass flow rate of H<sub>2</sub> is so low that the resulting flammable cloud will not interact with any of the obstacles present. Thus, the case is suited to analysis using simpler modelling tools, so doesn't need to be studied using CFD in the context of this project.

Sections 4.1.4.1 to 4.1.4.6 show, schematically, the set up for the release scenarios to be modelled. In the images, the wind direction (blue arrow), the dispenser at which the release originates (red circle) and the direction of the release (red arrow) are all shown.

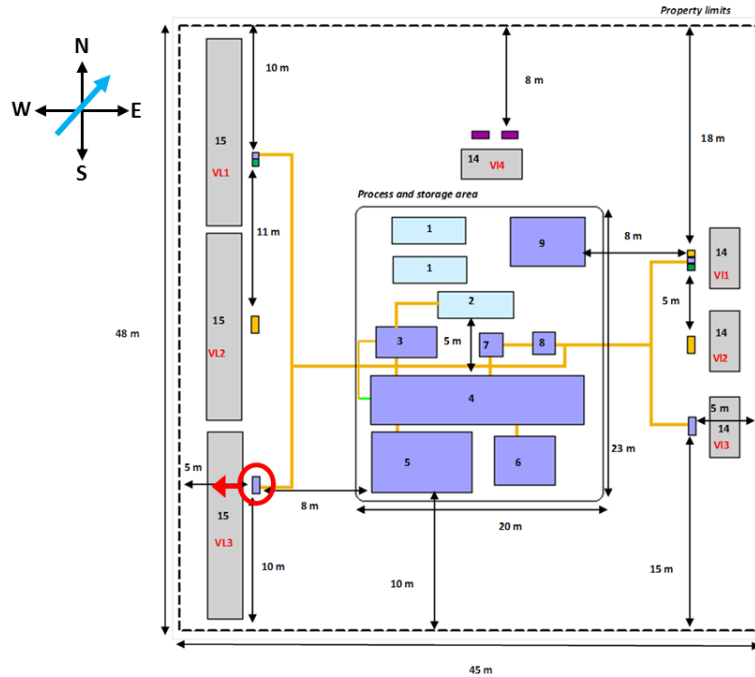
#### 4.1.4.1 Scenarios 1 – 4

Figure 24 presents a schematic of Scenarios 1-4. These cases use forecourt Configuration 1, the wind is from the South-East (as indicated by the blue arrow in the top-left of the Figure), the release is from the dispenser highlighted by the red circle and the release direction is shown by the red arrow.

#### 4.1.4.2 Scenario 7 & 8

#### 4.1.4.3 Scenario 9 – 12





**Figure 26 – Schematic of the setup for realistic release scenarios 9 – 12**

#### 4.1.4.4 Scenario 15 & 16

Figure 27 presents a schematic of Scenarios 15 & 16. These cases use forecourt Configuration 2, the wind is from the South-East and a different release dispenser and direction are used as compared to the other scenarios for Configuration 2, as highlighted by the red circle and red arrow, respectively. These scenarios use releases equivalent to those used in Scenarios 7 & 8.

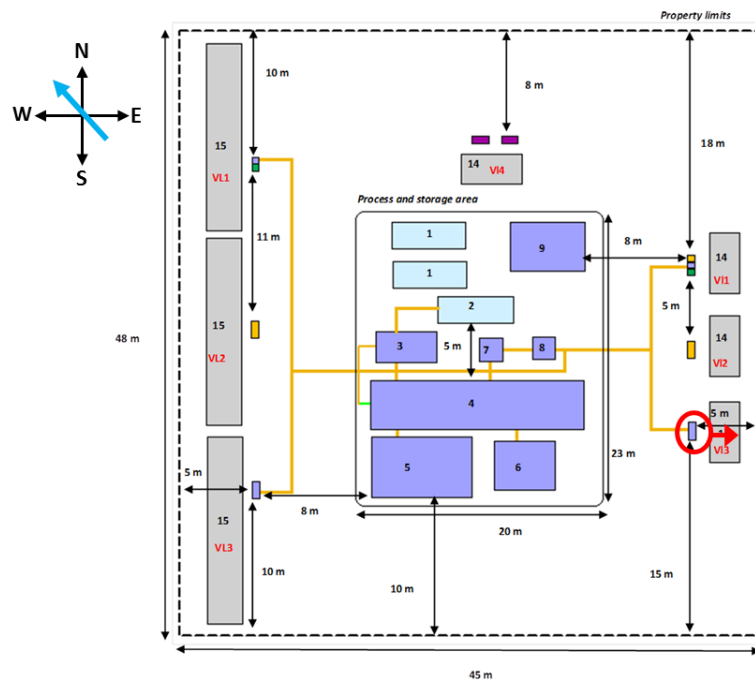


**Figure 27 – Schematic of the setup for realistic release scenarios 15 – 16**

#### 4.1.4.5 Scenarios 17 – 20

Figure 28 shows a schematic for Scenarios 17-20. For these cases, forecourt Configuration 3 is used,

the wind is from the South-East and the releases occur inside the dispenser cabinet and thus result in two release directions, where gas escapes from the upper ventilation openings in the dispenser (see Section 4.1.6 for further details). Again, the release dispenser and release directions are shown by the red circle and red arrows, respectively.

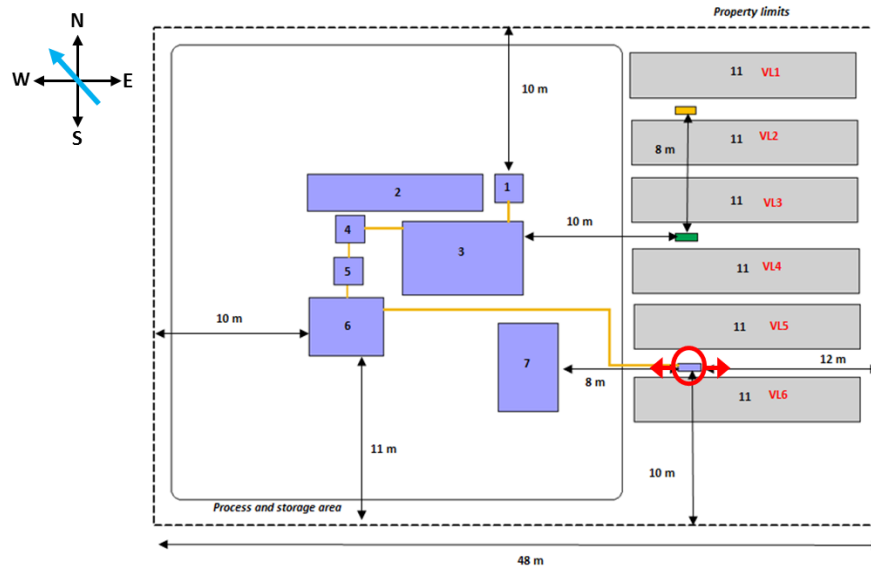


**Figure 28 – Schematic of the setup for realistic release scenarios 17 – 20**

#### 4.1.4.6 Scenarios 23 – 28

Figure 29 shows a schematic for Scenarios 23-28. These cases involve external releases from a dispenser of forecourt Configuration 3. The wind is from the South-East and the release dispenser and direction are indicated by the red circle and red arrow, respectively. As showed in Table 14, Scenarios 23-26 use the same release conditions as Scenarios 1-4 and 9-12, for forecourt configurations 1 and 2, respectively.

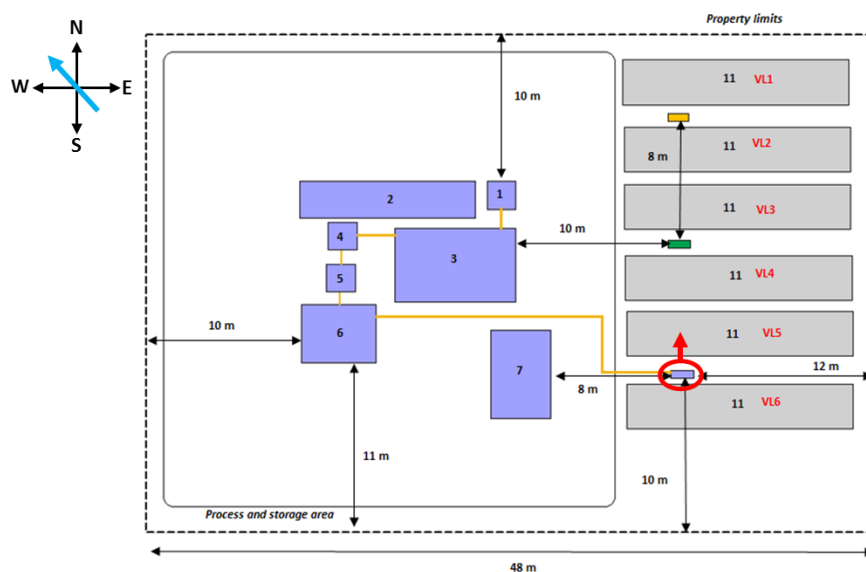


**Figure 29 – Schematic of the setup for realistic release scenarios 23 - 28**

#### 4.1.5 Atmospheric Conditions

For each of the realistic release scenarios, two separate wind conditions are considered. These wind conditions represent those commonly used in regulatory frameworks. Specifically, wind speeds (at a reference height of 10 m) of 1.5 m/s and 5 m/s will be used, together with atmospheric stability classes of F (stable) and D (neutral), respectively (i.e. F1.5 and D5). For the modelling performed as part of the present study, the aerodynamic roughness was taken to be 0.1 m. However, this was only used to define the wind profiles. The model set up used smooth wall conditions for the ground which, whilst representing a simplification of real conditions, is considered the most suitable approach for the present analysis. This is because the approach enables higher levels of grid resolution to be used without breaching recommended meshing limits for capturing the effects of rough walls in CFD models. Furthermore, within the context of the overall limitations of the modelling, the use of smooth walls is unlikely to significantly influence the model results.

The consequences of H<sub>2</sub> releases, in terms of flammable cloud, are maximised when the temperature difference between the release and ambient temperatures is greatest. As such, it makes sense to use a relatively high, but realistic, ambient temperature. Thus, standard conditions of 20 °C and a pressure of 101325 Pa will be used.

#### 4.1.6 Release Conditions

The releases are assumed to be at a process temperature -40 °C, which corresponds to the dispenser delivery temperature.

For the external releases, i.e. the scenarios in which the leak is assumed to originate from the delivery hose, the leak location is taken to be at a height of 1.2 m, approximately the height of the nozzle, and at the dispenser end of the hose. The release direction for each scenario is shown in the schematic diagrams of the forecourts shown in Sections 4.1.4.1 to 4.1.4.6. Figure 30 shows the release location on the dispenser for the external release cases modelled.

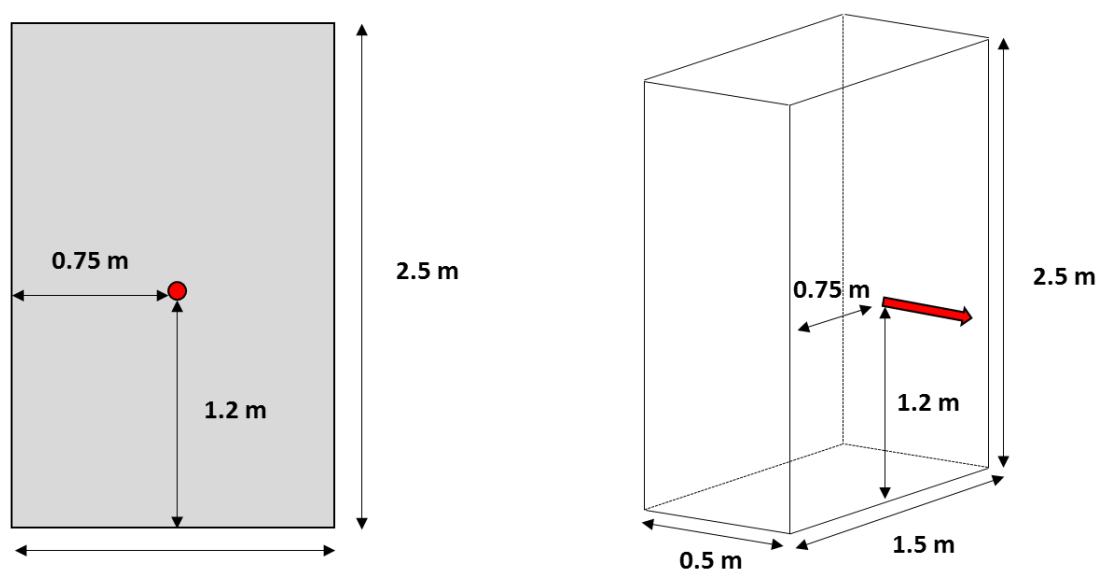


**Figure 30 – Modelled leak configuration for the external release scenarios**

For the internal releases, i.e. leaks in pipework within the dispenser, the release is initially modelled using a simple ventilation model (Linden, 1999; Jallais et al., 2013) to estimate the

equilibrium  $H_2$  concentration inside the dispenser. The release is then simulated in the CFD model as two external releases through 0.19 m x 0.5 m ventilation openings at the top of the dispenser. The imposed mass flow rate and  $H_2$  concentration at these ventilation openings is taken from the results of the simple model. Figure 31 shows how these releases were set up in the CFD model. The ventilation opening size was selected to be consistent with that used in the WP3 risk assessment analyses described in deliverable D3.5.

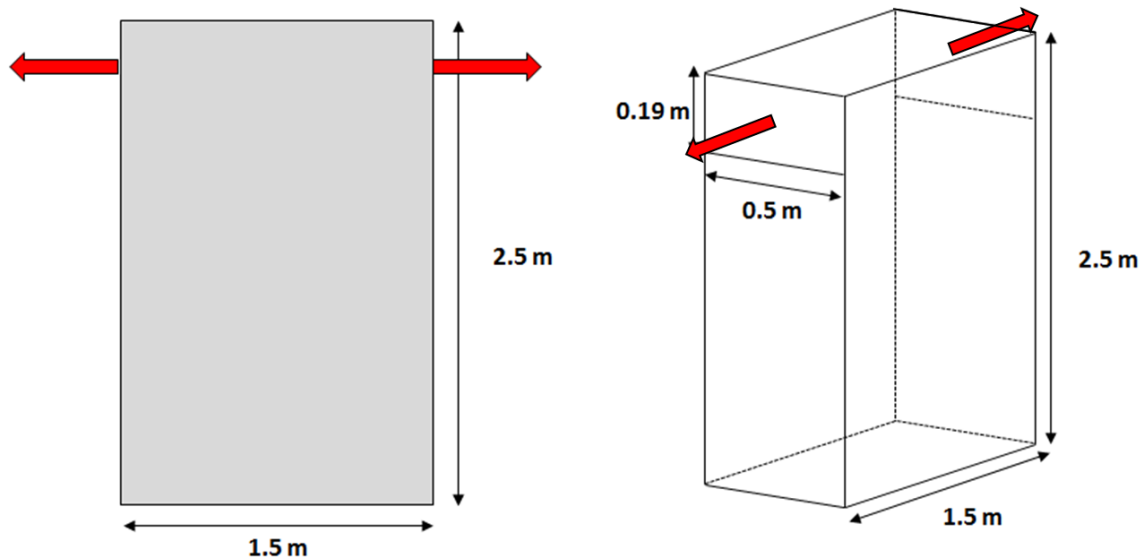


Figure 31 – Modelled leak configuration for the internal release scenarios

## 4.2 Modelling Approaches Used

### 4.2.1 Forecourt Geometry

Three-dimensional (3D) representations of the three forecourt configurations introduced in MultHyFuel deliverable D3.1 – *State of the art on Hydrogen Technologies and Infrastructures regarding a Multi-Fuel Station Environment* were created for use in the CFD modelling described in this report. The geometry files were based on the 2D plans presented in deliverables D3.1, D3.3, D3.4 and D3.5, with the details of building/equipment heights agreed in advance with the MultHyFuel consortium.

The 3D models include representative canopies above the dispenser locations. Whilst the modelled canopies may not reflect a specific canopy design used in practice, they capture some of the common features seen at  $H_2$ -refuelling sites. An alternative option would have been to model the releases without including a canopy, but excluding the canopy entirely was deemed unsatisfactory as this would not be representative of real-World refuelling stations. Thus, the representative canopy designs used give an acceptable compromise for the purposes of this study.

The 3D geometry files were shared with the task partners to ensure that there were no variations in geometry introduced by the different partner representations of the agreed forecourt configurations.

#### 4.2.1.1 Configuration 1 – Ready-to-deploy Multi-fuel Station

Figure 32 shows the 3D representation of forecourt Configuration 1. The dark grey objects

represent buildings and equipment within the process and storage area. The blue structures are representative canopy designs over each dispensing location, with the dispensers and vehicles shown in green. The extent of the forecourt area is shown by the light grey object representing the ground.

To convert the configuration layout from WP3 into a 3D geometry (see Figure 69 in Appendix 1), some assumptions about obstacle heights were necessary. For this configuration, the buildings and equipment in the process area were modelled as 2.5 m in height, except for the chiller unit which was set at a height of 2 m. The dispensers were taken as 2.5 m tall, with a minimum canopy height of 4.5 m, extending to 5 m above the refuelling area.

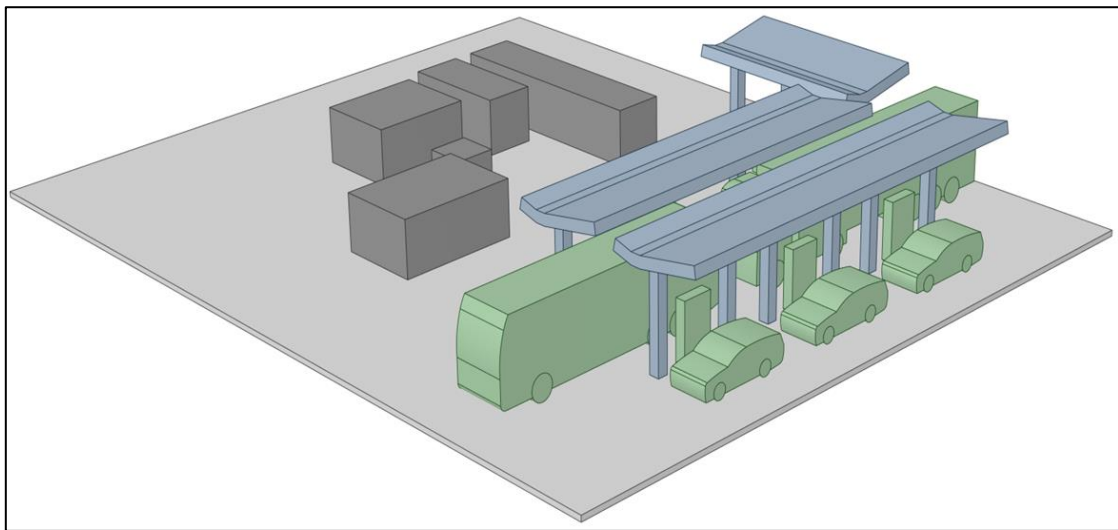


**Figure 32 – Perspective view of the 3D geometry for Configuration 1**

The vehicles included on the forecourt were taken to be representative versions of cars, trucks and buses/coaches. The vehicles were simplified as far as possible to enable them to be more easily captured with the computational meshes used in the CFD models. The same modelled vehicles were used across all three forecourt configurations.

#### 4.2.1.2 Configuration 2 – On Site $H_2$ Production Multi-fuel Station

Figure 33 shows the 3D representation of forecourt Configuration 2. The dark grey object represents a boundary wall around the process and storage area, with the buildings and equipment in that area shown to be enclosed by the wall. The blue structures are representative canopy designs over each of the dispenser locations. The dispensers themselves and all of the vehicles on the site are shown in green. The extent of the forecourt area is illustrated by the light grey object representing the ground.

Again, in order to define a 3D geometry from the 2D forecourt layout defined for Configuration 2 (see Figure 70 in Appendix 1), it was necessary to define heights for the buildings and equipment on the forecourt. For Configuration 2, the same dispenser and canopy heights were used as for configuration 1. The process area buildings and equipment were all set at heights of 2.5 m and 2.6 m for the electrolyser units (to represent the dimensions of an ISO container). The boundary wall around the process area was modelled as 3 m tall.



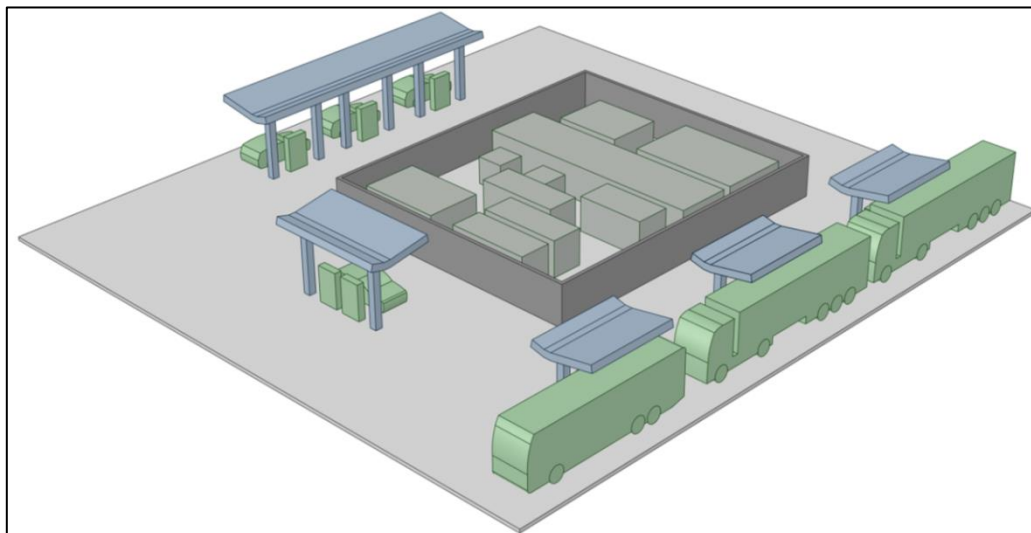


**Figure 33 – Perspective view of the 3D geometry for Configuration 2**

#### 4.2.1.3 Configuration 3 – High Capacity & High Filling Multi-fuel Station

Figure 34 shows the 3D representation of forecourt Configuration 3. The dark grey object represents a boundary wall around the process and storage area, with the buildings and equipment in that area shown to be enclosed by the wall. The blue structures are representative canopy designs over each of the dispenser locations. The dispensers themselves and all of the vehicles on the site are shown in green. The extent of the forecourt area is illustrated by the light grey object representing the ground.

To convert the Configuration 3 layout, as defined in WP3, into a 3D geometry, the buildings and equipment in the process and storage area were taken to have a height of 2.5 m. The modelled LH2 storage cylinder was taken to have a 2 m diameter and 6 m height. The boundary wall enclosing the process area was set as 3 m high, as for configuration 2. The dispenser and canopy heights were taken to be the same as for the other two geometries. However, the canopy shape for configuration 3 is slightly different, due to the canopies each covering back-to-back dispensing areas on the forecourt.

Additionally, the distance between the rearmost part of the trucks and the process and storage area wall is set to 10 m, following consultation with the MultHyFuel consortium. This does not align with the information given in the WP3 deliverables but was considered more appropriate than the dimensions given previously.

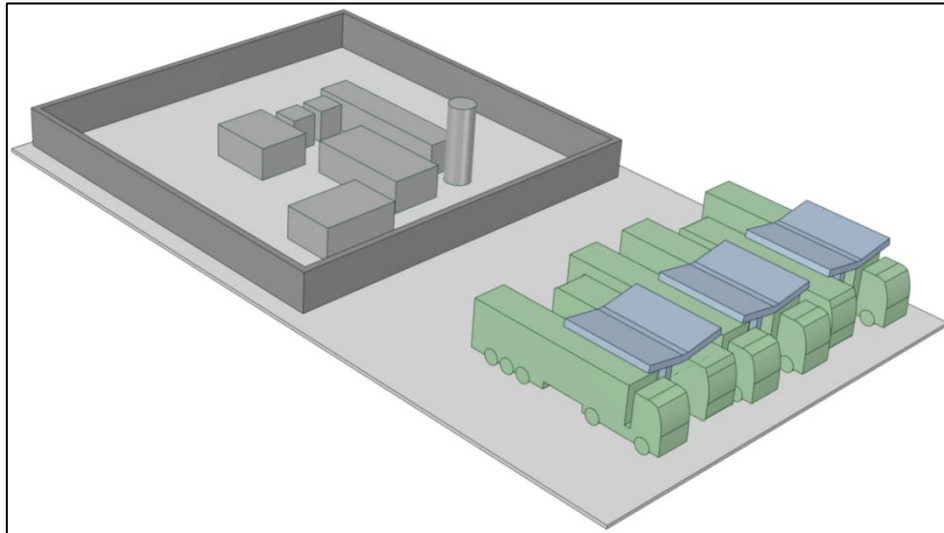


**Figure 34 – Perspective view of the 3D geometry for Configuration 3**

#### 4.2.2 Domain and Computational Mesh

The computational domain used for the realistic release modelling encompasses the full geometry of interest as well as a sufficiently large surrounding area so that the flow field is not influenced by the domain boundaries. Figure 35 shows an example of the simulation domain used for the modelling involving forecourt Configuration 1. The Figure shows a range of relevant dimensions, each assigned a letter as an identifier. The values of the dimensions used for the realistic release simulations in each CFD model are summarised in Table 15. Note that for the OpenFOAM v1912+ modelling, the simulation domain was oriented with the wind, so the values of  $a$ ,  $b$ ,  $c$  and  $d$  in Table 15 represent the shortest distances to the domain boundary from the forecourt, approximately.

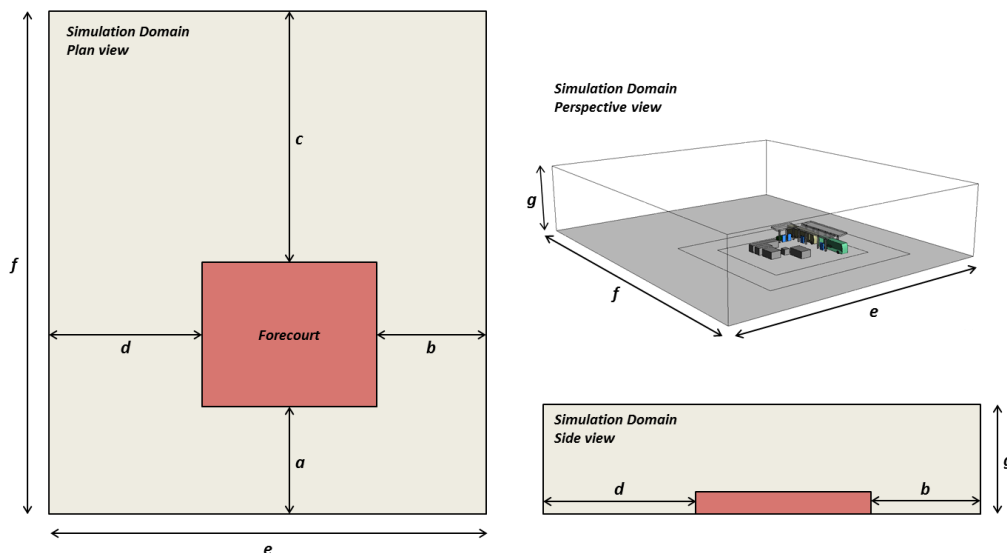


**Figure 35 – Simulation domain used: plan view (left), side view (bottom right) and perspective view (top right)**

Domain Dimension	Configuration 1	Configuration 2	Configuration 3	
	CFX v19.0	OpenFOAM v1812	FLACS v10.6	OpenFOAM v1912+
a	24.5 m	~25 m	n/a	~50 m
b	25.0 m	~25 m	n/a	~50 m
c	57.5 m	~25 m	n/a	~50 m
d	35.0 m	~25 m	n/a	~50 m
e	100.0 m	~100 m	33 m	164 m
f	115.0 m	~100 m	58 m	164 m
g	25.0 m	~25 m	12.2 m	40 m

**Table 15 – Domain extent used for the realistic release simulations. Refer to Figure 35 for further details.**

Regarding the computational meshes used, each of the CFD models was set up slightly differently. For example, the mesh used in the CFX modelling is based on an unstructured tetrahedral grid with refinement in the region of the forecourt. Further refinement is also made at the source of the release. This meshing approach enables the obstacles to be captured explicitly in the model. Figure 36 shows a plan view of the CFX mesh viewed on a plane at the height of the releases, i.e. 1.2 m above the ground.

Several different mesh resolutions were used in CFX to assess the sensitivity of the model predictions to the grid choice. For this grid sensitivity analysis, the mesh was successively refined to the point where the differences between the predicted flammable volume deviated by less than 5%. This level of grid independence was deemed acceptable for the purposes of the present analysis.

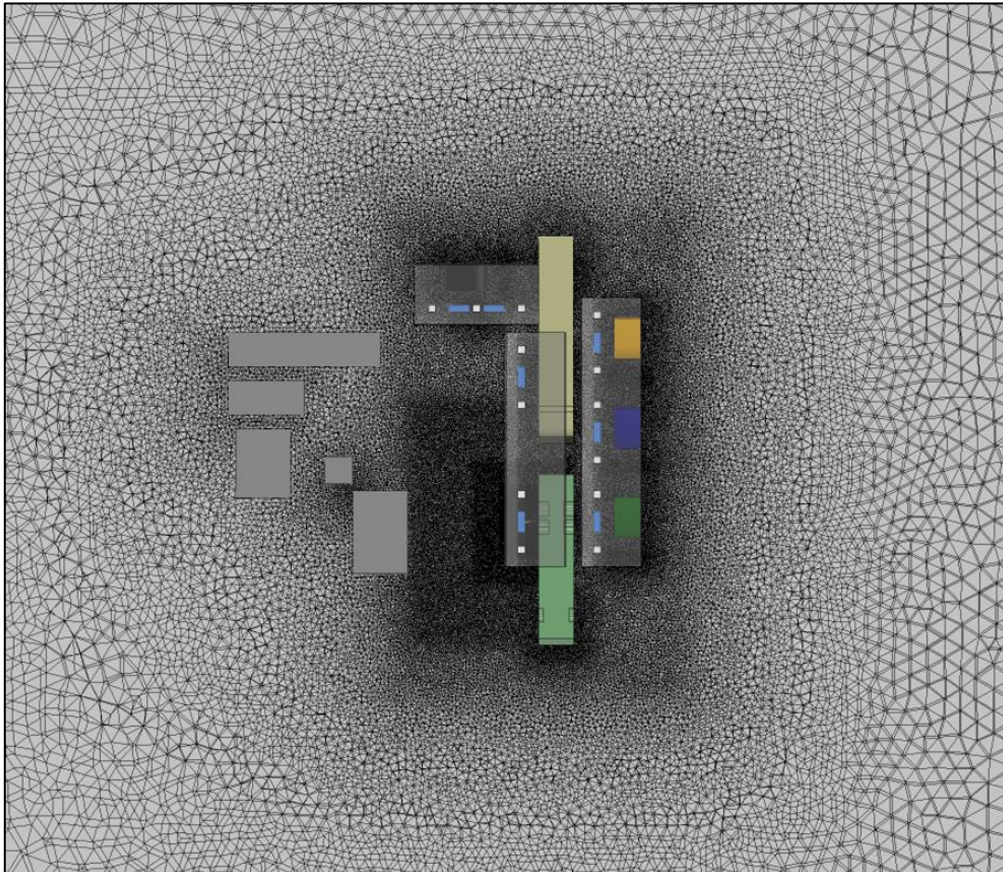


**Figure 36 – Plan view of the mesh used in CFX on a plane 1.2 m above the ground (the height of the realistic releases)**

The mesh used in the FLACS simulations is quite different to that used in CFX, as shown in Figure 37. The FLACS model uses a structured Cartesian mesh and assigns volume and area porosities to each cell to capture the influence of obstructions (as described in Section 3.2.1.3). From Figure 37 it can be seen that the vehicles and dispensers, shown in the right-hand side of the image, are aligned with the mesh, whereas the process and storage area to the left-hand side of the image, is more loosely captured using this distributed porosity approach. The purpose of this is to ensure that in the region of interest, i.e. near to the release, the porosity model does not adversely affect results, but further from the release, the mesh constraints are less stringent, allowing for a reduced mesh size overall.

Figure 38 presents an example of the type of meshing approach adopted in the modelling performed using OpenFOAM 1812. The approach is based on a hexahedral dominant mesh with adaption in regions of interest. This enables the mesh to use refinement around key obstacles, e.g. the cars shown in the Figure, without unnecessarily increasing the mesh requirements elsewhere in the simulation domain. Figure 39 and Figure 40 show examples of the meshes used in the OpenFOAM 1912+ and KFX modelling, respectively. Both of these models used structured Cartesian meshes with refinement close to the source. A disadvantage of this type of meshing approach is the use of excessive grid resolution in areas of the simulation domain which are not of interest. Figure 40 clearly illustrates this, with the band of refinement near the dispenser, and thus the source, extending across the full domain width. These three Figures illustrate that the obstacles are captured more crudely than is the case with an unstructured mesh. With sufficient grid resolution, the step-wise representation of obstacle edges is unlikely to have a significant impact on model predictions.



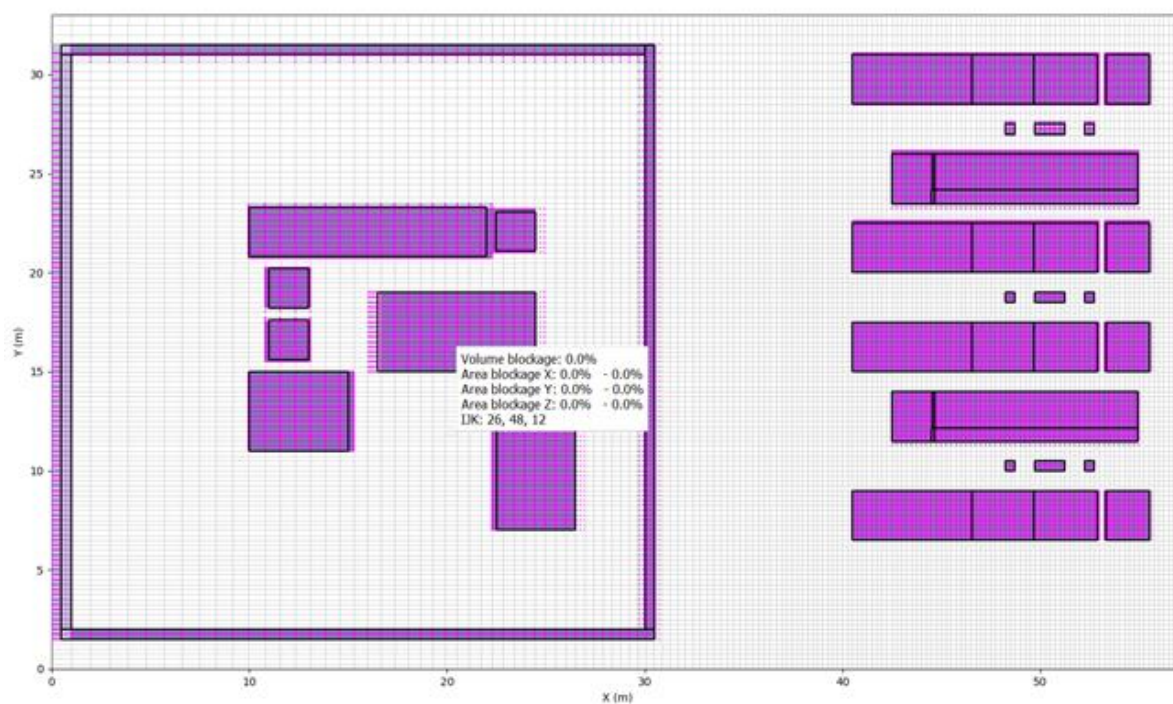


Figure 37 – Porosity distribution on the computational mesh used in the FLACS simulations of Scenarios 17-20

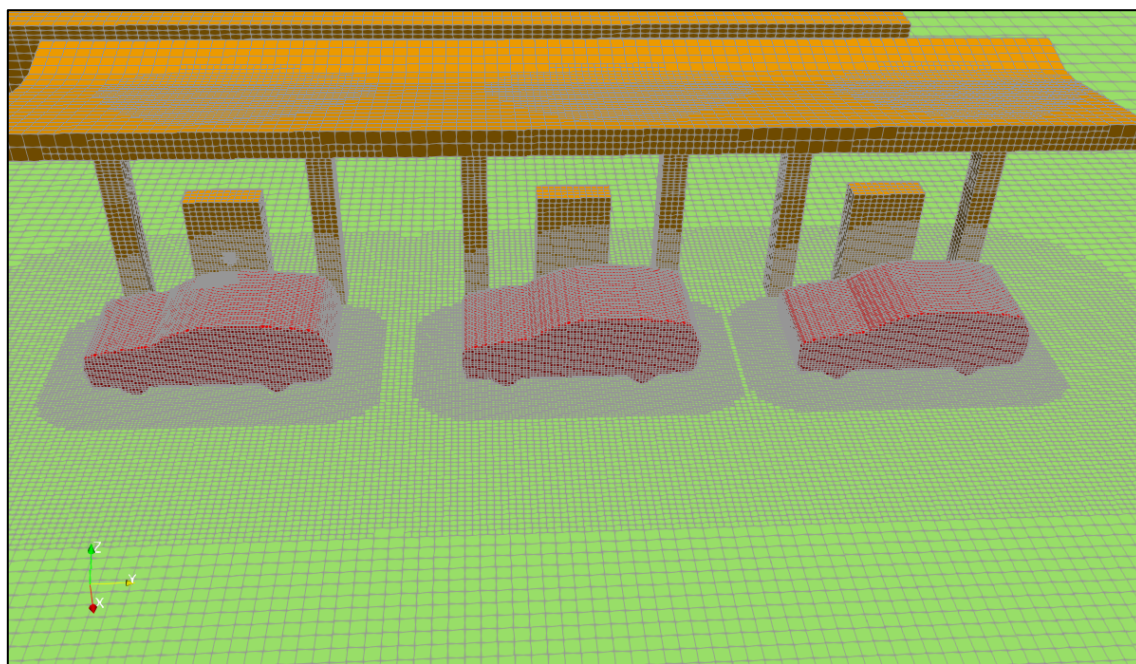
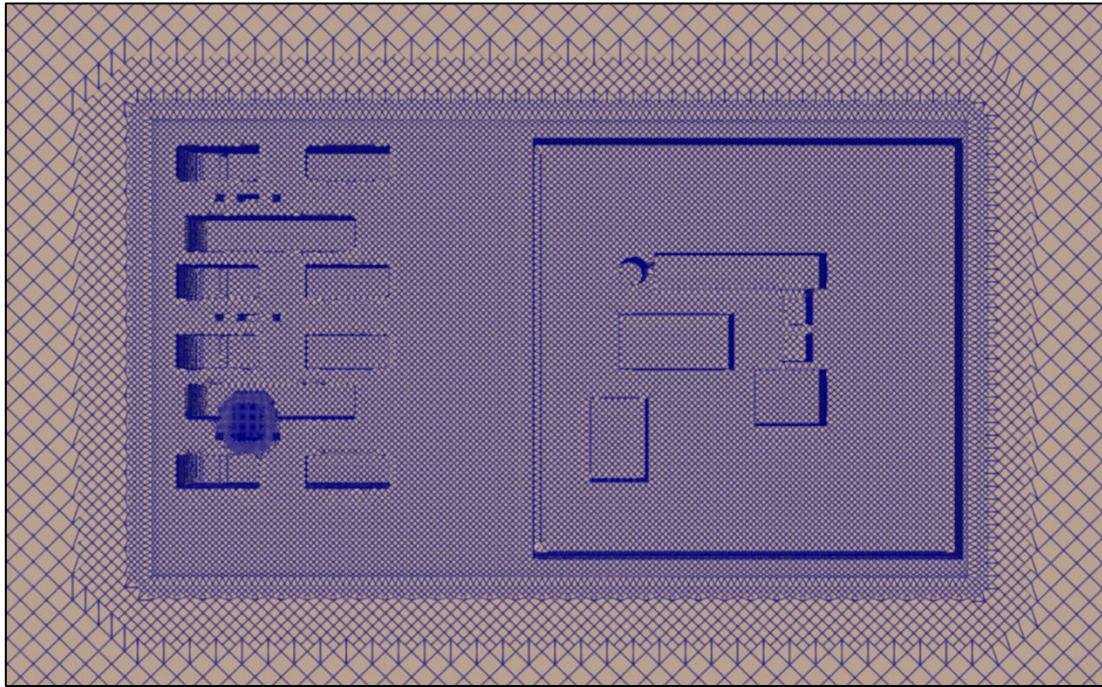
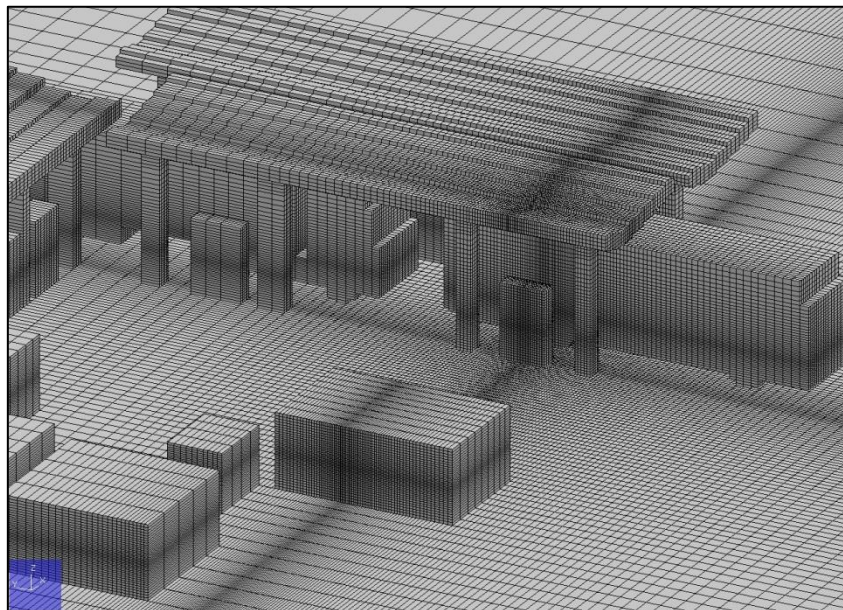


Figure 38 – Example of the meshing approach used in the OpenFOAM 1812 simulations of realistic releases for forecourt Configuration 2





**Figure 39 - Example of the meshing approach used in the OpenFOAM 1912+ simulations of realistic releases for forecourt Configuration 3. A focus is made on the area of interest**



**Figure 40 – Example of the meshing approach used in KFX for simulation of Scenario 4**

For reference, Table 16 summarises the mesh sizes used for the realistic release simulations by the task partners. As shown in the Table, for the external hose releases using CFX, OpenFOAM and KFX, cell/node counts of around 2-2.8 million have been used. For the FLACS simulations of the internal release scenarios, the cell count is much smaller. One of the benefits of using the distributed porosity concept to capture obstacles on the numerical mesh is that a much smaller grid is required overall, as there is no need for extensive grid refinement around obstructions. However, this does mean that flow features close to obstacles are unlikely to be as well resolved as they

would be if a finer mesh were used. All task partners performed mesh sensitivity studies as part of the modelling exercise. This showed that for the model predictions of interest, i.e. the flammable cloud volume, there was limited sensitivity to the choice of grid resolution.

Scenario No.	Configuration	Mesh Type	Total Cell/Node Count		
1	1	Unstructured tetrahedral (CFX)	2,236,662 (CFX)		
2			2,297,268 (CFX)	2,770,950 (KFX)	
3					
4					
5		Structured Cartesian (KFX)	n/a		
6			2,532,698 (CFX)		
7					
8					
9	2	Hexahedral with mesh adaption (OpenFOAM)	2,587,443 (OpenFOAM)		
10			2,587,301 (OpenFOAM)	2,237,928 (KFX)	
11					
12			1,490,832 (KFX)		
13		Structured Cartesian (KFX)	n/a		
14			2,545,529 (OpenFOAM)		
15					
16			1,989,504 (KFX)		
17	3	Structured Cartesian	802,854 (FLACS)		
18			n/a		
19					
20					
21		Structured Cartesian	1,926,942 (OpenFOAM)		
22			1,993,646 (KFX)		
23			1,926,942 (OpenFOAM)		
24					
25					
26					
27					
28					

**Table 16 – Summary of the mesh sizes used for the realistic release simulations described in this report**

### 4.2.3 Wind Profile Boundary Conditions

The exact approach used for applying wind boundary conditions varies across the range of CFD models used. However, across all four simulation tools, the same general approach has been applied. This general approach follows Monin-Obhukov similarity theory to model the atmospheric boundary layer (ABL). This approach relies on the use of inlet boundaries on the upstream (with respect to the wind direction) faces of the computational domain, at which vertical profiles of velocity, temperature (for stable atmospheric conditions), turbulent kinetic energy, and turbulent dissipation are applied.

At the downstream domain boundaries, pressure boundaries are typically used, which allow flow into/out of the domain in accordance with the predicted flow field. In the modelling performed here, the ground has been simulated as a smooth wall which, whilst not strictly consistent with the imposed wind profiles, simplifies the modelling approach.

There are known deficiencies of CFD modelling when it comes to simulating the atmospheric boundary layer (Batt et al., 2018), with models typically unable to maintain the desired wind profiles throughout the simulation domain. However, this is typically more of an issue for large-scale dispersion modelling, whereas in the analysis presented here, the main feature of interest is localised dispersion of momentum-dominated jet releases. Thus, the wind modelling element of the study is of less importance and is unlikely to significantly impact predictions of the flammable cloud. As such, whilst acknowledging the limitations in the modelling approaches used, the associated uncertainty is considered acceptable for the purposes of the present analysis.

Further details of the atmospheric conditions imposed in the different models are given in Appendix 2. Figure 41 shows a comparison of the imposed wind velocity profiles for the two atmospheric conditions considered. The dashed black horizontal line indicates the wind profile reference height and the two dashed vertical lines indicate the reference wind speeds of 1.5 m/s (blue) and 5 m/s (red), for the F1.5 and D5 conditions, respectively. The aerodynamic roughness length for the ground was taken to be 0.1 m for these profiles, as described in further detail in Appendix 2.

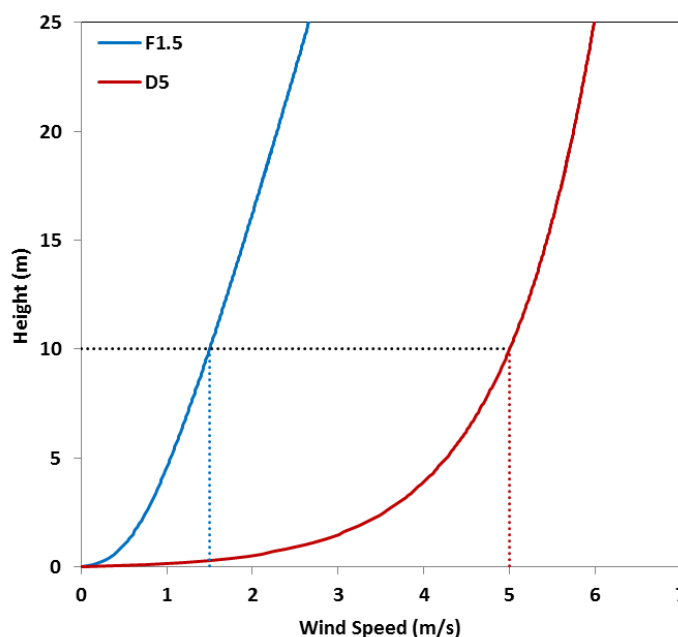


**Figure 41 – Comparison of the wind velocity profiles imposed for the F1.5 and D5 atmospheric conditions considered**

#### 4.2.4 H<sub>2</sub> Source Term

An important element of modelling the H<sub>2</sub> releases is the representation of the source of release. For the majority of the scenarios considered, the source will be a sonic H<sub>2</sub> jet, similar to those studied as part of the model validation work described in Section 3.

For the realistic release modelling, all of the scenarios involving jet releases have used source term inputs generated using the AEROPHUME sub-model within the Shell modelling package FRED. This



is the same approach which was used to generate the source term used for the OpenFOAM 1812 modelling described in Section 3. The model validation results presented in Section 3 demonstrated that this source term representation gave good agreement with the measured data for both the unobstructed and obstructed jet cases modelled with both the CFX and OpenFOAM CFD models. Thus, to ensure consistency across the scenarios, the same method is used by all the task partners.

Table 17 presents a summary of the calculated inlet conditions for the jet release scenarios listed in Table 14. For some of the scenarios modelled, the mass flow rate of the release is restricted to the delivery flow rate for the dispenser hose. These cases are highlighted in Table 17 with an asterisk (\*). AEROPLUME was still used to predict the source term conditions for the CFD models, but with the mass flow rate of H<sub>2</sub> imposed as a constraint.

	350 bar		700 bar	
Leak Type	10% Hose	Full Bore	Full Bore <i>Light Duty</i>	Full Bore <i>Heavy Duty</i>
Diameter (mm)	18.2	34.2	22.6	52.9
Velocity (m/s)	671.5	704.6	775.0	768.0
Temperature (K)	280.7	280.7	255.6	245.9
H <sub>2</sub> Mass Fraction	0.29	0.52	0.55	0.50
H <sub>2</sub> Mass Flow Rate (g/s)	14.8	120.0 *	60.0 *	300.0 *

**Table 17 - Summary of the H<sub>2</sub> jet source term parameters (calculated using Shell's AEROPLUME model) used by all modellers for the realistic release simulations. Where the mass flow rates include an asterisk (\*), this indicates that the flow rate has been capped at the dispenser delivery flow rate**

## 4.3 Simulation Results

### 4.3.1 Initial Velocity Field

The H<sub>2</sub> release simulations undertaken with CFX are initialised from a steady-state solution with the wind only. This enables the atmospheric profiles imposed as boundary conditions in the model to become established and provides a better *initial guess* of the wind field around the obstacles present on the representative forecourts. Performing the simulations in two-stages can help models achieve a converged solution and avoid some of the numerical difficulties which can be associated with introducing a high-speed jet flow into a quiescent environment.

Figure 42 and Figure 43 show the initial wind fields for the D5 and F1.5 wind conditions for forecourt Configuration 1. The two images show broadly similar patterns in the velocity field, with a large area of low velocity on the leeward side of the obstacles. For the simulations using forecourt Configuration 1, the wind is directed from the bottom-right to top-left of these two Figures, representing a South-Easterly wind.

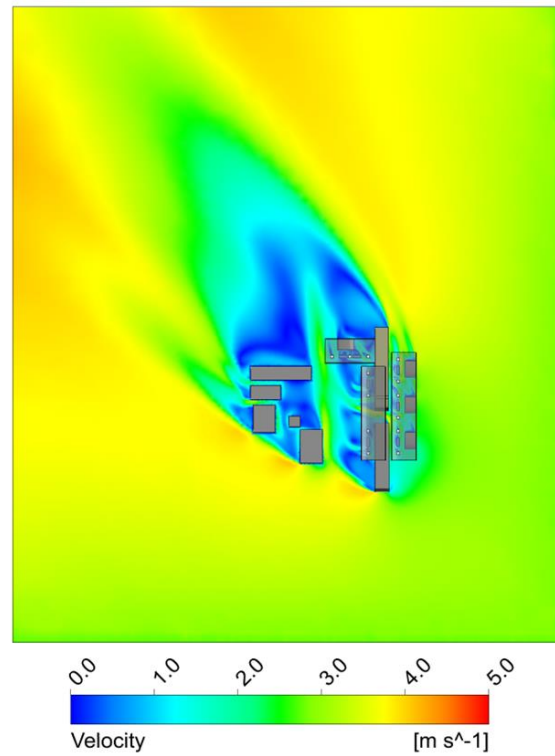


**Figure 42 – Initial velocity field for forecourt Configuration 1 with D5 atmospheric wind conditions at a height of 1.2 m above the ground (corresponding to the release height used for the external H<sub>2</sub> leaks)**

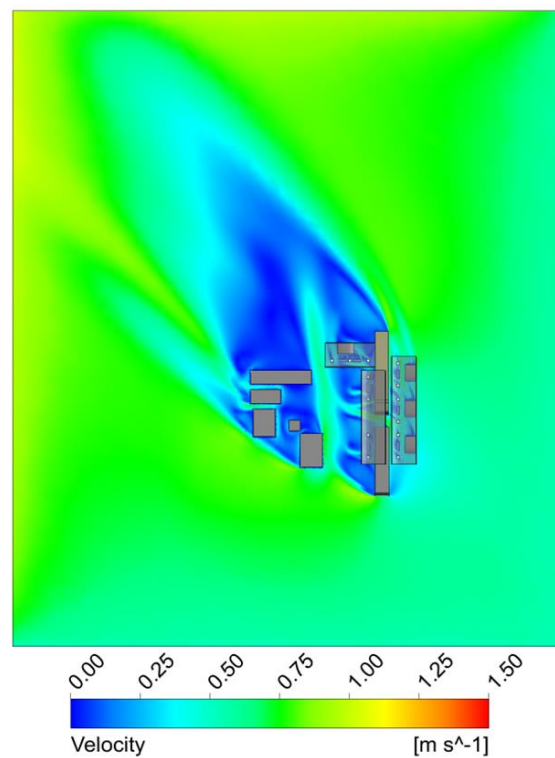


**Figure 43 – Initial velocity field for forecourt Configuration 1 with F1.5 atmospheric wind conditions at a height of 1.2 m above the ground (corresponding to the release height used for the external H<sub>2</sub> leaks)**

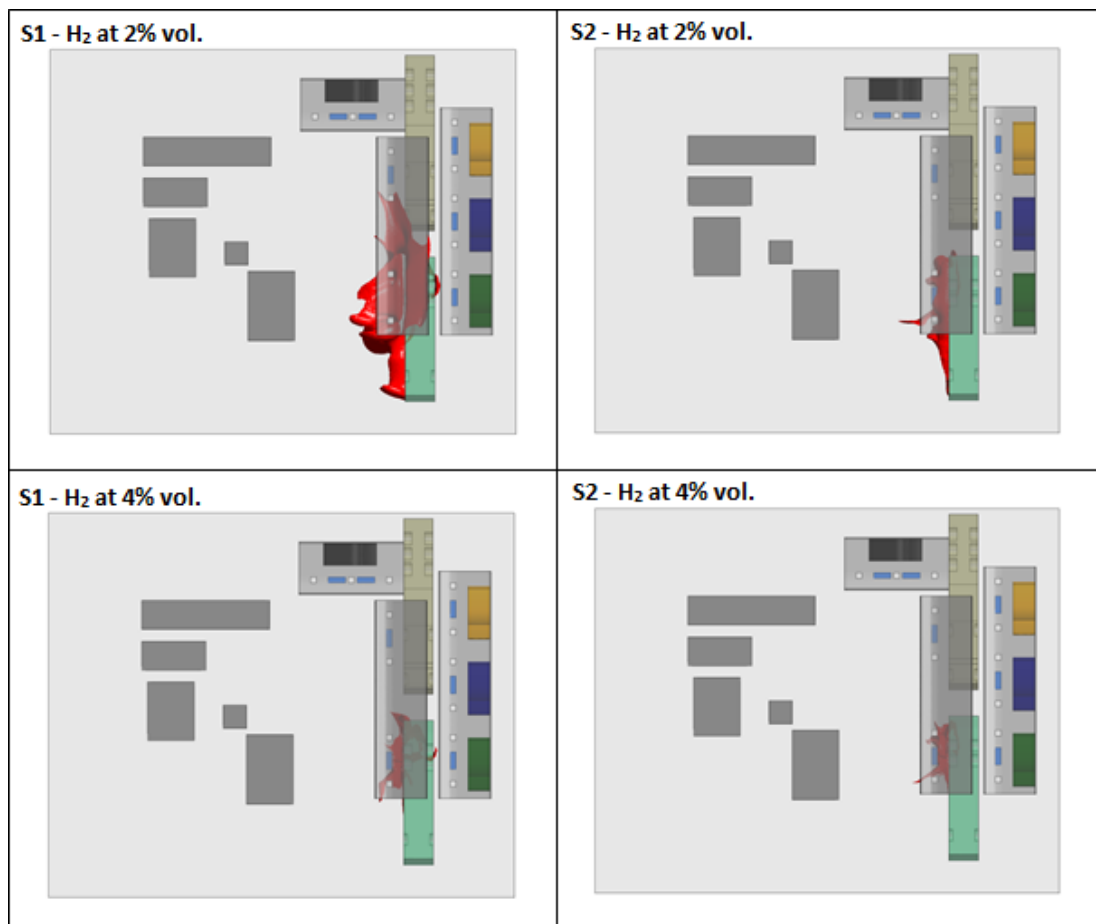
Whilst initialising the wind field was a step taken in the CFX modelling presented here, it is not

always necessary to follow this approach. The modelling performed with the other simulation tools selected did not follow the same approach. For these simulations both the wind and the H<sub>2</sub> release were started at the same time, usually with the initial wind profiles imposed as an initial condition everywhere within the simulation domain, and the models were run until a steady-state solution was obtained. The same approach could have been taken in CFX, but experience has shown that initialising the wind field first can lead to achieving a converged solution more easily.

#### 4.3.2 Scenarios 1 & 2

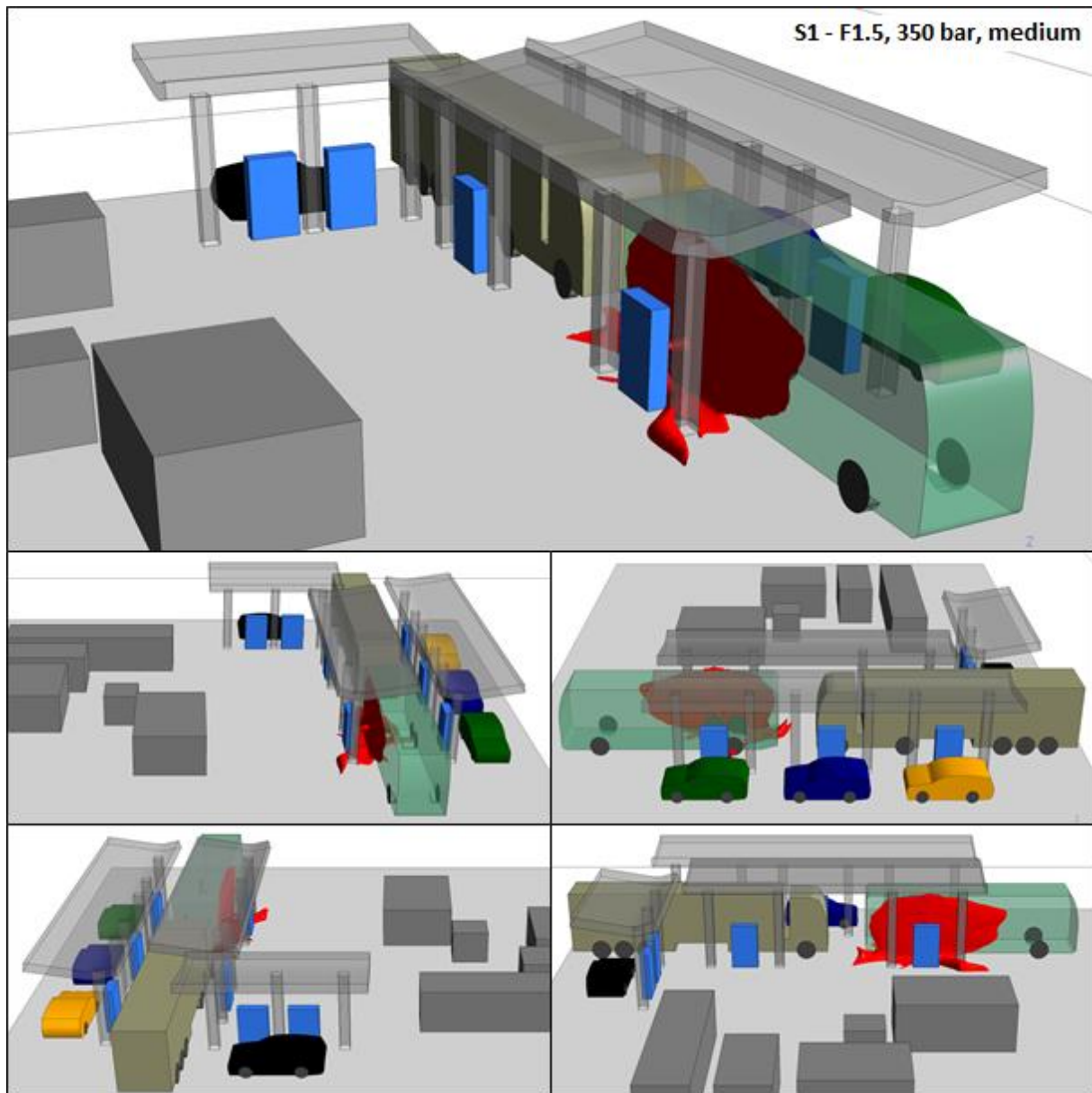
Scenarios 1 (F1.5) and 2 (D5) involve releases from a 350 bar H<sub>2</sub> delivery hose through an opening size equal to 10% of the hose diameter, approximately 0.95 mm. The geometry used for these scenarios is forecourt Configuration 1 (see Section 4.1.1 and 7.1.1). The release results in an H<sub>2</sub> mass flow rate of 14.8 g/s. Full details of the set up are described in Sections 4.1.

Figure 44 shows a comparison of the H<sub>2</sub>/air cloud spread at 2% and 4% (v/v) concentrations, i.e. ½ LFL and LFL, respectively. Iso-surfaces at these concentrations are shown in red within the Figure. The results were obtained using the CFX model. Whilst the spread of the cloud at the LFL concentration is similar under both F1.5 (Scenario 1) and D5 (Scenario 2) wind conditions, the spread of the cloud at the ½ LFL is substantially greater for Scenario 1. The ½ LFL concentration is typically used as the basis of hazardous area zoning and to define the area at risk of flash fire. As such, the results suggest that the lower wind speed case, Scenario 1, presents a risk of fire/explosion over a larger area of the forecourt than Scenario 2.



**Figure 44 – Plan-view of H<sub>2</sub>/air cloud at the ½ LFL (2% vol.) and LFL (4% vol.) concentrations for Scenarios 1 (F1.5) & 2 (D5) as predicted using CFX**

Figure 45 and Figure 46 show perspective views of the flammable cloud, i.e. where the  $H_2$  concentration is between 4% and 75% (v/v), for Scenarios 1 and 2, respectively. As shown in the Figures, the distribution of  $H_2$  is similar in both cases, with the cloud shape predominantly dictated by the jet release impinging on the side of the bus (green vehicle in Figures). Given that the wind direction in these two cases is from the South-East (refer back to Figure 42 and Figure 43), the bus itself provides substantial shelter to the dispenser at which the release originates. This, combined with the fact that these two scenarios use a relatively small mass flow rate of  $H_2$ , results in a small influence of the wind on the flammable cloud size.



**Figure 45 – Perspective view of the flammable cloud (iso-surface showing  $H_2$  at 4% vol.) for Scenario 1 (F1.5) as predicted using CFX**

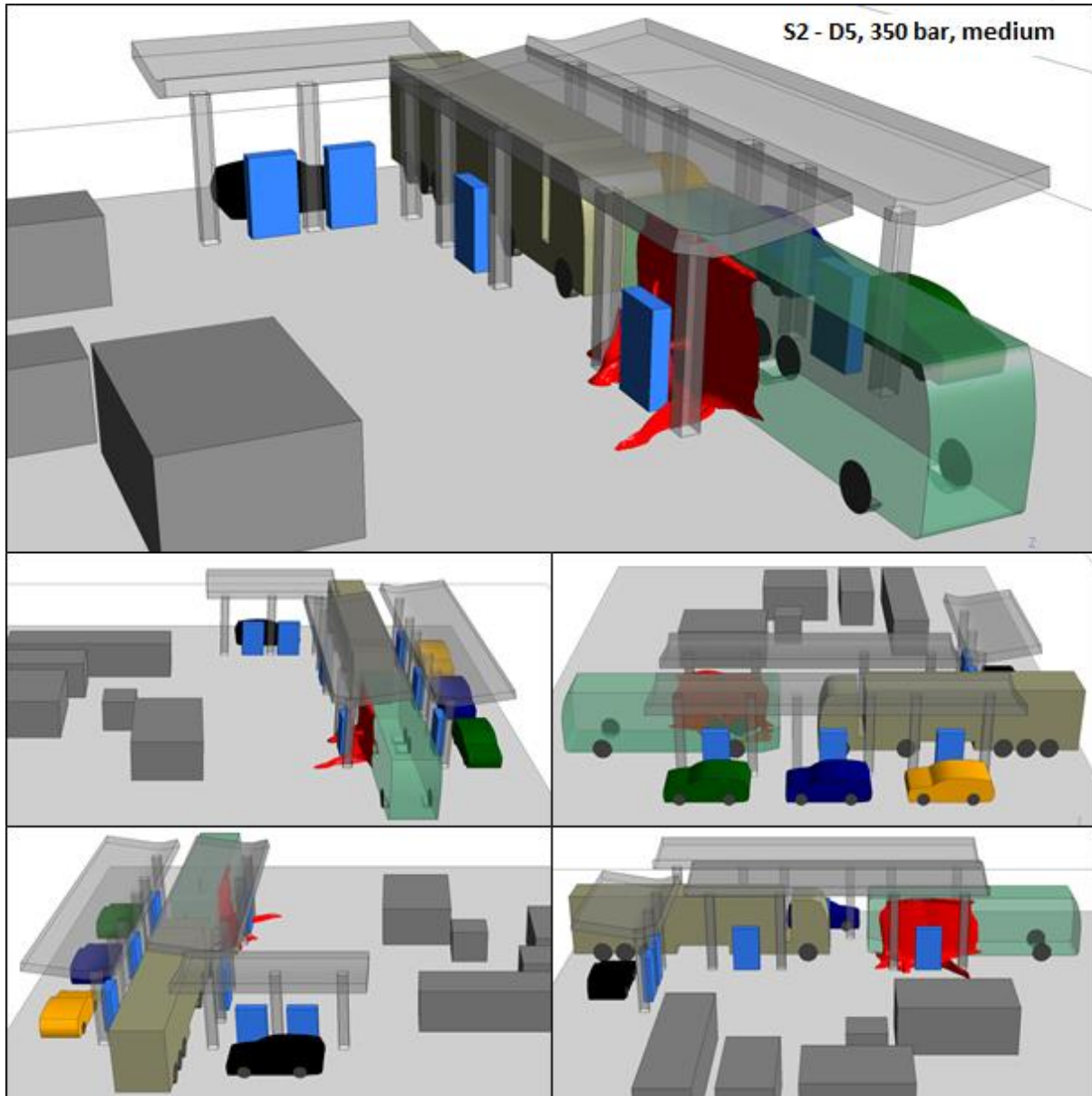


**Figure 46 – Perspective view of the flammable cloud (iso-surface showing H<sub>2</sub> at 4% vol.) for Scenario 2 (D5) as predicted using CFX**

For Scenarios 1 and 2, the mass of H<sub>2</sub> within the flammable cloud is small, approximately 17.3 g and 18.0 g, respectively. Regarding the flammable cloud volume, both Scenarios result in similarly sized clouds, as shown in the previous Figures. The predicted flammable volumes for these cases were 4.2 m<sup>3</sup> and 4.1 m<sup>3</sup> for Scenarios 1 and 2, respectively.

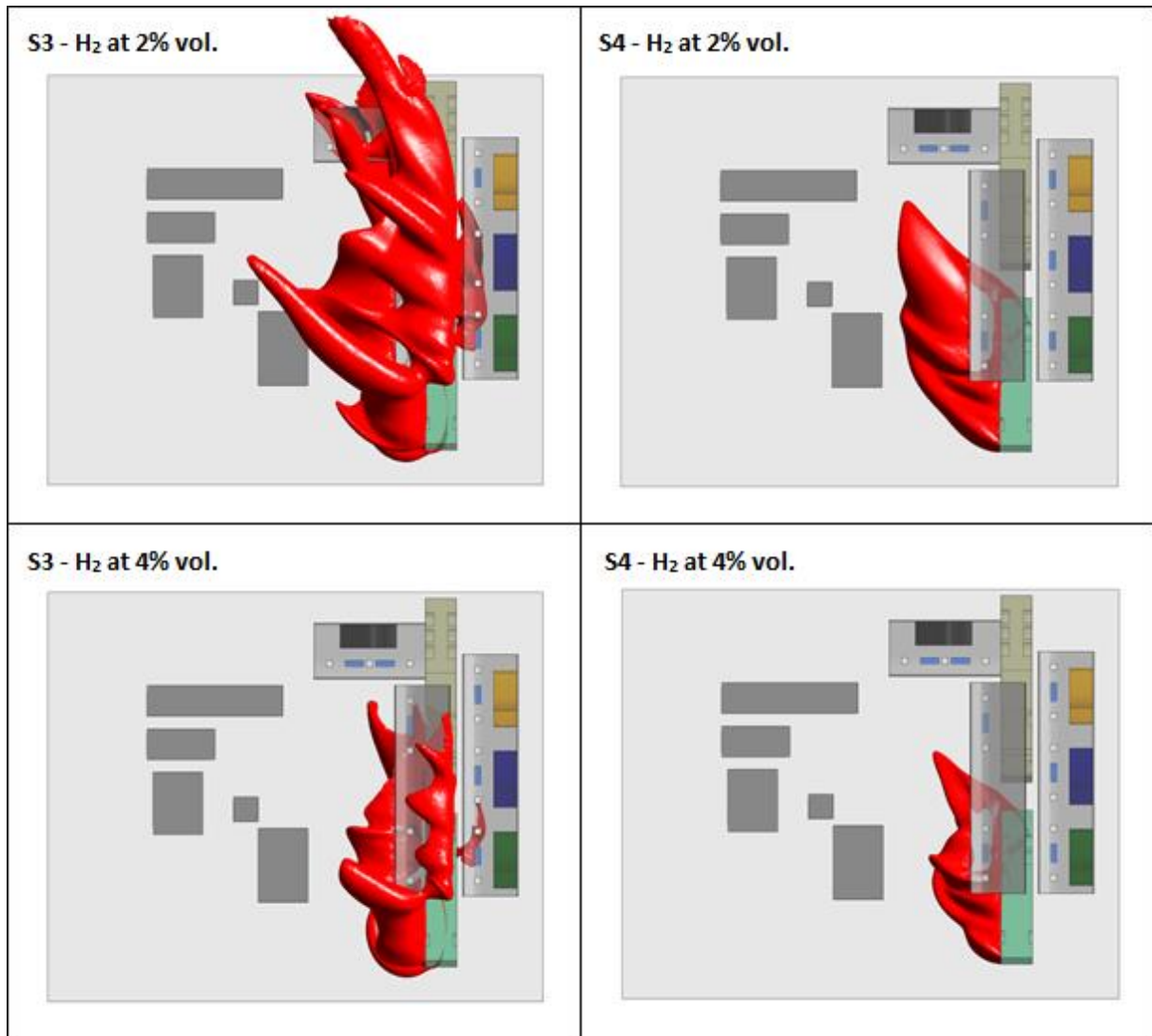
#### 4.3.3 Scenarios 3 & 4

Scenarios 3 (F1.5) and 4 (D5) involve a full bore rupture of a 3/8 inch, 350 bar H<sub>2</sub> delivery hose on forecourt Configuration 1. The release results in an H<sub>2</sub> mass flow rate of 120 g/s, corresponding to the maximum delivery flow rate of the dispenser. Full details of the set up are described in Sections 4.1 and 4.1.4.1.

Figure 47 shows a comparison of the H<sub>2</sub>/air cloud spread at 2% and 4% (v/v) concentrations, as predicted using CFX. It is clear from the Figure that the F1.5 weather condition (Scenario 3) results



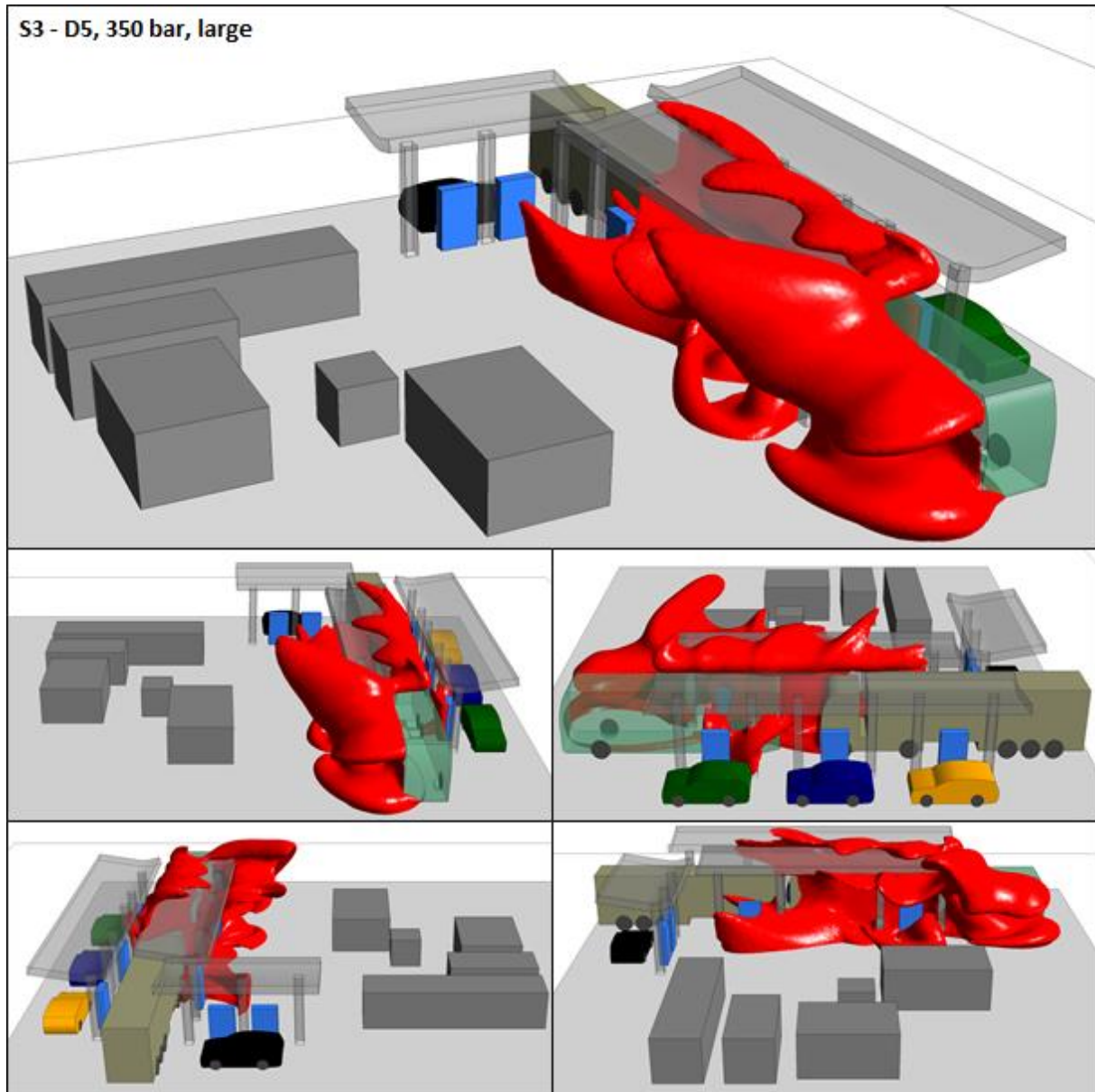
in a much larger flammable cloud. For Scenario 3, the  $\frac{1}{2}$  LFL cloud extends beyond the limits of the forecourt area (shaded light grey) and engulfs a large proportion of the refuelling area in the forecourt configuration used. Thus, this release scenario presents a significant hazard, particularly to people on site during such a release.



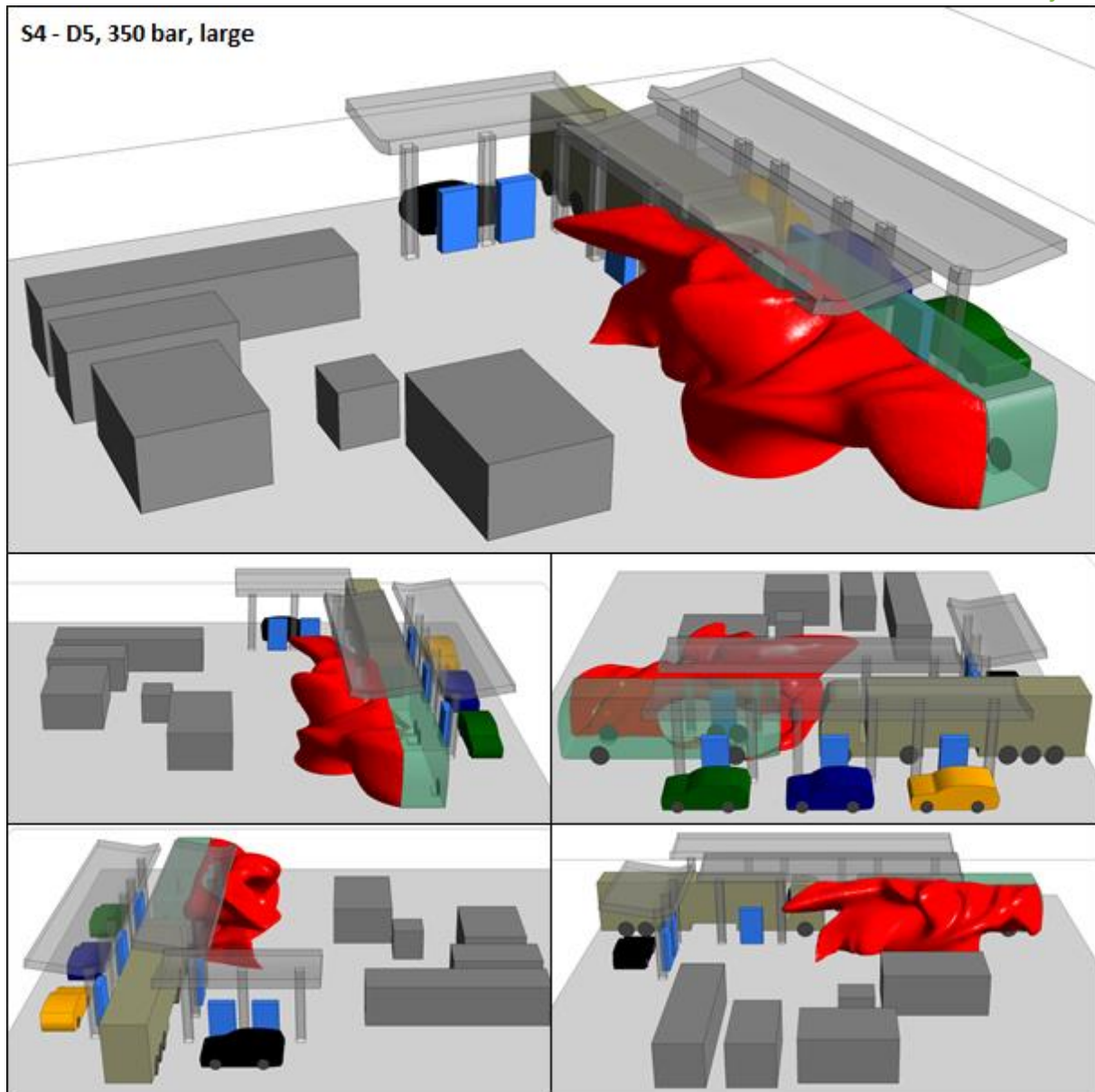
**Figure 47 – Plan-view of H<sub>2</sub>/air cloud at the  $\frac{1}{2}$  LFL (2% vol.) and LFL (4% vol.) concentrations for Scenarios 3 (F1.5) & 4 (D5) as predicted using CFX**

Figure 48 and Figure 49 present perspective views of the flammable cloud, i.e. where the H<sub>2</sub> concentration is between 4% and 75% (v/v), for Scenarios 3 and 4, respectively. The full bore release modelled for these scenarios clearly results in a significantly sized flammable cloud. For both the F1.5 and D5 wind conditions, the flammable region engulfs the dispenser area and the full length of the vehicle being refuelling (a bus in this instance). For Scenario 3 there is substantial interaction of the flammable cloud with the canopies above the refuelling areas and gas accumulates in the low-speed recirculation regions to the leeward side of other obstacles on the forecourt. For the higher wind speed case, Scenario 4, the flammable cloud remains below the canopy and stays together more as a single cloud structure. This is likely as a consequence of increased turbulent mixing giving more effective dilution of the cloud. Consequently, the flammable region is limited to a reduced volume for Scenario 4 than for Scenario 3. It should be noted that these results are based on the use of a RANS turbulence model, which

averages out much of the turbulence behaviour. In reality concentrations may fluctuate significantly in the region downstream of the dispenser and around the bus.



**Figure 48 – Perspective view of the flammable cloud (iso-surface showing H<sub>2</sub> at 4% vol.) for Scenario 3 (F1.5) as predicted using CFX**



**Figure 49 – Perspective view of the flammable cloud (iso-surface showing H<sub>2</sub> at 4% vol.) for Scenario 4 (D5) as predicted using CFX**

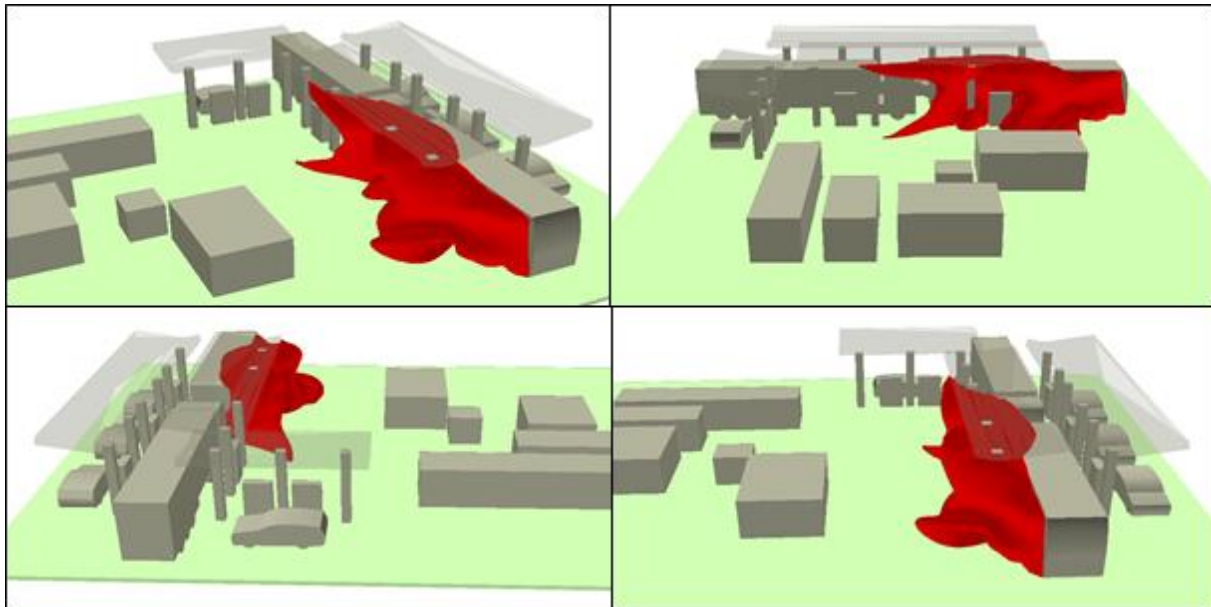
For the purposes of comparison, Scenario 4 was also simulated with KFX. This enables *cross-validation* between the CFX and KFX results to give an insight into how predictions from the two models compare. From such comparisons, it is also possible to infer how different scenarios compare, even if simulated with different models.

Figure 50 presents the KFX results for Scenario 4, showing the flammable cloud from a range of perspectives. Comparing the results shown in Figure 49 and Figure 50 illustrates that the modelling performed with CFX and KFX both results in very similar dispersion behaviour. The major qualitative features of the cloud are represented in the solutions from both models, with the gas cloud contained below the canopy. It is clear from the model results that there is significant shelter from the wind provided by the bus adjacent to the leaking dispenser, and this will clearly impact the shape and size of the predicted flammable clouds.

For both Scenarios 3 and 4, the CFX predictions of the mass of H<sub>2</sub> within the flammable cloud



exceeds 1 kg and the volume of the flammable cloud is substantial at approximately 230 m<sup>3</sup> and 200 m<sup>3</sup> for Scenarios 3 and 4, respectively. In comparison, KFX gives a predicted flammable volume of 132 m<sup>3</sup> for Scenario 4. Clearly there is a relatively large deviation between the two sets of model results, with CFX giving more conservative estimates of the flammable volume. However, the general agreement qualitatively between the predicted cloud shapes is good, showing that the two sets of simulations are broadly in line with each other, despite the use of different models.



**Figure 50 – Perspective view of the flammable cloud (iso-surface showing H<sub>2</sub> at 4% vol.) for Scenario 4 (D5) as predicted using KFX**

#### 4.3.4 Scenarios 7 & 8

Scenarios 7 (F1.5) and 8 (D5) involve a full bore rupture of a 700 bar light duty H<sub>2</sub> delivery hose on forecourt Configuration 1. The release results in an H<sub>2</sub> mass flow rate of 60 g/s, corresponding to the maximum delivery flow rate of the dispenser. As a consequence of the forecourt design, the dispenser at which the release is assumed to occur is located in a different position to the location used for the scenarios previously discussed. Full details of the setup are given in Sections 4.1 and 4.1.4.2.

Figure 51 shows a comparison of the H<sub>2</sub>/air cloud spread at 2% and 4% (v/v) concentrations for Scenarios 7 and 8. The results presented in the Figure were taken from CFX simulations. The two different wind conditions used, namely F1.5 and D5, clearly result in some significant differences in dispersion behaviour, flammable cloud size and extent.

For these two scenarios, the vehicle adjacent to the release location provides far less protection from the wind than was the case for the scenarios in which the jet impinges on the side of a bus. As a consequence, there is a more complex wind-induced flow field in the vicinity of the release as the wind catches the leading edges of the car, resulting in heavily disrupted flow onto the dispenser. Similarly, as the jet release impinges on the vehicle adjacent to the dispenser, the flow field that is formed by jet/obstacle interaction is far more complex than when the release impinged on the larger bus. These two features of the flow make for a turbulent flow field, causing the interesting cloud shapes shown in Figure 51.

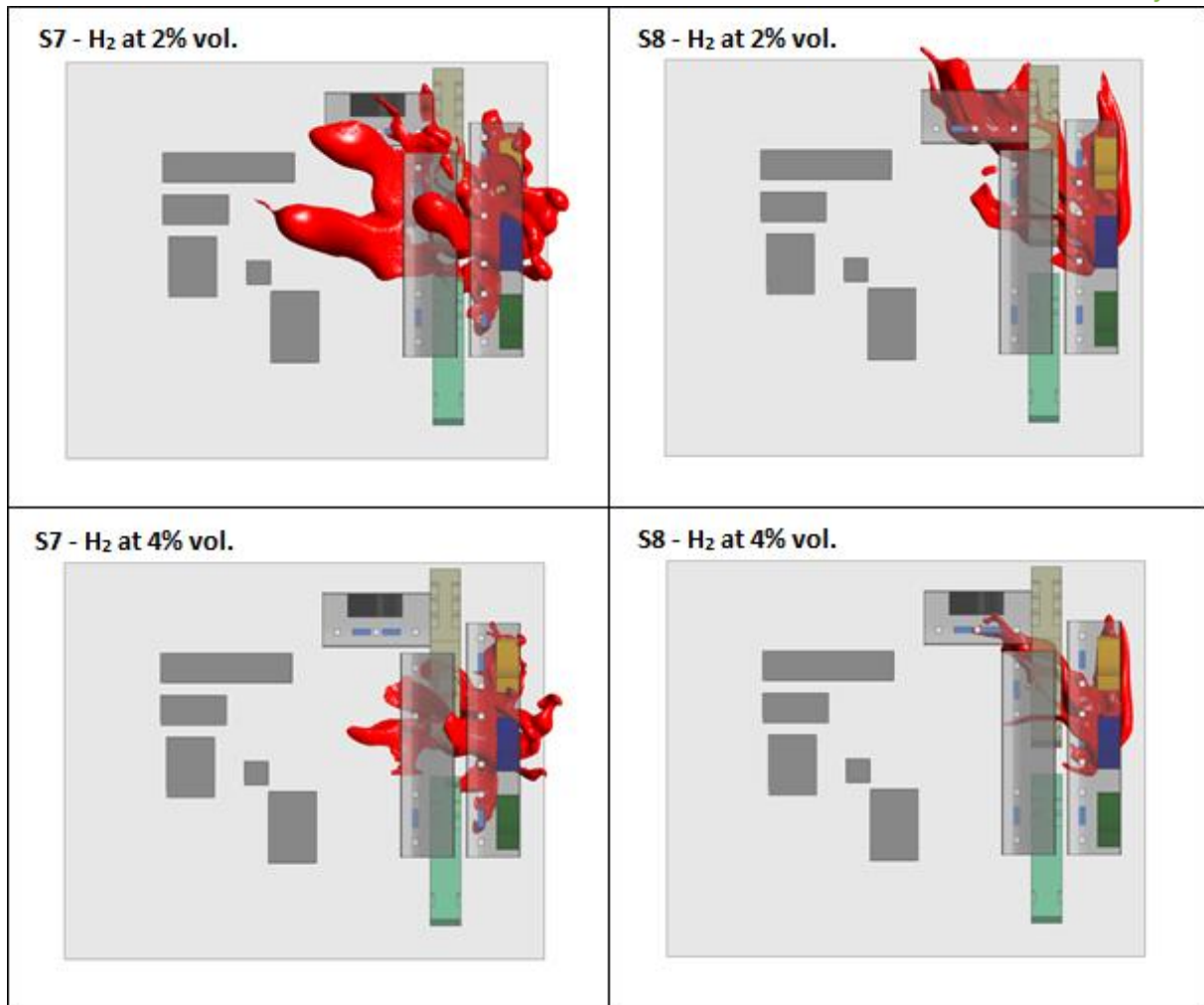


**Figure 51 – Plan view of H<sub>2</sub>/air cloud at the ½ LFL (2% vol.) and LFL (4% vol.) concentrations for Scenarios 7 (F1.5) & 8 (D5) as predicted using CFX**

Comparison of the ½ LFL cloud shapes shown in Figure 51 demonstrates that the two different wind conditions give slightly different general trajectories of the cloud. For the D5 case, Scenario 8, the H<sub>2</sub>/air cloud generally moves in the direction of the wind, i.e. from the bottom-right to the top-left of the image, whereas for the F1.5 conditions, Scenario 7, the cloud generally moves into the centre of the forecourt. This illustrates that the higher wind speed in Scenario 8 has more influence on the overall H<sub>2</sub> dispersion than for Scenario 7, where the flow induced by the jet release, and its interaction with obstacles, dominates.

Figure 52 and Figure 53 present perspective views of the flammable cloud, i.e. where the H<sub>2</sub> concentration is between 4% and 75% (v/v), for Scenarios 7 and 8, respectively. One immediately obvious difference between the two Scenarios is the height of the flammable cloud. For Scenario 7, the case with F1.5 wind conditions, the cloud rises more significantly than for Scenario 8 and as a result interacts with the canopies above the dispensing areas of the forecourt.

Again, as was the case when comparing Scenarios 3 and 4, the case with D5 wind conditions, Scenario 8, results in a flammable cloud with more smoothly rounded edges and fewer offshoots, particularly on the upwind side. Conversely, Figure 52 shows *fingers* of the cloud jutting off in different directions for Scenario 7, where the wind speed is lower.

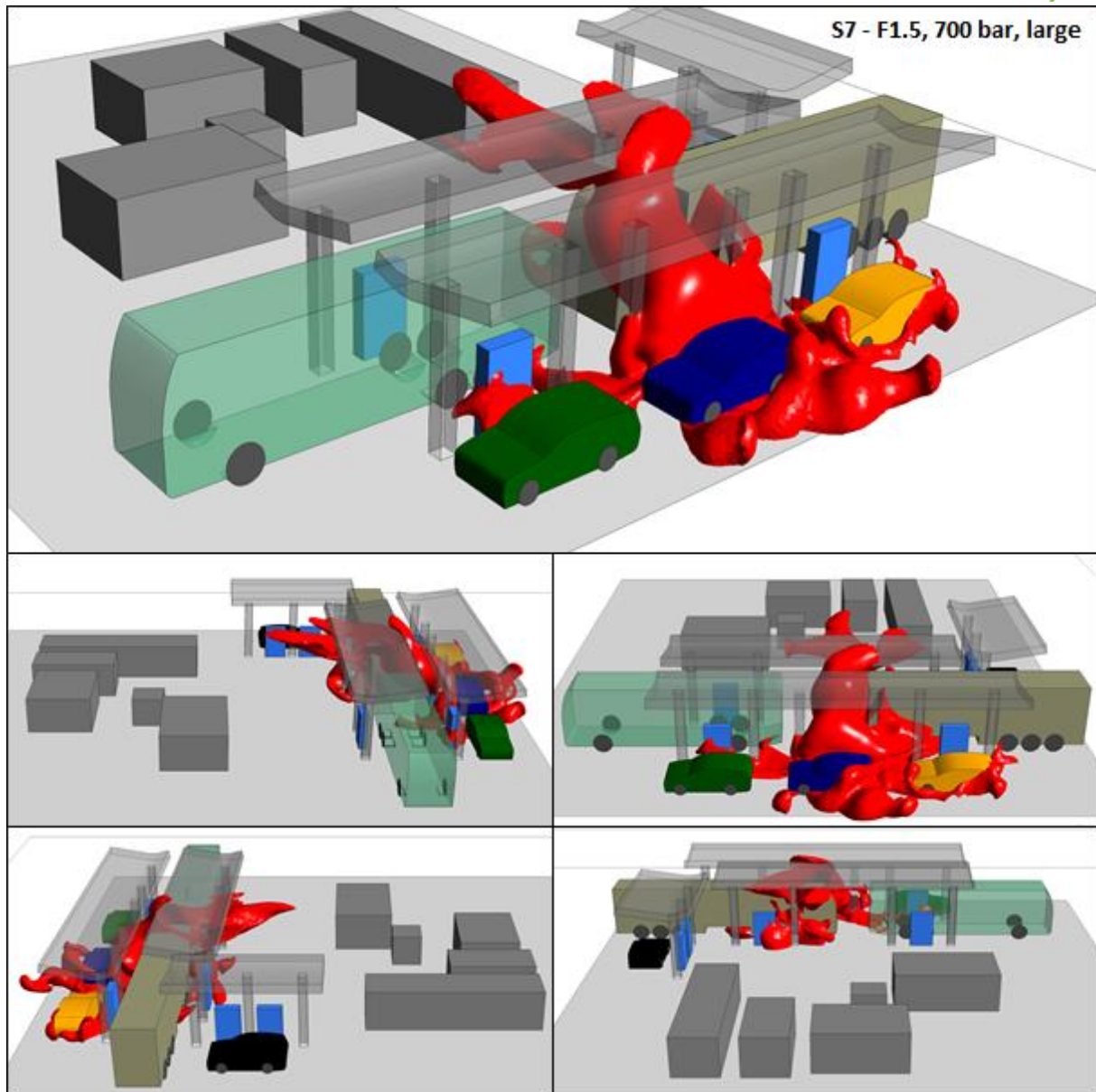
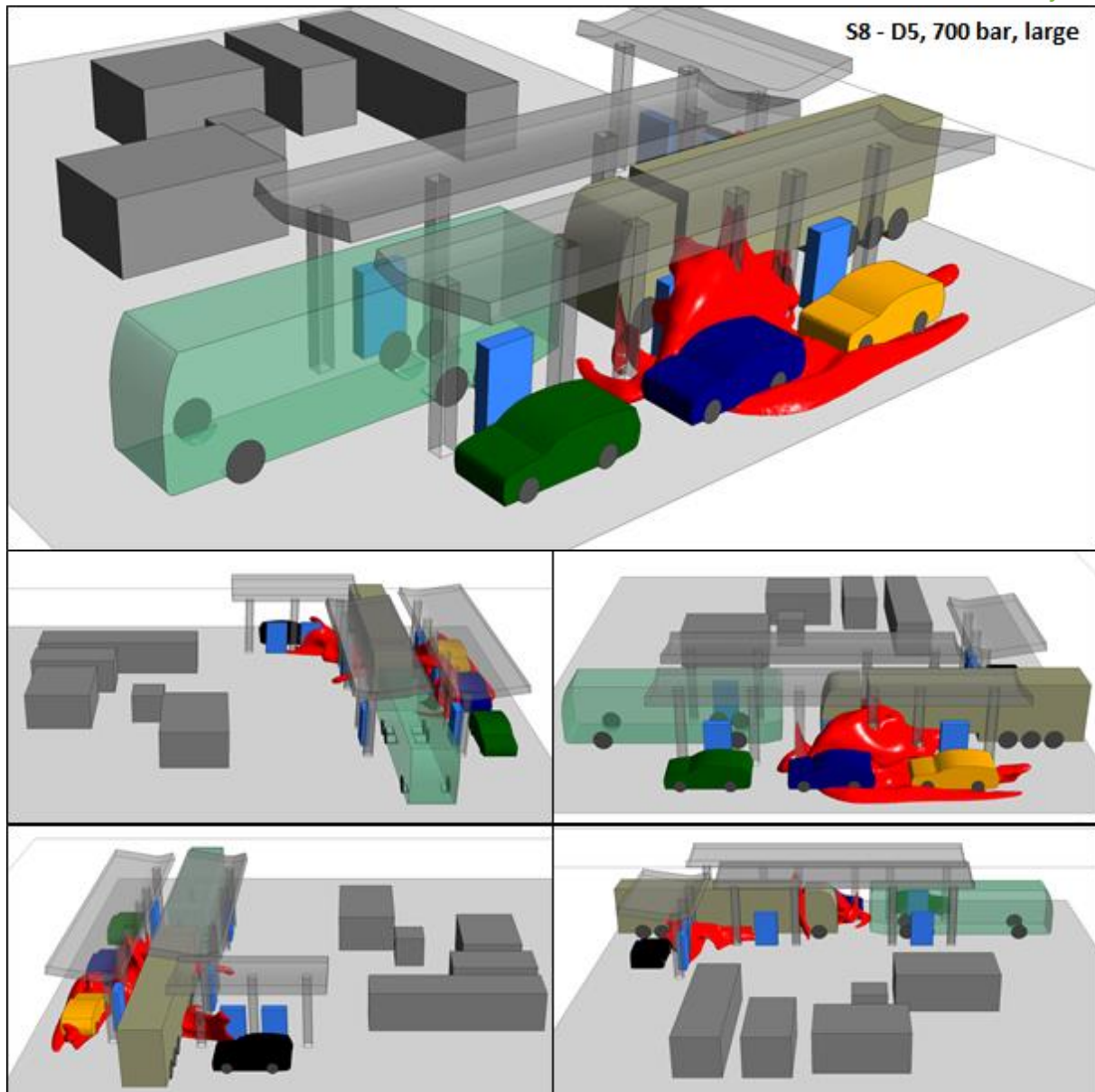


Figure 52 – Perspective view of the flammable cloud (iso-surface showing  $H_2$  at 4% vol.) for Scenario 7 (F1.5) as predicted using CFX



**Figure 53 – Perspective view of the flammable cloud (iso-surface showing H<sub>2</sub> at 4% vol.) for Scenario 8 (D5) as predicted using CFX**

In terms of the overall size of the flammable cloud, the CFX predictions give flammable volumes of around 100 m<sup>3</sup> and 50 m<sup>3</sup> for Scenarios 7 and 8, respectively. This is the most significant variation across the two wind conditions for all scenarios based on Configuration 1. There is a similar difference between the mass of H<sub>2</sub> within the flammable cloud at 0.55 kg and 0.28 kg for Scenarios 7 and 8, respectively.

#### 4.3.5 Scenarios 9 & 10

Scenarios 9 (F1.5) and 10 (D5) involve releases from a 350 bar H<sub>2</sub> delivery hose through an opening size equal to 10% of the hose diameter, approximately 0.95 mm. The geometry used for these scenarios is forecourt Configuration 2 (see Section 4.1.2 and 7.1.2). The release results in an H<sub>2</sub> mass flow rate of 14.8 g/s. These two scenarios are comparable to Scenarios 1 & 2 in terms of the H<sub>2</sub> release modelled. Full details of the setup are described in Sections 4.1.



Figure 54 shows perspective views of the H<sub>2</sub>/air clouds at concentrations of 2% and 4% (v/v), i.e. the ½ LFL and LFL concentrations, respectively, as predicted using OpenFOAM 1812. The Figure shows iso-surfaces at these concentrations in yellow. The Figure demonstrates that OpenFOAM predicts a larger flammable volume for Scenario 9, with F1.5 wind conditions, than Scenario 10, with D5 conditions. This is more clearly evident for the ½ LFL cloud, as was also the case when comparing Scenarios 1 and 2.

Comparing Figure 54 with Figure 45 and Figure 46, which show results for Scenarios 1 and 2, respectively, illustrates that CFX and OpenFOAM 1812 predict similar features of the flammable cloud shape for the same H<sub>2</sub> releases. Whilst different forecourt geometries were used across the scenarios, the main features of the flammable cloud appear similar, with *fingers* forming around the base of the dispenser and the cloud shape principally dictated by the flow formed by the jet impinging on the side of the vehicle. Similarly to Scenarios 1 and 2, the cloud defined by the ½ LFL concentration of H<sub>2</sub> is significantly larger than the LFL cloud.

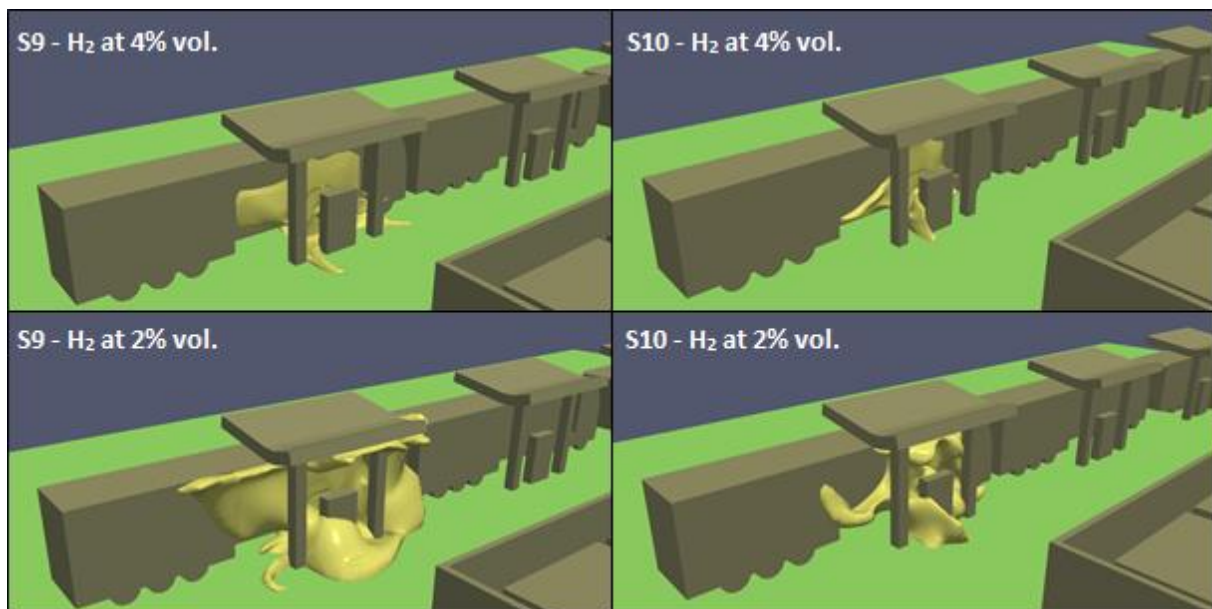


**Figure 54 – H<sub>2</sub>/air cloud at the ½ LFL (2% vol.) and the LFL (4% vol.) concentrations for Scenarios 9 (F1.5) & 10 (D5) as predicted using OpenFOAM 1812**

For Scenarios 9 and 10 the flammable volumes predicted with OpenFOAM 1812 are approximately 4.6 m<sup>3</sup> and 3.0 m<sup>3</sup>, respectively. These volumes are similar to those predicted using CFX for Scenarios 1 and 2, although the OpenFOAM results give a larger difference between the two wind conditions modelled.

#### 4.3.6 Scenarios 11 & 12

Scenarios 11 (F1.5) and 12 (D5) involve a full bore rupture of a 3/8 inch, 350 bar H<sub>2</sub> delivery hose on forecourt Configuration 2. The release results in an H<sub>2</sub> mass flow rate of 120 g/s, corresponding to the maximum delivery flow rate of the dispenser. Full details of the set up are described in Sections 4.1 and 4.1.4.3. In terms of the releases modelled, these scenarios are comparable to Scenarios 3 and 4.

Figure 55 shows a comparison of the H<sub>2</sub>/air cloud spread at 2% and 4% (v/v) concentrations predicted using OpenFOAM 1812. The Figure shows that Scenario 11, which uses F1.5 wind

conditions, results in a much larger, and more complex, cloud structure than is the case where D5 conditions were used in Scenario 12. This behaviour is consistent with the CFX results for Scenarios 3 and 4, i.e. the corresponding cases based on forecourt Configuration 1.

Comparing Figure 55 to Figure 47 shows a number of similarities in the dispersion behaviour between Scenarios 11 & 12 and Scenarios 3 & 4. Specifically, the D5 cases (Scenarios 4 and 12) result in more smoothly defined cloud geometries, whereas for the F1.5 cases (Scenarios 3 and 11), there are large offshoots of the gas clouds, particularly those defined by the  $\frac{1}{2}$  LFL concentration of  $H_2$ .

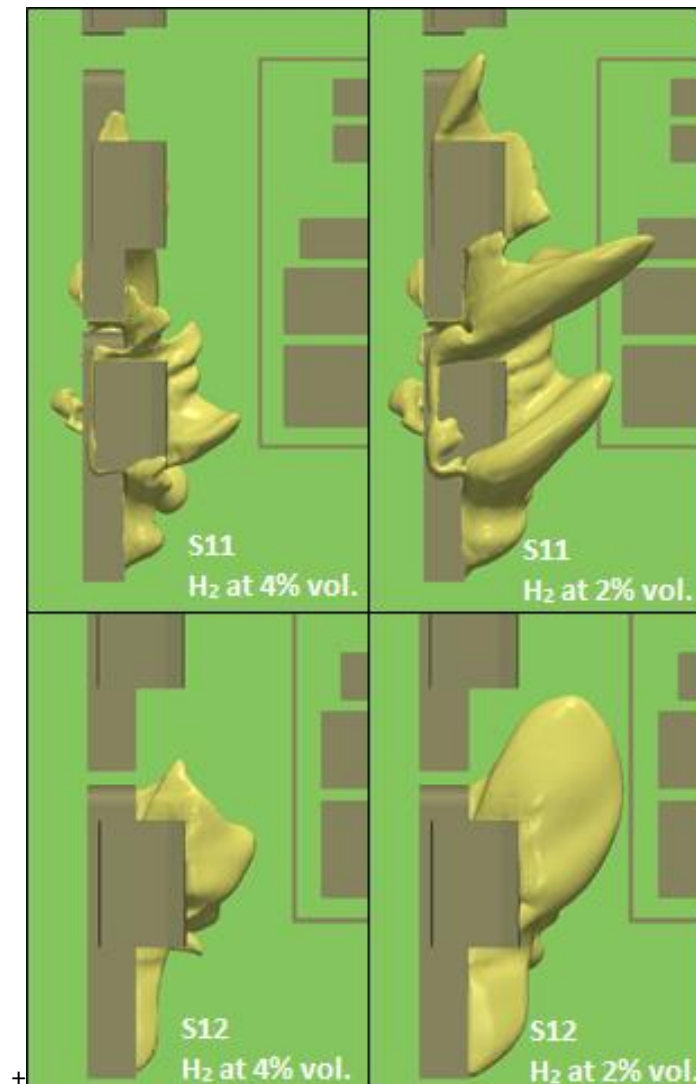


**Figure 55 – Plan view of  $H_2$ /air cloud at the  $\frac{1}{2}$  LFL (2% vol.) and LFL (4% vol.) concentrations for Scenarios 11 (F1.5) & 12 (D5) as predicted using OpenFOAM 1812**

In addition to the OpenFOAM 1812 simulations of Scenarios 11 & 12, the two scenarios were also modelled using KFX as a means of *cross-validation* between models. Figure 57 shows the KFX predicted  $H_2$ /air clouds at 2% and 4% (v/v) concentrations of  $H_2$  for Scenarios 11 and 12. Comparing the predictions to the cloud shapes/sizes obtained using OpenFOAM, as shown in Figure 56, indicates broadly comparable behaviour across the two sets of model results. Given that the OpenFOAM results also show similar behaviour to predictions made using CFX for comparable releases, this gives confidence in the general dispersion behaviour and cloud shapes predicted by the range of models used.

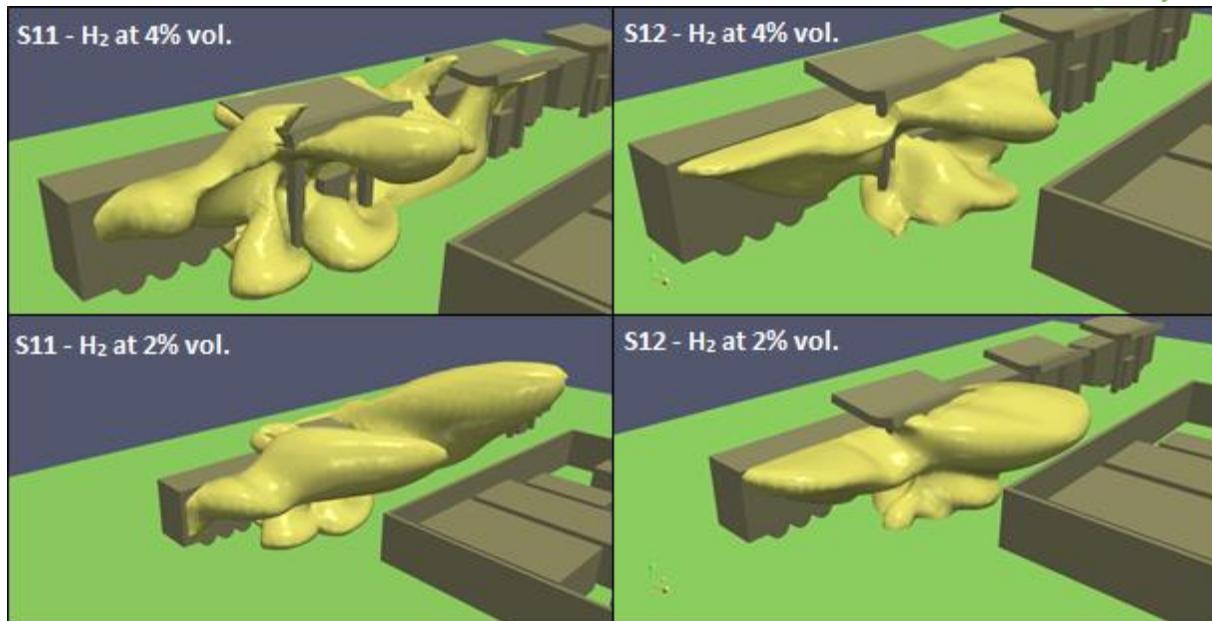


**Figure 56 – H<sub>2</sub>/air cloud at the ½ LFL (2% vol.) and the LFL (4% vol.) concentrations for Scenarios 11 (F1.5) & 12 (D5) as predicted using OpenFOAM 1812**

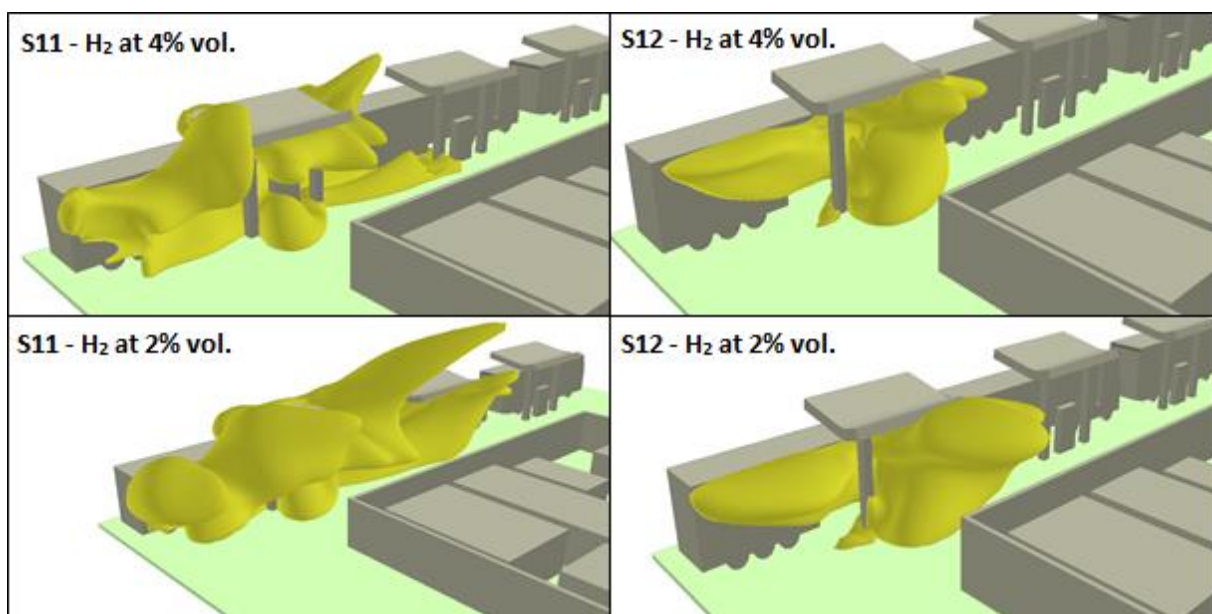


**Figure 57 – H<sub>2</sub>/air cloud at the ½ LFL (2% vol.) and the LFL (4% vol.) concentrations for Scenarios 11 (F1.5) & 12 (D5) as predicted using KFX**

For Scenarios 11 and 12 the flammable volumes predicted with OpenFOAM 1812 are 186 m<sup>3</sup> and 117 m<sup>3</sup>, respectively. These values exceed the KFX predictions of 155 m<sup>3</sup> and 85 m<sup>3</sup> for Scenarios 11 and 12, respectively.

#### 4.3.7 Scenarios 15 & 16

Scenarios 15 (F1.5) and 16 (D5) involve a full bore rupture of a 700 bar, light duty H<sub>2</sub> dispenser hose on forecourt Configuration 2. The release results in an H<sub>2</sub> mass flow rate of 60 g/s, corresponding to the maximum H<sub>2</sub> delivery flow rate of the dispenser. Full details of the set up are described in

Sections 4.1 and 4.1.4.4. These scenarios are equivalent to Scenarios 7 and 8, but using an alternative forecourt geometry.

Figure 58 compares plan views of the H<sub>2</sub>/air cloud defined by the ½ LFL and LFL concentrations Scenarios 15 and 16 as predicted using OpenFOAM 1812. The Figure illustrates that the two different wind conditions used result in significantly different cloud shapes and sizes, as was the case for the equivalent scenarios using Configuration 1, namely Scenarios 7 and 8.

For Scenario 16, the cloud trajectory is broadly in line with the wind direction, most clearly shown by the ½ LFL cloud in Figure 58. Conversely, for Scenario 15, the model predicts multi-directional spread of the cloud, resulting in a larger flammable volume. These OpenFOAM results are consistent with the predictions made using CFX for Scenarios 7 and 8, which showed similar behaviour with regards to the cloud shape and direction(s) of travel.

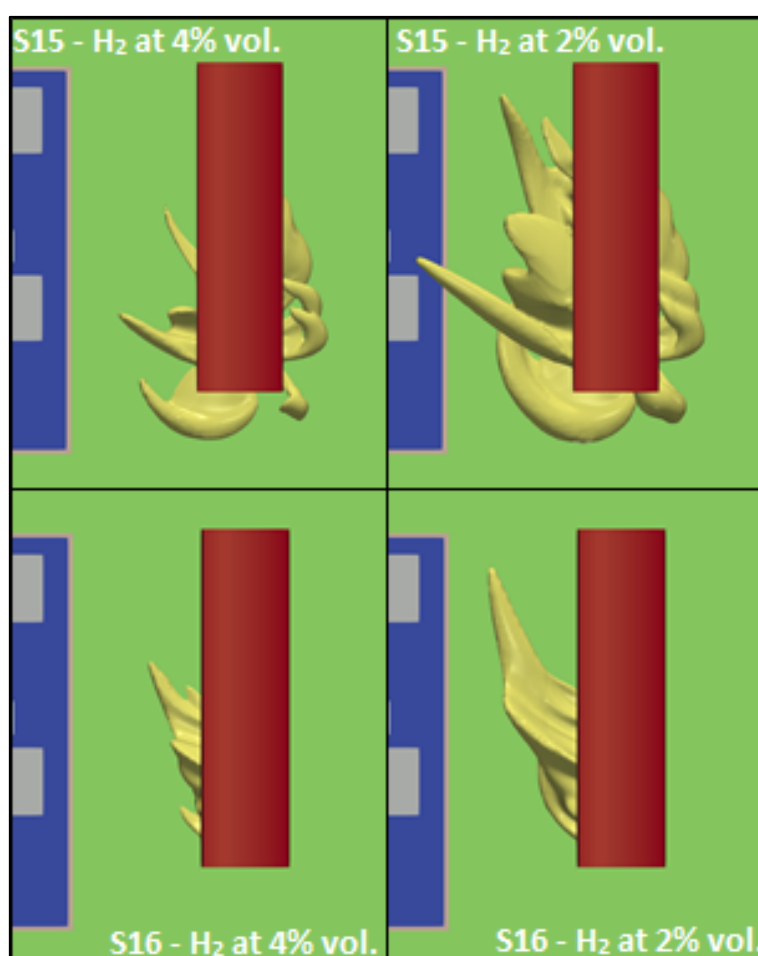


**Figure 58 – Plan view of H<sub>2</sub>/air cloud at the ½ LFL (2% vol.) and LFL (4% vol.) concentrations for Scenarios 15 (F1.5) & 16 (D5) as predicted using OpenFOAM 1812**

Figure 59 further illustrates the cloud shapes predicted for Scenarios 15 and 16 using OpenFOAM. The Figure shows perspective views of the H<sub>2</sub>/air clouds at the ½ LFL and LFL concentrations of H<sub>2</sub>. From this Figure, it is clear that the D5 wind conditions in Scenario 16 results in a cloud with reduced depth as compared to the cloud shape/size predicted for Scenario 15, with lower wind speed. Again, as has been a common theme throughout the realistic release modelling, the cloud shape under F1.5 conditions is more varied, with numerous offshoots in different directions.



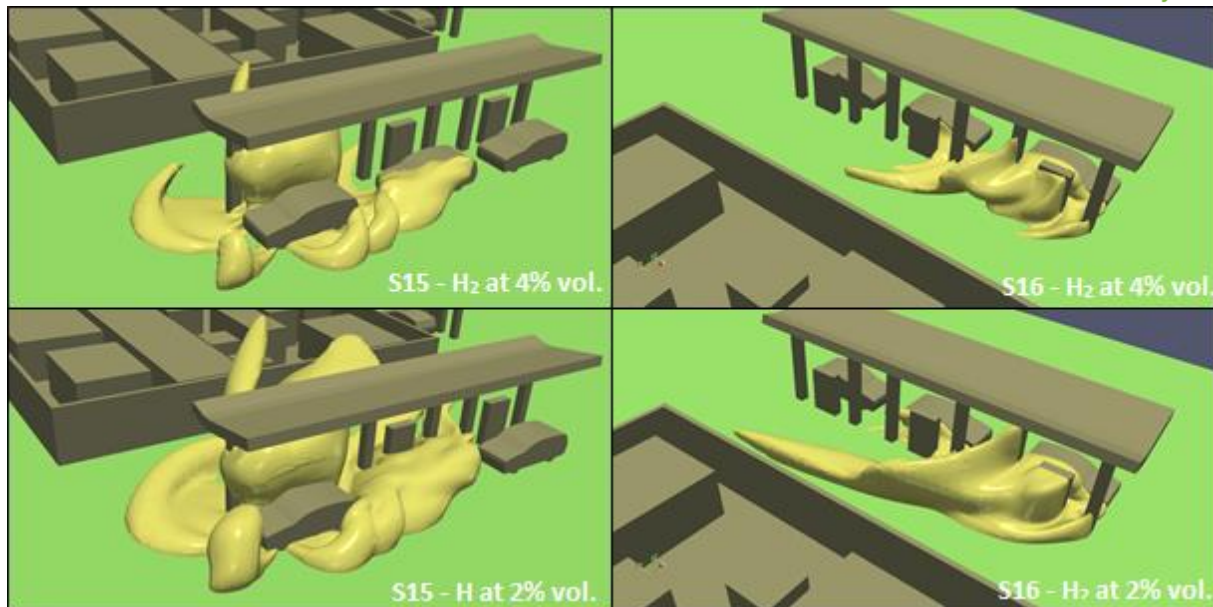


**Figure 59 – H<sub>2</sub>/air cloud at the ½ LFL (2% vol.) and the LFL (4% vol.) concentrations for Scenarios 15 (F1.5) & 16 (D5) as predicted using OpenFOAM 1812**

Figure 60 shows similar perspective views of the ½ LFL and LFL clouds for Scenarios 15 and 16 as predicted using KFX. Again, this is for the purposes of cross-validation between models and in order to see how predicted release behaviour varies with model choice. Comparison of Figure 59 and Figure 60 shows that there are a number of features of the H<sub>2</sub>/air cloud shapes that are captured by both OpenFOAM and KFX, most notably, the more compact cloud for Scenario 16 and the more chaotic cloud shape seen for Scenario 15. For Scenario 16, OpenFOAM clearly gives a larger downwind cloud extent, with a long tail predicted for the ½ LFL cloud in particular. Whereas for that Scenario, KFX gives a more bulbous cloud, confined around the region of the dispenser at which the H<sub>2</sub> release occurs.

Whilst there are some specific discrepancies in the predicted cloud shapes across the two sets of model predictions, the overall broad agreement in qualitative behaviour of the H<sub>2</sub> dispersion gives some confidence in the predictions as a whole.

For Scenarios 15 and 16 the flammable volumes predicted with OpenFOAM 1812 are 55 m<sup>3</sup> and 32 m<sup>3</sup>, respectively. For comparison, the KFX predictions give flammable volumes of 47 m<sup>3</sup> and 40 m<sup>3</sup> for Scenarios 15 and 16, respectively.

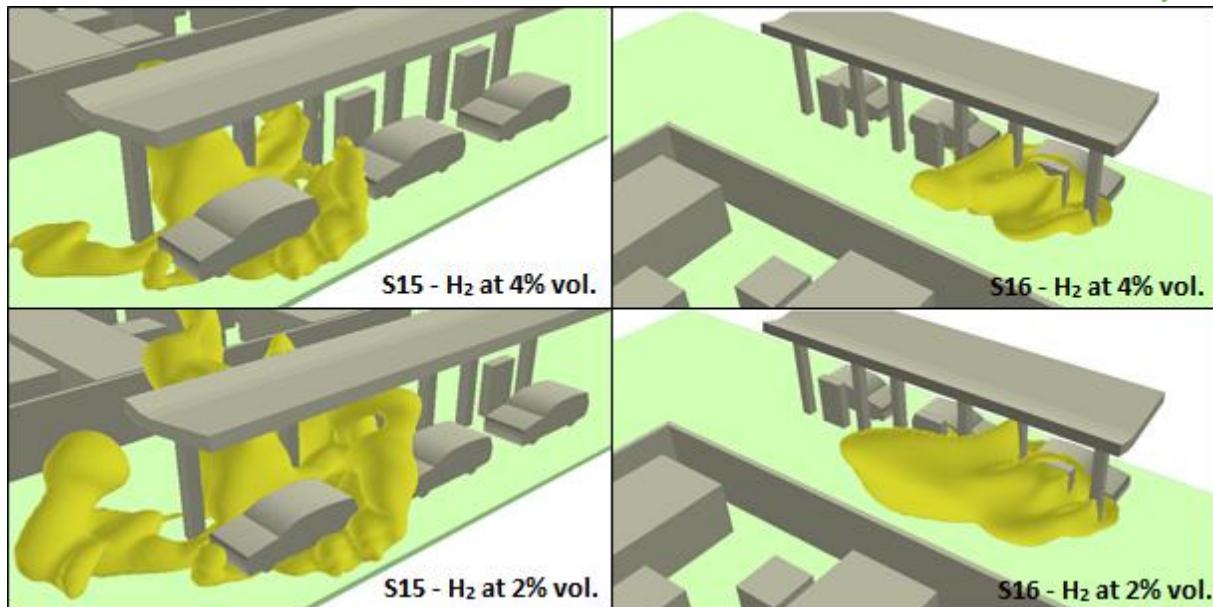


**Figure 60 – H<sub>2</sub>/air cloud at the ½ LFL (2% vol.) and the LFL (4% vol.) concentrations for Scenarios 15 (F1.5) & 16 (D5) as predicted using KFX**

#### 4.3.8 Scenarios 17 & 18

Scenarios 17 (F1.5) and 18 (D5) represent the first two cases where the release is modelled as emanating from pipework within the dispenser housing. These cases involve releases at 1000 bar through a 0.2 mm diameter hole in dispenser pipework, which results in an H<sub>2</sub> mass flow rate of 1.5 g/s. For these scenarios, forecourt Configuration 3 is used. The specific details of the scenarios can be found in Sections 4.1 and 4.1.4.5 and the manner in which the source term is captured in the CFD model is described in Section 4.1.6.

Figure 61 shows a comparison of the H<sub>2</sub>/air cloud spread at 2% and 4% (v/v) concentrations, i.e. the ½ LFL and LFL, respectively, for Scenarios 17 and 18. The results are taken from FLACS modelling of these scenarios. For both scenarios, the size of both the LFL and ½ LFL clouds are small, with very little interaction with the surrounding obstacles. What is clear from the Figure is that the cloud volume is larger for the lower wind speed case, Scenario 17, which is to be expected since this wind condition is likely to result in lower turbulent mixing of the cloud, and thus reduced levels of dilution compared to Scenario 18 in which a greater wind speed was used.

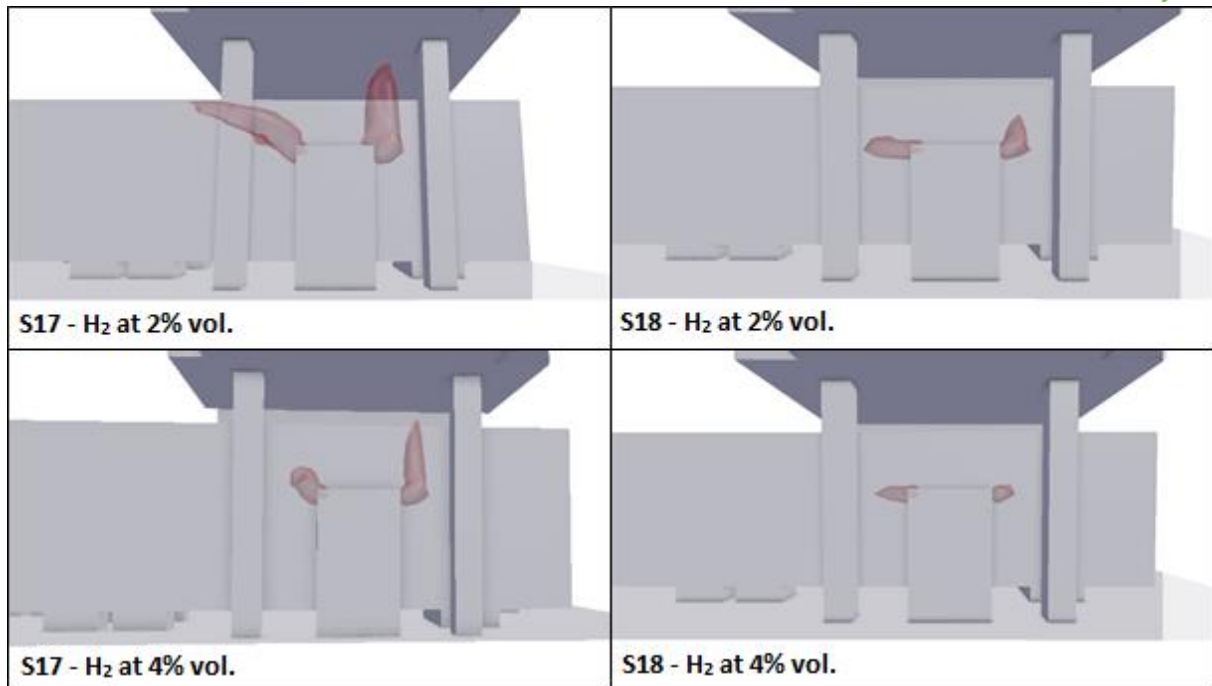


**Figure 61 – Perspective view of the H<sub>2</sub>/air cloud at the LFL and ½ LFL concentrations for Scenarios 17 (F1.5) and 18 (D5) as predicted with FLACS**

The predicted cloud volumes for these two cases are significantly smaller than for the other scenarios considered due to the substantially lower H<sub>2</sub> mass flow rate of 1.5 g/s. For these two cases the predicted flammable volumes, i.e. where the H<sub>2</sub> concentration is between 4% and 75% (v/v), were approximately 0.3 m<sup>3</sup> and 0.1 m<sup>3</sup> for Scenarios 17 and 18, respectively. Regarding the mass of H<sub>2</sub> within those flammable clouds, the model predicts 1.8 g and 0.6 g of H<sub>2</sub> in the cloud for Scenarios 17 and 18, respectively.

It should be noted that the results for the internal release scenarios (Scenarios 17–20) do not account for the H<sub>2</sub>/air mixture inside the dispenser itself, which may contribute significantly to the risk. For example, if the mixture inside the dispenser is within the flammability limits, then ignition of that mixture could generate a significant overpressure hazard, which is not accounted for in the dispersion modelling presented here.

#### 4.3.9 Scenarios 19 & 20

Scenarios 19 (F1.5) and 20 (D5) are the other two scenarios that also involve releases from pipework inside the dispenser casing. For these cases, the assumed leak is through an opening size corresponding to 10% of the diameter of the pipework, approximately 0.95 mm. It is assumed that the pipework has already undergone a pressure drop down to a dispensing pressure of 350 bar therefore, the H<sub>2</sub> mass release rate is 14.8 g/s, as for some of the earlier scenarios described. Full details of the scenario can be found in Sections 4.1 and 4.1.4.5.

Figure 62 shows a comparison of the H<sub>2</sub>/air cloud spread at 2% and 4% (v/v) concentrations, i.e. the ½ LFL and LFL, respectively, for Scenarios 19 and 20. The Figure shows the ½ LFL cloud interacting with the canopy above the dispenser and refuelling area for both of these two Scenarios and the cloud (at both concentrations shown) extends away from the dispenser with the wind.

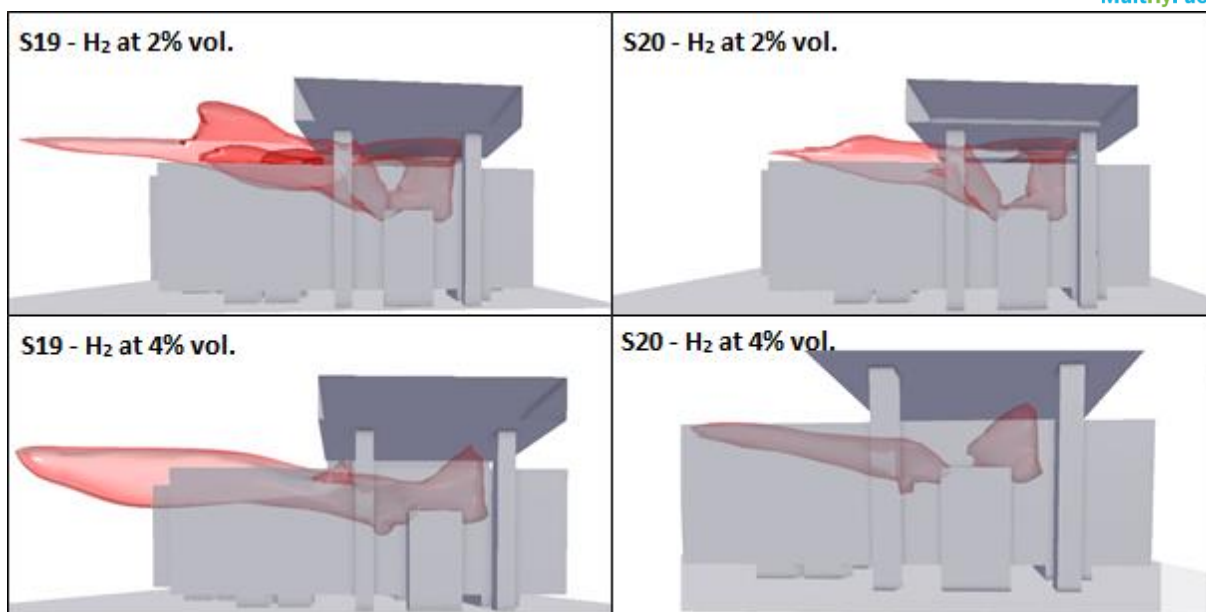


**Figure 62 – Perspective view of the H<sub>2</sub>/air cloud at the LFL and ½ LFL concentrations for Scenarios 19 (F1.5) and 20 (D5) as predicted with FLACS**

The F1.5 wind condition used in Scenario 19 results in a significantly larger flammable volume than the case with D5 conditions, i.e. Scenario 20. This is consistent with the general results seen across the range of other scenarios modelled. This is expected since the lower wind speeds associated with F1.5 lead to a reduction in turbulent mixing and dilution of the cloud occurs at a slower rate and over a larger region. For these two cases, the predicted flammable volumes and masses of H<sub>2</sub> in the cloud are approximately 7.6 m<sup>3</sup> and 49 g, respectively, for Scenario 19. For Scenario 20, these figures are approximately 2.3 m<sup>3</sup> for the flammable volume and 16 g for the mass of H<sub>2</sub> in the cloud.

Across both pairs of internal release scenarios (Scenarios 17–20) the F1.5 wind condition results in approximately a factor of 3 increase in both the flammable volume and mass within the resulting gas cloud. This indicates that the lower wind speed scenarios represent something closer to worst case, which is the expected result.

#### 4.3.10 Scenarios 23 & 24

Scenarios 23 (F1.5) and 24 (D5) involve releases from a 350 bar H<sub>2</sub> delivery hose through an opening with a size equal to 10% of the hose diameter, approximately 0.95 mm. The geometry used for these scenarios is forecourt Configuration 3 (see Section 4.1.3 and 7.1.3). The release results in an H<sub>2</sub> mass flow rate of 14.8 g/s. Full details of the set up are described in Sections 4.1.

The intention for these two scenarios was to simulate them using OpenFOAM 1912+. However, due to difficulties in getting the model to run correctly, no results have been obtained. This is not uncommon with CFD modelling as there is never a guarantee that satisfactory results will be produced. It is unfortunate in the context of this MultHyFuel task as it reduces the range of realistic release scenarios covered. However, it remains the case that the span of cases for which there are CFD model results provides sufficient information to meet the objectives of the CFD modelling work.

#### 4.3.11 Scenarios 25 & 26

Scenarios 25 (F1.5) and 26 (D5) involve a full bore rupture of a 3/8 inch, 350 bar H<sub>2</sub> delivery hose on forecourt Configuration 3. The release results in an H<sub>2</sub> mass flow rate of 120 g/s, corresponding to the maximum delivery flow rate of the dispenser. Full details of the set up are described in Sections 4.1 and 4.1.4.6.

The original intention for the realistic release modelling within MultHyFuel task 2.1.2 was for OpenFOAM 1912+ to be used to simulate the jet release scenarios involving forecourt Configuration 3. However, due to difficulties getting the model to run correctly, no results were generated using that code. As mitigation against having no results for forecourt Configuration 3 with an external H<sub>2</sub> leak (the results described for Scenarios 17 to 20 cover internal leak scenarios) additional simulations were undertaken using KFX to provide solutions for Scenarios 25 and 26. There was insufficient time and budget within the project task to run all of the Configuration 3 scenarios using KFX, so Scenarios 25 and 26 were chosen as they use an H<sub>2</sub> release condition which was also used for forecourt Configuration 1 (Scenario 3 & 4) and Configuration 2 (Scenarios 11 & 12). This enables a comparison of results across all three forecourt configurations to be made for identical H<sub>2</sub> release conditions.

Figure 63 shows plan views of the KFX predicted H<sub>2</sub>/air cloud at the ½ LFL and LFL for Scenarios 25 and 26. The Figure illustrates that the large flammable clouds are formed under both F1.5 and D5 wind conditions modelled. The ½ LFL cloud shows significant coverage of the forecourt, indicating a large area at risk of flash fire or explosion, should there be an ignition.

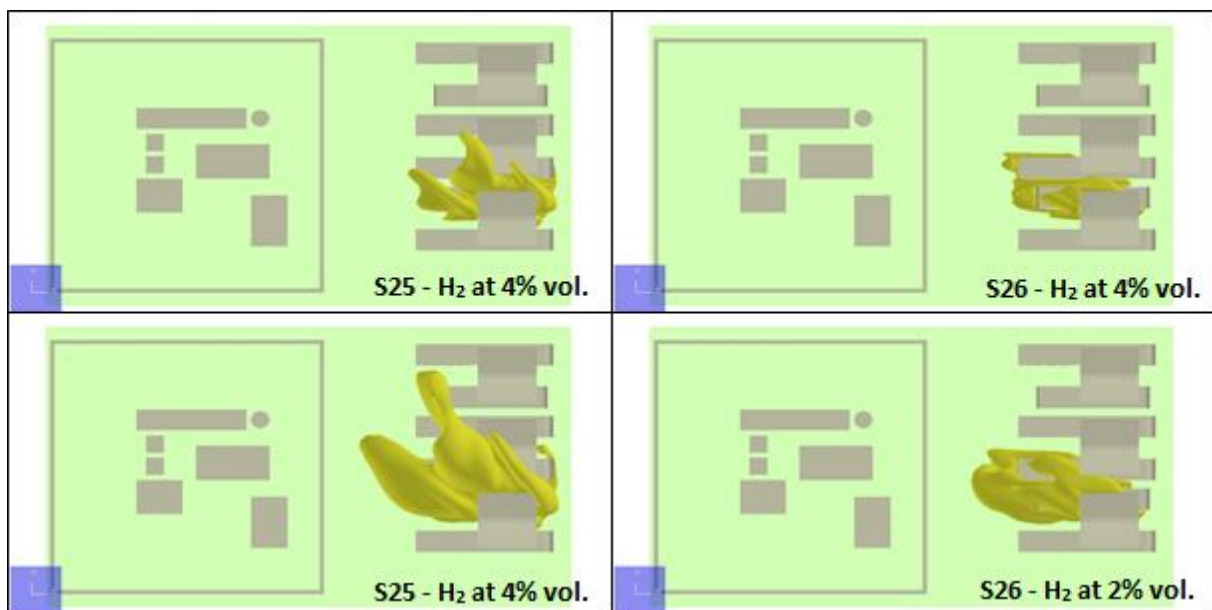


**Figure 63 – Plan view of H<sub>2</sub>/air cloud at the ½ LFL (2% vol.) and LFL (4% vol.) concentrations for Scenarios 25 (F1.5) & 26 (D5) as predicted using KFX**

Figure 64 shows perspective views of the same H<sub>2</sub>/air clouds presented in Figure 63. From Figure 64 it is clear that the F1.5 wind conditions result in significant cloud depth and extensive interaction with the canopy above the dispenser under which the release occurs. For Scenario 26, with the higher wind speed, the additional turbulence generated as the wind interacts with the vehicles and canopies increases turbulent mixing, and thus greater dilution, above the canopy, than is the case for Scenario 25. This is the likely to be the main reason for the difference in dispersion behaviour between the two cases.



It is quite difficult to draw too many comparisons between Scenarios 25 & 26 and the equivalent release scenarios for Configurations 1 and 2 due to the substantial differences in forecourt geometry. However, it is the case that F1.5 wind conditions consistently result in larger cloud volumes and that a full bore release at 120 g/s of H<sub>2</sub> produces a substantially sized cloud, and thus a significant risk of fire or explosion hazards on the forecourt.

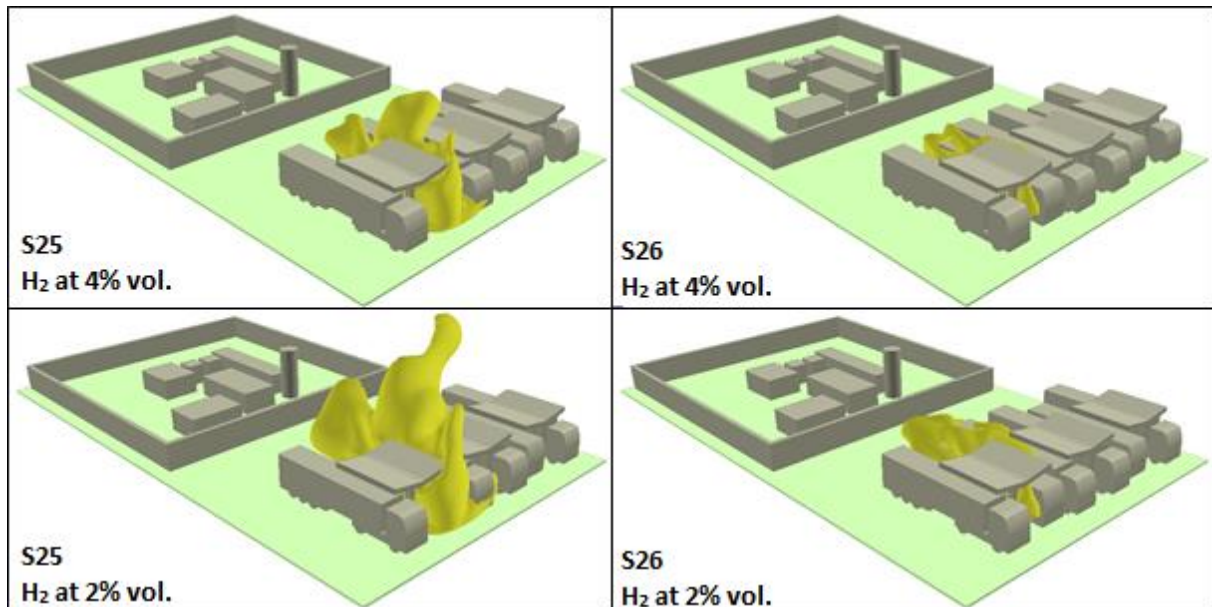


**Figure 64 – H<sub>2</sub>/air cloud at the ½ LFL (2% vol.) and the LFL (4% vol.) concentrations for Scenarios 25 (F1.5) & 26 (D5) as predicted using KFX**

For Scenarios 25 and 26 the flammable volumes predicted with KFX are 196 m<sup>3</sup> and 106 m<sup>3</sup>, respectively.

#### 4.3.12 Scenarios 27 & 28

Scenarios 27 (F1.5) and 28 (D5) involve a full bore rupture of a 3/8 inch H<sub>2</sub> delivery hose at 700 bar. These cases were intended to cover the hypothetical scenario of heavy duty refuelling at 700 bar with an H<sub>2</sub> mass flow rate of 300 g/s. Again, the intention was to simulate these scenarios using OpenFOAM 1912+, but due to the difficulties previously mentioned regarding obtaining viable solutions with that CFD model, we again have no outputs for these cases.

## 5 Discussion

### 5.1 Summary of Realistic Release Modelling Results

Figure 65 presents a summary of the flammable volumes predicted for the range of realistic release scenarios modelled. The Figure demonstrates that the F1.5 wind condition consistently results in a larger flammable cloud volume than the corresponding cases using the D5 wind condition. This is likely to be a consequence of there being less wind-induced turbulent mixing from wind interaction with the obstacles on the representative forecourts. The lower level of turbulent mixing results in less dilution of the released  $H_2$ , and thus larger flammable cloud volumes.

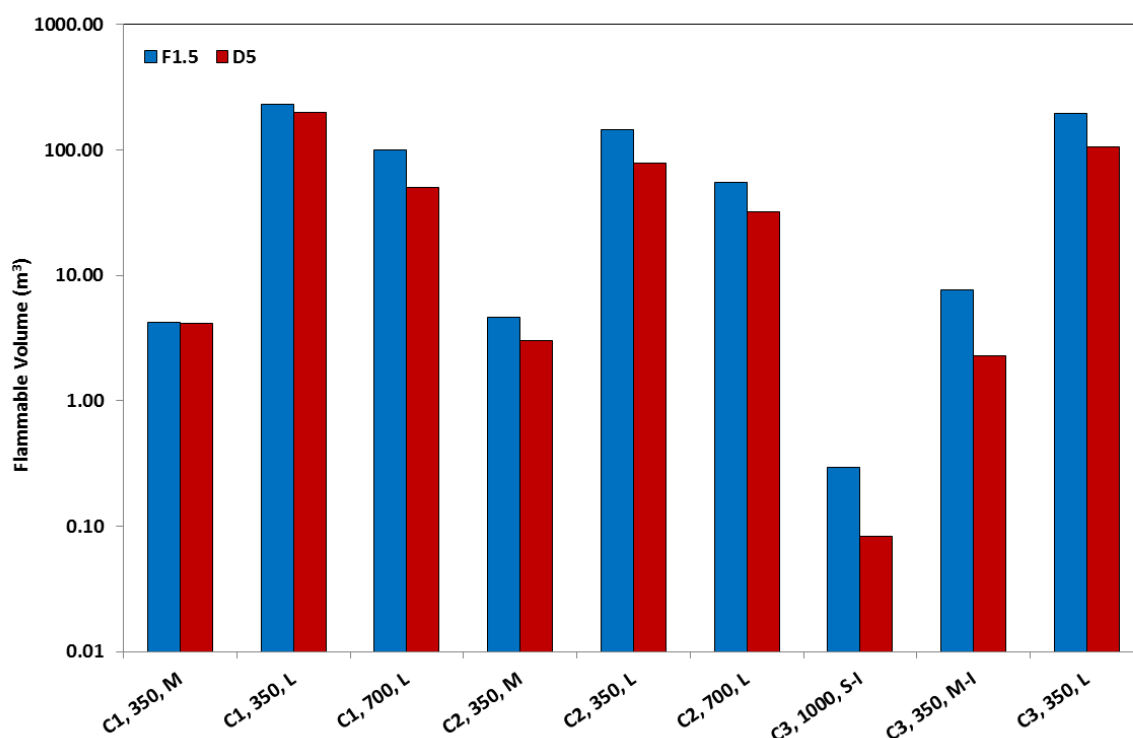


**Figure 65 – Comparison of the predicted flammable cloud volume across the range of realistic release scenarios modelled. Here, the column labels give Configurations 1, 2 and 3 as C1, C2 and C3, respectively, followed by the release pressure as a numerical value and the release size as small-internal (S-I), medium (M) and large (L). Results for the F1.5 and D5 wind conditions are shown as blue and red columns, respectively.**

Figure 66 presents a comparison of the predicted flammable cloud volume for the three pairs of realistic release scenarios that involved full bore rupture of a 3/8 inch 350 bar  $H_2$  delivery hose. Specifically, this Figure covers Scenarios 3 & 4 for Configuration 1, Scenarios 11 & 12 for Configuration 2, and Scenarios 25 & 26 for Configuration 3. The Figure shows predictions using CFX and KFX for Configuration 1 (note that only Scenario 3 was not modelling using KFX) and predictions using OpenFOAM 1812 and KFX were used to model the two scenarios for forecourt Configuration 2. For forecourt Configuration 3, only KFX predictions are available. From this Figure it is clear that the predicted flammable cloud sizes are large in all cases.

The cloud spread predicted for these cases, as shown and discussed in Section 4.3, covers large areas of the forecourt, engulfing the dispensing area and interacting significantly with the representative canopy above the dispenser. Whilst the aim of the present task is to consider dispersion behaviour, rather than consequences, it is clear that if such releases were to occur, there would be a very high risk of fire and/or explosion, with the potential for widespread damage to the site, and potentially hazardous conditions for people present on the forecourt. It is also

worth noting that the full bore releases modelled in this work used  $H_2$  mass flow rates which were capped at the dispenser delivery flow rate. If the flow rate restriction were to be lost at the same time as a full bore rupture of the hose, then the  $H_2$  mass flow rate would be around an order of magnitude greater, giving an even more substantial hazard than illustrated through the CFD modelling presented here.

Looking at how the predicted flammable cloud volume varies across the three forecourt configurations for the full bore releases, it is clear from Figure 66 that the influence of the wind condition for the CFX modelling is not as significant as for the results from the other models. For the KFX and the OpenFOAM 1812 modelling for Configurations 2 and 3, the D5 wind condition results in a flammable cloud volume around half that predicted for F1.5 wind conditions. Whereas, for the CFX modelling for Configuration 1, the difference in predicted flammable volume between wind conditions is around 15-20%. This is likely to be due to a combination of things, including how the atmospheric boundary layer has been defined in the models, the differences in the forecourt geometries and the meshing approach used around obstacles in each model.

Comparing the KFX predictions shown in Figure 66, which cover all three forecourt configurations, it is clear that the release on Configuration 1 results in the largest flammable cloud size. This can be attributed partly to the fact that the modelled bus provides greater shelter from the wind than the truck used in Configurations 2 and 3, but perhaps more significantly, as a consequence of the larger canopy above the dispensing area leading to a flow field around it that effectively captures the gas cloud and inhibits dispersion and mixing. This finding suggests that reducing the size of the canopies such that there are individual canopies above each dispenser could lead to enhanced turbulent mixing and thus more effective dilution and dispersion of any released gas. This highlights a need for further study into the influence of canopy design in future hydrogen research projects.

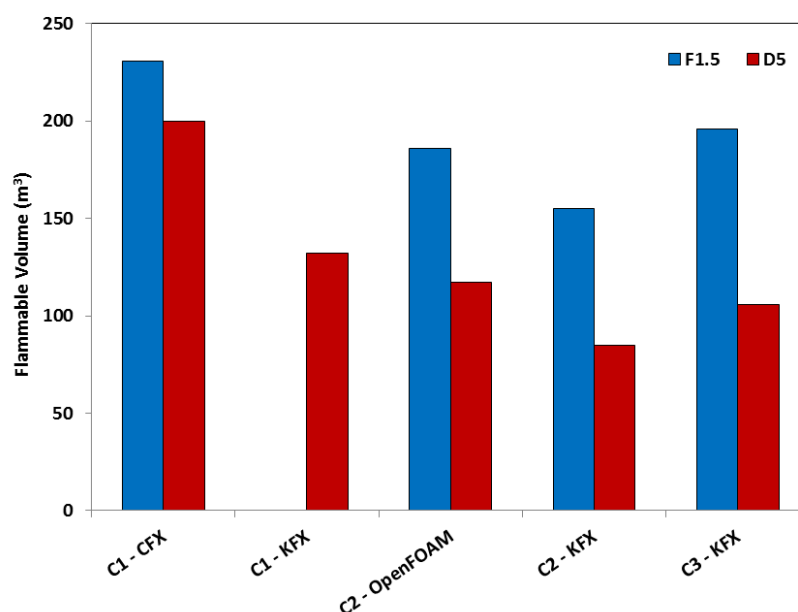


**Figure 66 – Comparison of the predicted flammable cloud volumes for the 350 bar, full bore rupture release scenarios across all three forecourt configurations**

Figure 67 presents the predicted flammable cloud volume for the 350 bar release through an opening of approximately 0.95 mm, corresponding to 10% of the  $H_2$  delivery hose diameter. The Figure shows a comparison of the results across the forecourt Configurations 1 and 2. The results show that these cases give comparable cloud volumes despite the difference in forecourt



geometry. The difference between the two wind conditions modelled is less pronounced than was the case for the full bore hose rupture scenarios. From the detailed CFD outputs presented in Section 4.3, it is evident that this is a consequence of the significant sheltering from the wind provided by the large vehicles adjacent to the leak location. As a consequence, the cloud volume is principally dictated by the interaction of the jet release with the vehicle, rather than the wind.

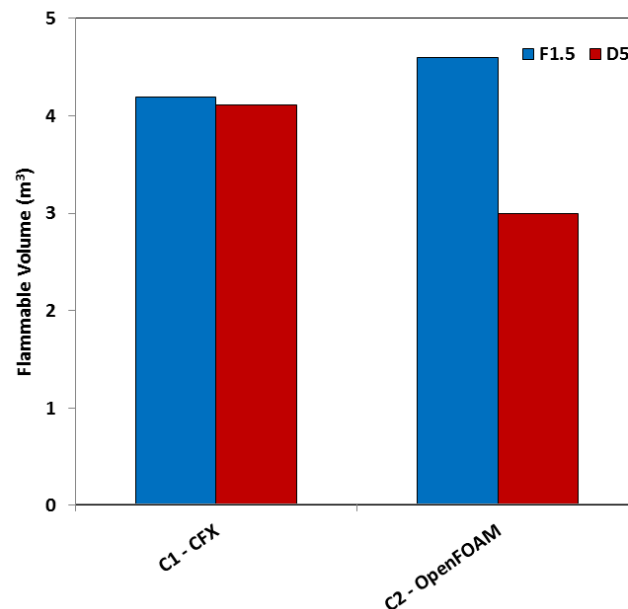


**Figure 67 – Comparison of the predicted flammable cloud volumes for the 350 bar, 10% hose diameter release scenarios for Configurations 1 and 2**

Figure 68 presents a comparison of the predicted flammable cloud volume across the set of realistic release scenarios involving full bore rupture of a 3/8 inch, 700 bar H<sub>2</sub> delivery hose. Specifically, the Figure shows results for Scenarios 7 & 8, for Configuration 1, and Scenarios 15 & 16, for Configuration 2. For the Configuration 2 cases, there are model predictions from both OpenFOAM 1812 and KFX. The Figure shows that, whilst the three predictions made with D5 wind conditions are broadly similar, and consistently smaller than with F1.5 wind conditions, there is a large discrepancy in the flammable volume predicted in the lower wind speed case. Here, CFX is predicting a cloud volume almost twice the size of that predicted using the other two models under D5 wind conditions.

Given the differences in the forecourt geometries used, meshing strategies and approaches, the potential for minor differences in the setup of the wind conditions and other choices of CFD sub-model, it is not unexpected to see the different models predicting different levels of variation in cloud volume across the two wind conditions tested. What is clear from the modelling work presented here, is that H<sub>2</sub> releases from full bore ruptures of the delivery hose present a significant hazard and should be mitigated against as far as is possible.

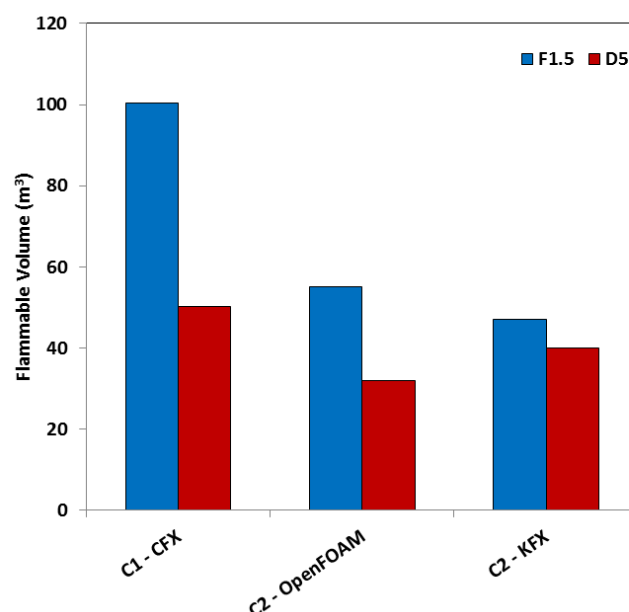


**Figure 68 – Comparison of the predicted flammable cloud volumes for the 700 bar, full bore rupture release scenarios for Configurations 1 and 2**

## 5.2 Limitations of Modelling Performed

As with any modelling study, there are a number of limitations which should be taken into consideration when evaluating model outputs. Some of the limitations and assumptions specific to the present analysis are described below.

Firstly, it is not possible to validate the simulations of realistic release scenarios as experimental data for that purpose does not yet exist. The model validation exercise described in Section 3 of this report was undertaken to partially mitigate against this, by providing direct comparison of the selected CFD model results to experimental data for scenarios sharing key physics with the anticipated critical scenarios (since the model validation preceded definition of the realistic releases). This exercise enabled the participants within the *Dispersion Characteristics* task to establish whether the models selected would be suitable for further use in the project and gave confidence in the results which could be produced both by the models and the modellers involved.

Secondly, the realistic release scenarios themselves include significant simplification. For example, we have representative multi-fuel forecourt configurations from WP3, but in reality these forecourts would have specific environments around them, e.g. an urban area, which could substantially influence the results. Without basing the simulations on a specific, pre-existing real-world location, nothing further can be done to mitigate against this. Thus, evaluation of the model predictions should take this simplification into account.

There are also further simplifications to the forecourt geometries themselves. For example, the vehicles included in the models are of simple shape and design, whereas in reality there are a range of more complex vehicle shapes that could be present on an actual forecourt at any given time. Furthermore, the representative canopy design used in the modelling does not necessarily match the specific design of an actual canopy used on a multi-fuel forecourt. However, the model predictions indicate that there is significant interaction between the release  $H_2$  and the structures present on the forecourt.

An additional limitation of the modelling is the simulation of the atmospheric boundary layer and the wind field present on the modelled forecourts. An urban environment surrounding a multi-fuel forecourt could drastically alter the wind field, leading to significant changes in the predicted flammable cloud volumes and H<sub>2</sub> dispersion behaviour. Furthermore, as described in Section 4.2.3, there are known deficiencies with CFD modelling of ABL's, particularly in the case of a stably-stratified atmosphere, such as has been used for the F1.5 wind condition simulated in this work. However, given the other limitations of the modelling undertaken as part of this project, this is unlikely to have a significant impact on the findings, particularly since all realistic release scenarios are equally affected.

### 5.3 Areas for Extending the Research in Future Projects

Whilst this work has presented CFD simulations of a broad spectrum of releases identified through WP3, and Task 3.5 specifically, as *critical* scenarios, an alternative approach would have been to focus on a few specific examples and to study them in further detail. This, of course, leads to the conclusion that it would be useful to extend the modelling work presented in this report to look further at the impacts of, for example, canopy geometry, wind conditions, release direction, the environment around the forecourt etc. Clearly this is beyond the scope, and budget, of the MultHyFuel project and thus lends itself to further study in a follow-on piece of research work. It is recommended that any future project also considers undertaking case study simulations for real sites intended for conversion to multi-fuel use.

Additionally, the present study has included an element of model validation in order to give confidence in the selected CFD models before studying the realistic scenarios. However, as discussed in Section 5.2, there is no validation of the models against data for the types of realistic releases considered. Other parts of MultHyFuel WP2 are seeking to generate this type of data, so a useful further project could include validation against the data generated through the experimental research undertaken as part of the present project.

## 6 Conclusions

The main aim of WP2 is to **produce the data missing to implement usable risk analysis and mitigation activity** for Hydrogen Refuelling Stations (HRS) in a multi-fuel context. The WP is divided into the following tasks:

- **Task 2.1 – Leakage Characterisation of H<sub>2</sub> Dispensers**
  - Task 2.1.1 – Leakage Characteristics
  - Task 2.1.2 – Dispersion Characteristics
  - Task 2.1.3 – Ignition Probabilities
  - Task 2.1.4 – Efficiency of Safety Barrier
- **Task 2.2 – Fire and Explosion Hazards**
  - Task 2.2.1 – Defining a Zoning Threshold
  - Task 2.2.2 – Domino Effect arising from Faults on H<sub>2</sub> Dispensers
  - Task 2.2.3 – Vulnerability of H<sub>2</sub> Dispensers to Incidents Involving Other Fuel Dispensers

This report is the main output of WP2 *Task 2.1.2 – Dispersion Characteristics*. The principal aim of this task is to study realistic releases of H<sub>2</sub> on representative multi-fuel forecourts using CFD.

In this report, the CFD modelling performed as part of the *Dispersion Characteristics* task is described and the range of realistic release scenarios considered, and their links to the critical scenarios identified through the risk assessment work conducted in WP3, are presented. The report presents demonstration solutions, including predicted flammable cloud volumes, for the critical scenarios considered.

The task has been conducted in two stages as follows:

- **Model Validation** – to evaluate the CFD models selected by the task partners and evaluate their performance through comparison to experimental data
- **Realistic Release Modelling** – to perform demonstration simulations of a range of critical scenarios, identified through WP3 HAZID workshops and subsequent risk assessment analyses, which could not be adequately studied using simpler modelling tools

The model validation exercise shows that the CFD models selected by the task partners can reasonably reproduce the measured data across a range of H<sub>2</sub> release scenarios. The experiments used as the basis of the exercise include underexpanded H<sub>2</sub> jet releases in the open atmosphere and issuing into an obstacle array, as well as buoyancy-driven releases inside a naturally ventilated enclosure. These scenarios are considered to span a range of key physics associated with the critical scenarios also studied in this work. The results of the model validation exercise show that the models produce acceptable solutions when compared to measured data and provide confidence in the ability of the models, and the modellers, to capture the behaviour of the realistic releases adequately.

One of the key findings from the model validation cases involving jet releases is that the specification of the source term is critical to model performance. For the modelling presented in this report, the choice of CFD model is shown to be of less importance than the definition of the source term, since multiple CFD codes give comparable results when using the same imposed

source condition. The model validation results suggest that jet release modelling in CFD studies should use source term input values taken from a suitable jet model at the point in the jet where the local Mach number is close to 1.

For the realistic release modelling, it was necessary for the selected cases for simulation to link into the risk assessment work performed in Task 3.1 through to Task 3.5 of WP3. These tasks led to the identification of a range of *critical scenarios* associated with multi-fuel forecourts. The outputs of Task 3.5, in particular, formed the basis of scenario selection in the present task. For the CFD modelling task, it was necessary to reduce the number of identified critical scenarios to a subset which could be managed within the context of the task. As such, the decision was taken to focus on releases at the dispenser, i.e. no scenarios involving pipework upstream of the dispenser are considered in the present study.

The realistic release simulation results presented span nine base scenarios, each with two separate wind conditions, to give 18 cases in total. The cases cover all three forecourt configurations defined in MultHyFuel WP3 and involve H<sub>2</sub> releases ranging from 1.5 to 120 g/s through hole sizes with diameters of 0.2 mm, 10% of the hose diameter (~ 0.95 mm) and full bore rupture of a 3/8 inch hose (~9.5 mm). The wind conditions modelled involve a stable atmospheric boundary layer (ABL) with a wind speed of 1.5 m/s at a reference height of 10 m above the ground (F1.5) and a neutral ABL with a wind speed of 5 m/s at a reference height of 10 m (D5).

The simulation results illustrate a consistent trend of the F1.5 conditions giving larger flammable cloud volumes than the corresponding scenario with D5 wind conditions. This illustrates that a stable atmosphere with low wind speed is likely to give a better representation of worst-case conditions for the purposes of risk assessment analyses.

The predicted cloud volumes across the range of scenarios considered ranges from around 0.1 – 230 m<sup>3</sup>, depending on the size of the release, the forecourt geometry and the selected CFD model. The results show that the full bore rupture releases present a significant hazard, with flammable clouds fully engulfing the dispensing area and spreading over a large proportion of the forecourt. Conversely, the medium-sized (10% hose diameter) H<sub>2</sub> releases give greatly reduced flammable cloud volumes, although they still present a credible hazard in the vicinity of the release point. For the smallest release considered, the predicted cloud volumes are small and show no interaction with the obstacles present on the forecourt. As such, it would be reasonable to study the smallest releases using simpler, engineering type tools, rather than CFD.

One of the benefits of having studied these scenarios with CFD models is being able to obtain a visual representation of the flammable cloud and to thus be able to see the interaction of the cloud with obstacles on the forecourt. From the results presented in this report, it is clear that there can be extensive interaction of the flammable cloud with the canopy above the dispensing area. As such, it is recommended that additional work is undertaken in a future project to study the influence of canopy design.

The work described in this report has gone as far as it is possible to within the scope and budget of the MultHyFuel *Dispersion Characteristics* task. However, it is clear that this work can only be considered as having taken a first step into the study of H<sub>2</sub> releases on multi-fuel forecourts. There is clearly scope for extension of this modelling study to consider real-world multi-fuel forecourt case studies and to further evaluate the choice of model input parameters and forecourt geometry on predicted flammable cloud volumes. The results of this study highlight the canopy as having a strong influence on the dispersion. It is recommended that future research seeks to continue this work.

## 7 Appendix

### 7.1 Appendix 1 – Forecourt Configurations

#### 7.1.1 Configuration 1 – Ready-to-Deploy Multi-fuel Station

Figure 69 shows the layout used in the MultHyFuel project as a representative design for a *ready-to-deploy* multi-fuel forecourt. For the purposes of the risk assessment analysis in WP3 it is assumed that forecourt Configuration 1 is located in an urban environment containing 600 people per hectare.

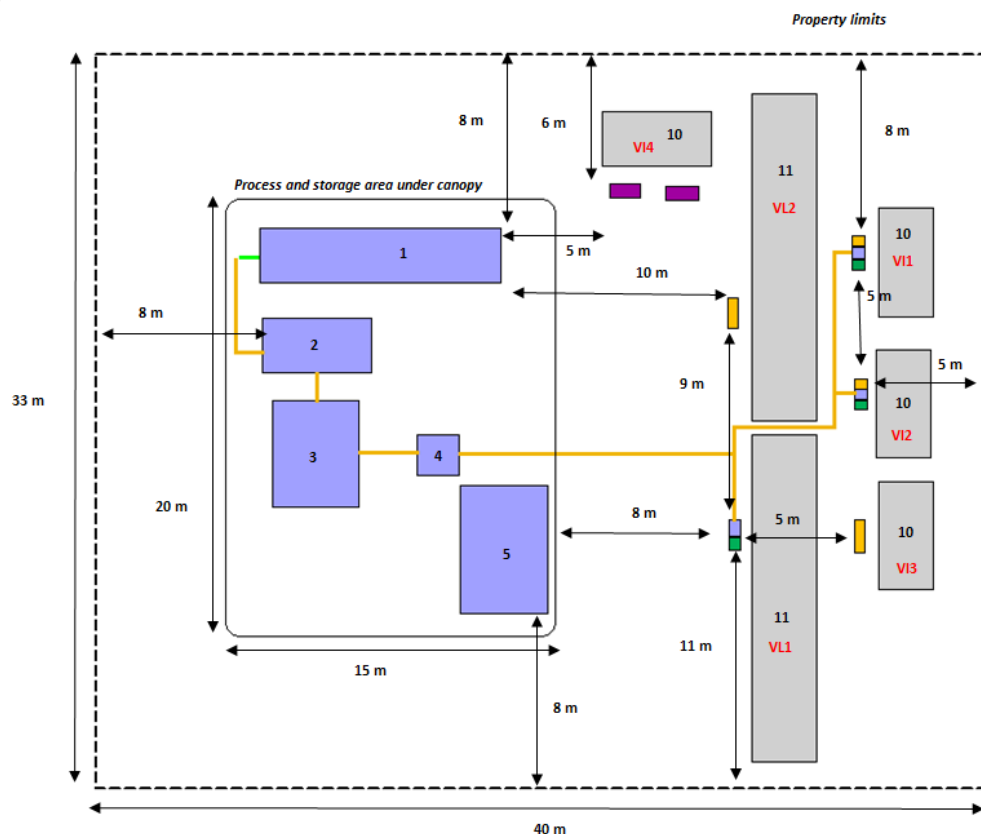








**Figure 69 – Layout of the *ready to deploy* multi-fuel forecourt from deliverable D3.5. Table 19 presents descriptions of the items included in this forecourt layout**

Table 18 summarises the assumptions used in the risk assessment analysis regarding the distribution of vehicles and members of the public present for forecourt Configuration 1. The critical scenarios identified in Section 4.1 are taken for the arrangement described in this Table.

Dispenser	Cars	Buses/Heavy duty vehicles
<b>H<sub>2</sub></b>	1 car (4 people) (VI1) 1 car (1 person) (VI2)	1 bus (2 people) (VL1)
<b>Other</b>	1 car (4 people) (VI3) 1 car (1 person) (VI4)	1 truck (2 people) (VL2)

**Table 18 – Assumed distribution of vehicles and members of the public present on the forecourt for Configuration 1**

Table 19 provides information on the dimensions of the footprint occupied by each piece of equipment and the distribution areas for Configuration 1.

N°	Installation/ equipment	Size of installation/equipment [m]
1	Gaseous hydrogen storage area	11 m x 2,5 m (trailer area)
2	Compression skid	5 m x 2,5 m (for one compressor)
3	MP & HP buffers	5 m x 4 m
4	Chiller	2 m x 2 m
5	Control & technical room	6 m x 4 m
6	Conventional fuel dispensers 	1,5 m x 0,5 m
7	Multi-fuel dispensers 	1,5 m x 0,5 m
8	H <sub>2</sub> dispersing 	1,5 m x 0,5 m
9	Electric charging point 	1,5 m x 0,5 m
10	Distribution area for cars	5 m x 2,5 m
11	Distribution area for buses and heavy-duty vehicles	15 m x 3 m
12	Delivery connection (for trailer) 	n/a
13	Pipes H <sub>2</sub> 	n/a

**Table 19 – Summary of the footprint size for equipment and distribution areas for Configuration 1**

### 7.1.2 Configuration 2 – On Site H<sub>2</sub> Production Multi-fuel Station

Figure 70 shows the layout used to represent a multi-fuel forecourt with on-site H<sub>2</sub> production. For the purposes of the risk assessment analysis, it was assumed that such a station would be located in a suburban area containing 50 people per hectare.

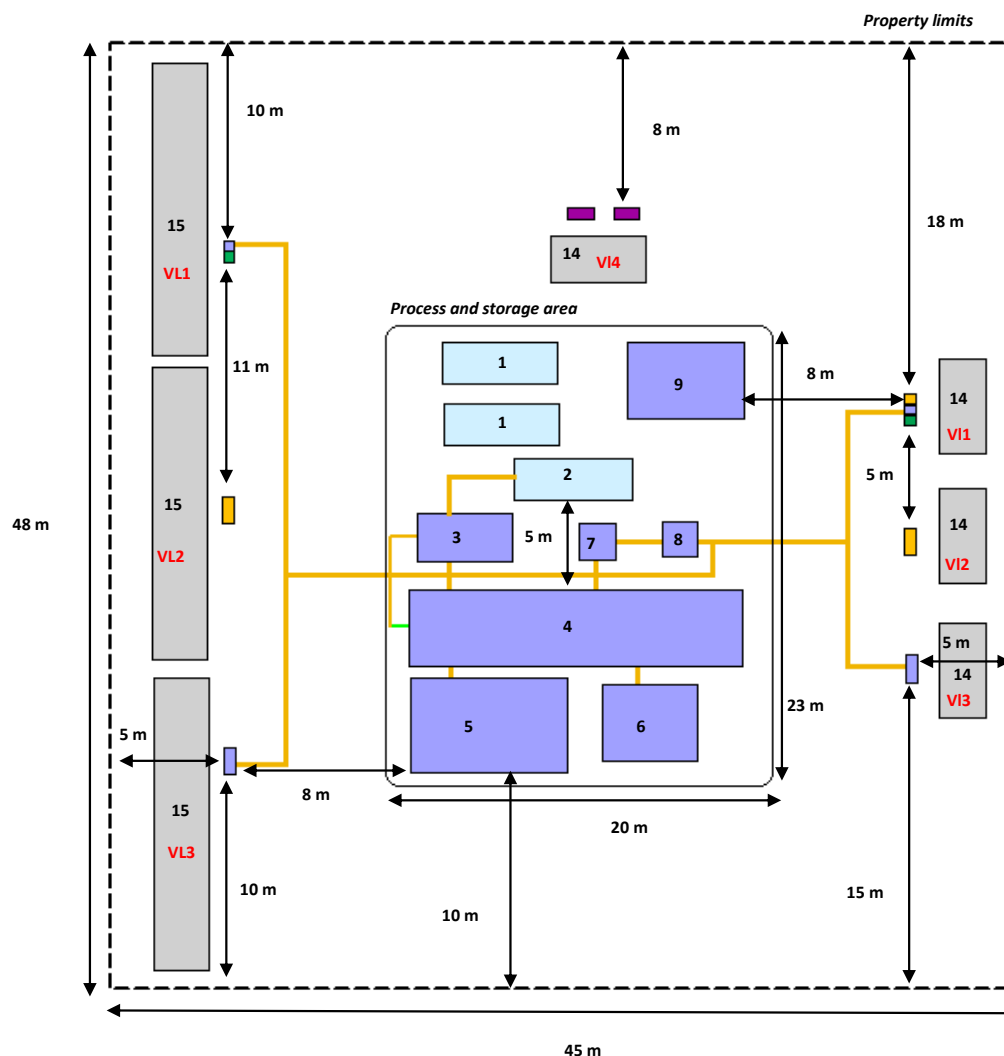


**Figure 70 – Layout of the on site H<sub>2</sub> production multi-fuel forecourt from deliverable D3.5. Table 21 presents descriptions of the items included in this forecourt layout**

Table 20 summarises the assumptions used in the risk assessment analysis regarding the distribution of vehicles and members of the public present for forecourt Configuration 2. The critical scenarios identified in Section 4.1 are taken for the arrangement described in this Table.

Dispenser	Cars	Buses/Heavy duty vehicles
<b>H<sub>2</sub></b>	1 car (4 people) (VL1) 1 car (1 person) (VL3)	1 bus (2 people) (VL1) 1 truck (2 people) (VL3)
<b>Other</b>	1 car (4 people) (VL2) 1 car (1 person) (VL4)	1 truck (2 people) (VL2)

**Table 20 – Assumed distribution of vehicles and members of the public present on the forecourt for Configuration 2**



Table 21 provides information on the dimensions of the footprint occupied by each piece of equipment and the distribution areas for Configuration 2.

N°	Installation/ equipment	Size of installation/equipment [m]
1	Power container	6 m x 2,3 m (for one container)
2	PEM electrolyser	6 m x 2,3 m (for one container)
3	Compression skid	5 m x 2,5 m (for one compressor)
4	BP Buffer / Trailer area	17 m x 4 m
5	MP Buffer	8 m x 5 m
6	HP Buffer	5 m x 4 m
7	Chiller	2 m x 2 m
8	HX (heat exchanger)	2 m x 2 m
9	Control & technical room	6 m x 4 m
10	Conventional fuel dispensers 	1,5 m x 0,5 m
11	Multi-fuel dispensers 	1,5 m x 0,5 m
12	H <sub>2</sub> dispersing 	1,5 m x 0,5 m
13	Electric charging point 	1,5 m x 0,5 m
14	Distribution area for cars	5 m x 2,5 m
15	Distribution area for buses and heavy duty vehicles	15 m x 3 m
16	Delivery connection (for trailer) 	n/a
17	Pipes H <sub>2</sub> 	n/a

**Table 21 – Summary of the footprint size for equipment and distribution areas for Configuration 2**

### 7.1.3 Configuration 3 – High Capacity & High Filling Multi-fuel Station

Figure 71 shows the layout used to represent a high capacity and high filling multi-fuel forecourt. For the purposes of the risk assessment analysis it was assumed that such a station would be located in an industrial zone in a rural area containing 20 people per hectare. Furthermore, it was also assumed that there would be a highway located 35 m away from the station

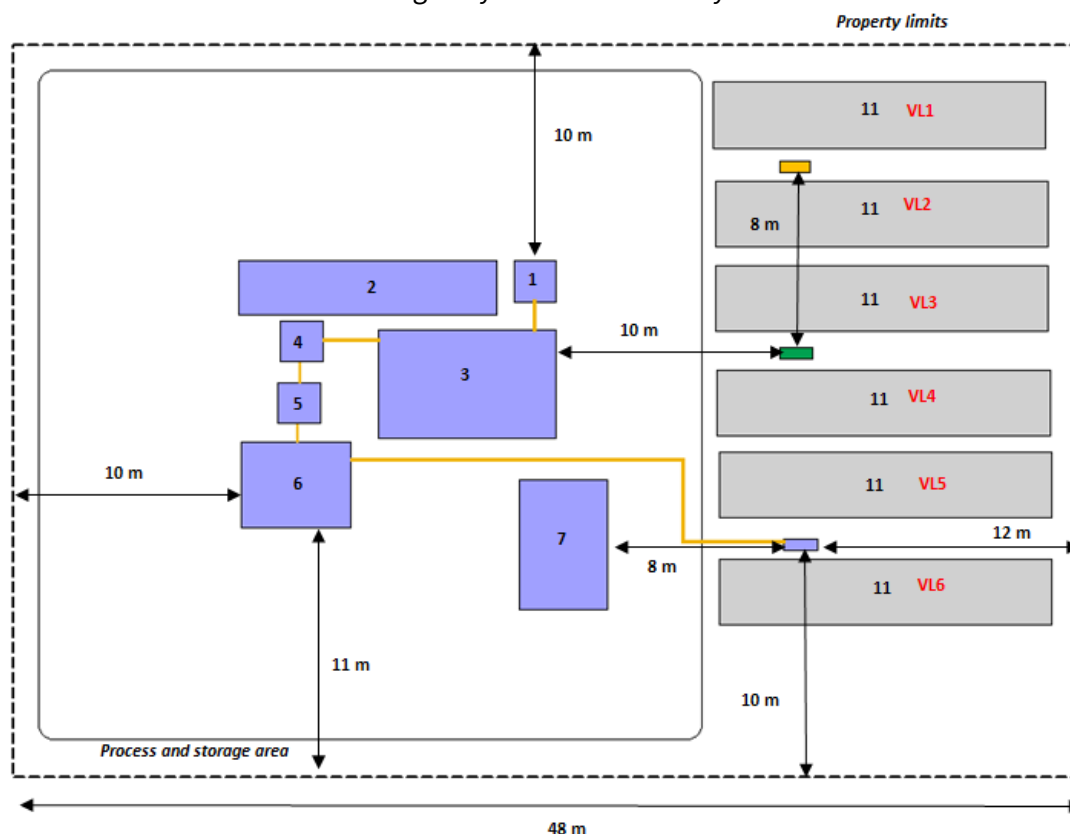






**Figure 71 – Layout for the *high capacity* multi-fuel forecourt from deliverable D3.5. Table 23 presents descriptions of the items included in this forecourt layout**

Table 22 summarises the assumptions used in the risk assessment analysis regarding the distribution of vehicles and members of the public present for forecourt Configuration 3. The critical scenarios identified in Section 4.1 are taken for the arrangement described in this Table.

Dispenser	Buses/Heavy duty vehicles
<b>H<sub>2</sub></b>	1 bus (2 people) (VL5) 1 truck (2 people) (VL6)
<b>Other</b>	1 bus (2 people) (VL2) 3 trucks (2 people each) (VL1, VL3, VL4)

**Table 22 – Assumed distribution of vehicles and members of the public present on the forecourt for Configuration 3**

Table 23 provides information on the dimensions of the footprint occupied by each piece of equipment and the distribution areas for Configuration 3.

N°	Installation/ equipment	Size of installation/equipment [m]
1	Liquid hydrogen storage area	2 m x 2 m (vertical storage usually)
2	Trailer area	12 m x 2,5 m
3	Pumping skid	8 m x 4 m
4	Vaporizer	2 m x 2 m (vertical vaporizer usually)
5	Compression skid	2 m x 2 m
6	HP buffers	5 m x 4 m
7	Control & technical room	6 m x 4 m
8	Conventional fuel dispensers 	1,5 m x 0,5 m
9	L-CNG dispensing 	1,5 m x 0,5 m
10	H <sub>2</sub> dispersing 	1,5 m x 0,5 m
11	Distribution area for buses and heavy duty vehicles	15 m x 3 m
12	Pipes H <sub>2</sub> 	n/a

**Table 23 - Summary of the footprint size for equipment and distribution areas for Configuration 3**

## 7.2 Appendix 2 – Atmospheric Boundary Layer

In order to capture the influence of different wind conditions in the realistic release modelling it is necessary to specify atmospheric boundary layer profiles as inlet conditions, and often as initial conditions, in the various CFD models used in this MultHyFuel task. As described in Section 4.1.5 two sets of atmospheric conditions have been used as follows:

- **D5** – corresponding to a neutral atmospheric boundary layer with a wind speed of 5 m/s at a reference height of 10 m above the ground.
- **F1.5** – corresponding to a stable atmospheric boundary layer with a 1.5 m/s at a reference height of 10 m above the ground.

The following subsections of this Appendix outline the equations used to describe the two wind conditions listed above.

### 7.2.1.1 Neutral Boundary Layer

For the case of neutral atmospheric stability, it is necessary to impose profiles of the turbulent kinetic energy,  $k$ , the turbulent dissipation rate,  $\varepsilon$ , and the wind speed,  $U$ , as the inlet boundaries of the CFD simulation domain. In addition, it can be beneficial to also use the same profiles as initial conditions throughout the domain to aid with numerical convergence.

The profiles used in this work, shown below as Equations (1)-(4), follow the approach given in Richards and Hoxey (1993), where  $U(z)$  represents the vertical velocity field, with  $z$  taken as the height above the ground,  $k$  is the turbulent kinetic energy,  $\varepsilon(z)$  gives the vertical profile for the turbulent dissipation rate,  $u_*$  is the friction velocity,  $U_{ref}$  is the reference wind speed,  $z_{ref}$  is the reference height for the reference wind speed,  $\kappa = 0.41$  is the von Karmann constant,  $z_0 = 0.1$  m is the aerodynamic roughness height and  $C_\mu = 0.09$  is the default value of one of the model constants used in the  $k$ - $\varepsilon$  turbulence model (Launder and Spalding, 1972).

Equations (1)-(4) deviate slightly from the original Richards and Hoxey (1993) approach by including an adjustment to the height to avoid taking the natural logarithm of, or dividing by, zero. Whilst each of the modellers involved in this task has used a wind profile based on profiles such as those given below, there may be minor differences from model to model. These differences are likely to be minor and are thus considered unimportant in the context of the overall analysis.

$$u_* = \frac{U_{ref} \kappa}{\ln\left(\frac{z + z_0}{z_0}\right)} \quad (1)$$

$$U(z) = \frac{u_*}{\kappa} \ln\left(\frac{z + z_0}{z_0}\right) \quad (2)$$

$$k = \frac{u_*^2}{\sqrt{C_\mu}} \quad (3)$$

$$\varepsilon(z) = \frac{u_*^3}{\kappa(z + z_0)} \quad (4)$$

### 7.2.1.2 Stable Boundary Layer

For the case of the stable boundary layer it is also necessary to prescribe a vertical profile for temperature as well as the velocity and turbulence parameters. Typically, the temperature is specified via the potential temperature,  $\theta(z)$ . Equations (5)-(12) have been used in the CFX modelling presented in this report to specify the F1.5 wind conditions. The specific approaches used by the other task partners may deviate slightly from this equation set, but not substantially so, particularly for the velocity profile. It is expected that any difference in the prescribed wind conditions will have little influence on the model results.

The expressions for the velocity and the potential temperature are taken from Alinot and Masson (2005), given below as Equations (8) and (10), respectively. These equations rely on the use of an additional parameter  $L$ , which is the Monin-Obhukov length for the boundary layer profile. For a stable atmospheric boundary layer  $L > 0$ . Equation (5) presents one approach for estimating the value of  $L$ . This equation is taken from the FLACS User Manual (Gexcon, 2014), where  $L_s = -31.323$  m and  $z_s = 19.36$  m. The different task partners used minor variations in approach for estimating  $L$  but all obtained comparable values.

The turbulence parameters for the stable boundary layer are specified here following Equations (11) and (12), originally given by Han et al. (2000). Additionally, the atmospheric boundary layer height,  $h$ , is estimated from Equation (7), where  $f = 0.0001 \text{ s}^{-1}$  is the Coriolis parameter.

$$\frac{1}{L} = \frac{1}{L_s} \log_{10} \left( \frac{z}{z_s} \right) \quad (5)$$

$$u_* = \frac{U_{ref} \kappa}{\ln \left( \frac{z + z_0}{z_0} \right) + 5 \frac{z}{L}} \quad (6)$$

$$h = 0.4 \left( \frac{u_* L}{f} \right)^{1/2} \quad (7)$$

$$U(z) = \frac{u_*}{\kappa} \left[ \ln \left( \frac{z + z_0}{z_0} \right) + 5 \frac{z}{L} \right] \quad (8)$$

$$\theta_* = \frac{u_*^2 \theta_0}{g \kappa L} \quad (9)$$

$$\theta(z) = \theta_0 + \frac{\theta_*}{\kappa} \left[ \ln \left( \frac{z + z_0}{z_0} \right) + 5 \frac{z}{L} \right] \quad (10)$$

$$k(z) = 6 u_*^2 (1 - z)^{1.75} \quad (11)$$

$$\varepsilon(z) = \frac{u_*^3}{\kappa(z + z_0)} \left( 1.24 + 4.3 \frac{z}{L} \right) \left( 1 - 0.85 \frac{z}{h} \right)^{\frac{3}{2}} \quad (12)$$

For the turbulence parameters specified above, i.e.  $k(z)$  and  $\varepsilon(z)$  given by Equations (11) and (12), respectively, the work of Alinot and Masson (2005) and Han et al. (2000) are based on the use of  $C_\mu = 0.033$  as a constant in the k- $\varepsilon$  turbulence model. In the modelling performed here, a value of  $C_\mu = 0.09$  is used, which is the default value from the standard k- $\varepsilon$  model formulation. In order

to ensure that the correct turbulence profiles are specified, it is necessary to scale Equation (11) down, and Equation (12) up, by around 20-30%, to match what would be obtained using  $C_\mu = 0.033$ . This scaling has been applied in the modelling described here.

## 8 References

- Alinot, C. and Masson, C., (2005), k- $\epsilon$  model for the atmospheric boundary layer under various thermal stratifications, *Transactions of the American Society of Mechanical Engineers (ASME)*, **127** (2005), 438-443
- ANSYS, 2019, ANSYS CFX Solver Theory Guide Release 19.0, ANSYS Inc.
- Batt, R., Gant, S., Lacome, J-M, Truchot, B. and Tucker, H., (2018), CFD modelling of dispersion in neutrally and stably-stratified atmospheric boundary layers: results for Prairie Grass and Thorney Island, *International Journal of Environment and Pollution*, **63** (1-2)
- Bernard-Michel, G. and Houssin-Agbomson, D., (2017), Comparison of helium and hydrogen releases in 1 m<sup>3</sup> and 2 m<sup>3</sup> two vents enclosures: Concentration measurements at different flow rates and for two diameters of injection nozzle, *International Journal of Hydrogen Energy*, **42** (2017), 7542-7550
- Betteridge, S., (2022), Shell FRED 2022 Technical Guide, Shell Global Solutions
- Daubech, J., Hebrand, J., Jallais, S., Vyazmina, E., Jamois, D. and Verbecke, F., (2015), Un-ignited and ignited high pressure hydrogen releases: Concentration – turbulence mapping and overpressure effects, *Journal of Loss Prevention in the Process Industries*, **36** (2015), 439-446
- DNV, (2001), Kameleon FireEx 2000 Theory Manual, Report R0123
- Ewan, B.C.R. and Moodie, K., (1986), Structure and velocity measurements in underexpanded jets, *Combustion Science and Technology*, **45** (5-6), 275-288
- Gexcon, (2014), FLACS v10.3 User's Manual, 20<sup>th</sup> June 2014, Gexcon AS, Norway
- Han, J., Arya, S.P., Shen, S. and Lin, Y.-L., (2000), An estimation of turbulent kinetic energy and energy dissipation rate based on atmospheric boundary layer similarity theory, Report No. NASA/CR-2000-210298, National Aeronautics and Space Administration (NASA)
- Jallais, S., Houssin-Agbomson, D. and Cariteau, B., (2013), Application of natural ventilation engineering models to hydrogen build-up in confined zones, International Conference of Hydrogen Engineering (ICHES), Brussels, Belgium, 9<sup>th</sup>-11<sup>th</sup> September 2013
- Linden, P. (1999), The fluid mechanics of natural ventilation, *Annual Review of Fluid Mechanics*, **31** (1999), 201-238
- McFarlane, K., (1991) Development of Plume and Jet Release Models, International Conference on Modelling and Mitigating the Consequences of Accidental Release of Hazardous Materials, New Orleans, Proceedings pp 657-688
- Papanikolaou, E., Baraldi, D., Kuznetsov, M. and Venetsanos, A., (2012), Evaluation of notional nozzle approaches for CFD simulations of free-shear under-expanded hydrogen jets, *International Journal of Hydrogen Energy*, **37** (2012), 18563-18574
- Richards, P.J. and Hoxey, R.P., Appropriate boundary conditions for computational wind



engineering models using the k- $\epsilon$  turbulence model, *Journal of Wind Engineering and Industrial Aerodynamics*, **46 & 47** (1993), 145-153

## What is MultHyFuel?

The goal of MultHyFuel is to contribute to the effective deployment of hydrogen as an alternative fuel by developing a common strategy for implementing Hydrogen Refueling Stations (HRS) in multi-fuel contexts, contributing to the harmonization of existing laws and standards based on practical, theoretical and experimental data as well as on the active and continuous engagement of key stakeholders.

MultHyFuel is a project funded by the Fuel Cells and Hydrogen 2 Joint Undertaking (FCH 2 JU).

Further information can be found under <https://www.multyfuel.eu>.

For feedback on the MultHyFuel project or the published deliverables, please contact [info@multyfuel.eu](mailto:info@multyfuel.eu).

### *The MultHyFuel Consortium*



**BESPOKE RESEARCH AND  
CONSULTANCY FROM**

